University of Wollongong

Research Online

University of Wollongong Thesis Collection 2017+

University of Wollongong Thesis Collections

2017

Advanced suspension system using magnetorheological technology for vehicle vibration control

Xin Tang
University of Wollongong

Follow this and additional works at: https://ro.uow.edu.au/theses1

University of Wollongong

Copyright Warning

You may print or download ONE copy of this document for the purpose of your own research or study. The University does not authorise you to copy, communicate or otherwise make available electronically to any other person any copyright material contained on this site.

You are reminded of the following: This work is copyright. Apart from any use permitted under the Copyright Act 1968, no part of this work may be reproduced by any process, nor may any other exclusive right be exercised, without the permission of the author. Copyright owners are entitled to take legal action against persons who infringe their copyright. A reproduction of material that is protected by copyright may be a copyright infringement. A court may impose penalties and award damages in relation to offences and infringements relating to copyright material. Higher penalties may apply, and higher damages may be awarded, for offences and infringements involving the conversion of material into digital or electronic form.

Unless otherwise indicated, the views expressed in this thesis are those of the author and do not necessarily represent the views of the University of Wollongong.

Recommended Citation

Tang, Xin, Advanced suspension system using magnetorheological technology for vehicle vibration control, Doctor of Philosophy thesis, School of Mechanical, Materials, Mechatronic & Biomedical Engineering, University of Wollongong, 2017. https://ro.uow.edu.au/theses1/208

Research Online is the open access institutional repository for the University of Wollongong. For further information contact the UOW Library: research-pubs@uow.edu.au

UNIVERSITY
OF WOLLONGONG
AUSTRALIA

Advanced suspension system using magnetorheological technology for vehicle vibration control

A thesis submitted in partial fulfilment of the requirements for the award of the degree of

Doctor of Philosophy

from

University of Wollongong

by

Xin Tang

School of Mechanical, Materials, Mechatronic & Biomedical Engineering

Faculty of Engineering and Information Sciences

October 2017

DECLARATION

I, Xin Tang, declare that this thesis, submitted in partial fulfilment of the requirements for the award of Doctor of Philosophy, in the school of Mechanical, Materials, Mechatronic, and Biomedical Engineering, University of Wollongong, is wholly my own work unless otherwise referenced or acknowledged. The document has not been submitted for qualifications at any other academic institution.

Xin Tang

26 October 2017

ABSTRACT

In the past forty years, the concept of controllable vehicle suspension has attracted extensive attention. Since high price of an active suspension system and deficiencies on a passive suspension, researchers pay a lot attention to semi-active suspension. Magneto-rheological fluid (MRF) is always an ideal material of semi-active structure. Thanks to its outstanding features like large yield stress, fast response time, low energy consumption and significant rheological effect. MR damper gradually becomes a preferred component of semi-active suspension for improving the riding performance of vehicle. However, because of the inherent nonlinear nature of MR damper, one of the challenging aspects of utilizing MR dampers to achieve high levels of performance is the development of an appropriate control strategy that can take advantage of the unique characteristics of MR dampers. This is why this project has studied semi-active MR control technology of vehicle suspensions to improve their performance.

Focusing on MR semi-active suspension, the aim of this thesis sought to develop system structure and semi-active control strategy to give a vehicle opportunity to have a better performance on riding comfort.

The issues of vibration control of the vehicle suspension were systematically analysed in this project. As a part of this research, a quarter-car test rig was built; the models of suspension and MR damper were established; the optimization work of mechanical structure and controller parameters was conducted to further improve the system performance; an optimized MR damper (OMRD) for a vehicle suspension was designed, fabricated, and tested. To utilize OMRD to achieve higher level of performance, an appropriate semi-active control algorithm, state observer-based Takagi-Sugeno fuzzy controller (SOTSFC), was designed for the semi-active suspension system, and its feasibility was verified through an experiment. Several tests

were conducted on the quarter-car suspension to investigate the real effect of this semi-active control by changing suspension damping.

In order to further enhance the vibration reduction performance of the vehicle, a full-size variable stiffness and variable damping (VSVD) suspension was further designed, fabricated, and tested in this project. The suspension can be easily installed into a vehicle suspension system without any change to the original configuration. A new 3-degree of freedom (DOF) phenomenological model to further accurately describe the dynamic characteristic of the VSVD suspension was also presented. Based on a simple on-off controller, the performance of the variable stiffness and damping suspension was verified numerically. In addition, an innovative TS fuzzy modelling based VSVD controller was designed. The TS fuzzy modelling controller includes a skyhook damping control module and a state observer based stiffness control module which considering road dominant frequency in real-time. The performance evaluation of the VSVD control algorithm was based on the quarter-car test rig which equipping the VSVD suspension. The experiment results showed that this strategy increases riding comfort effectively, especially under off-road working condition.

The semi-active control system developed in this thesis can be adapted and used on a vehicle suspension in order to better control vibration.

ACKNOWLEDGEMENTS

I would like to express my gratitude to all those who helped me during the writing of this thesis. I gratefully acknowledge the help of my supervisor, Prof. Weihua Li, an expert in magneto-rheological area, for all the support and encouragement he provided to me, during my entire Ph.D. program. His constant guidance has walked me through all the stages of the writing of this this thesis. His encouragement and unwavering support has also sustained me through frustration and depression. Under his unselfish guidance, I am growing up to not only an eligible Ph.D. student but a person of courage and honesty in life.

I also would like to extend my sincere gratitude to my co-supervisors, Prof. Haiping Du and Prof. Gursel Alici, for their instructive advice and useful suggestions on my research progress. I also owe a special debt of gratitude to all my good friends and colleagues, Shuaishuai Sun, Donghong Ning, Jian Yang, Dan Yuan, Xinxin Shao, Tanju Yildirim, Haiqiu Zhang, Han Wang, Wenfei Li in SMART Infrastructure Facility, and Zhiwei Xing, Rui Yan, Man Zhang, from whose happiness shared with me in daily life and enlightening brainstorming in study I have benefited a lot.

Last, I should like to express my gratitude to my beloved parents who have always been helping me out of difficulties and supporting without a word of complaint, without which this work would have been impossible.

TABLE OF CONTENTS

LIST OF FIGURES

LIST OF TABLES

1 INTRODUCTION

1.1 Background and motivation

Since the first vehicle was invented in 1880, the transportation conception of human being has significantly changed. In the development of automobile technology, riding comfort is one of the most significant benchmark to evaluate vehicle's performance. Comparing to other sub-systems, suspension system is more crucial for vehicle's performance which can transfer the force from road excitation and attenuate the vibration to vehicle body. Owing to the close relationship between the performance of a vehicle and the suspension system, it is important to improve the performance of suspension system to get better riding comfort. As the development of vehicle technology, traditional passive suspension confronts the bottleneck of performance because of its "passive" characteristic that it is hard to balance the vehicle comfort, stability and safety during riding. But an adjustable semi-active suspension system can deal with this imbalance by adjusting the suspension status depending on the driving condition. To further improve the riding performance of a suspension, numerous studies have been carried on in the past 50 years. The theoretical results show that the damping and stiffness are the parameters most closely related to the performance of a vehicle suspension to increase riding comfort. Many researchers have done very excellent work on the adjustable semi-active control of vehicle [1-3], and the application of magneto-rheological (MR) technology applied on vehicle has been reported continuously [4, 5].

The parameters of a damper are very influential to the damper's performance in vibration control [6]. Therefore, optimizing the parameters has been a very important program in damper design. Apart from the optimization work of the damper structure,

suitable controller and algorithms are the other important components of semi-active suspension system. With the collaborative design of excellent controlling algorithm and optimized damper structure, MR damper can perform excellent damping ability. In order to improve the effectiveness of the semi-active control, a multi-objective optimization program was done in this thesis to support the synthesis design of the MR damper and its controller.

Due to the hysteretic feature of MR damper, many classical semi-active controllers are hard to estimate it accurately to achieve better control effect. Modern control strategies such as Fuzzy control, Robust control, and neural networks have the potential to improve an MR damper performance because of the ability to handle nonlinear systems [7]. To improve the performance of MR damper in real-time control, many researches have done excellent work on developing method to effectively handle the nonlinearity of MR system [8]. However, the above research mainly focused on controller design and theoretically verification, especially in Takagi-Sugeno (TS) fuzzy control, the corresponding experimental investigation which considering practical application has not been achieved. In order to help fill this gap, this research developed a state observer based TS fuzzy controller for MR damper. It was evaluated on a quarter-car suspension with MR damper experimentally.

As well as the suspension damping, the stiffness value is another important component that affects the performance of a suspension. To date, passive spring has been widely used in vehicle suspension, and while having harder stiffness guarantees stability on a road profile, it leads to bad riding comfort to the driver and passengers. An idealized suspension spring is supposed to provide appropriate stiffness value depending on the specific driving and road condition. With this characteristic, the suspension with variable stiffness spring can provide hard stiffness to ensure no end-stop and proper

stiffness to support riding comfort based on specific road condition. To improve suspension performance, variable damping control has been studied and used in semi-active system control for many years. However, variable stiffness and variable damping suspension systems with better vibration control behaviour than the system with only variable damping is rarely been investigated in existing literature. Recently, some variable stiffness and damping structures have been designed and tested [9, 10]. Despite of the verification of the superiority of the variable stiffness and damping system, devices capable of varying stiffness and damping for practical applications have not been developed. Based on this motivation, our research group developed a compact variables stiffness and damping damper for vehicles [11]. However, the damping variation range of this structure is relatively small to a real vehicle suspension. To compensate for this deficiency, this thesis developed a full-size variable stiffness and variable damping MR suspension for vehicle whose damping variation range has been significantly improved.

For the response analysis of variable stiffness and variable damping (VSVD) instrument, Some MR VSVD models have been proposed. For instance, Sun et al. [11] developed a simple condition criterion based model for a VSVD damper. The variable stiffness system can be described as two states, including ‘loose’ and ‘block’. Nevertheless, the model performs quite well in the corresponding analysis. It is still not adequate for control analysis yet. In many cases, the stiffness system stays somewhere in between the ‘loose’ and ‘block’ with more complex dynamics characteristic. Comparing with the condition criterion based model, the one applying Newton’s second law could describe the dynamic response of the suspension more accurately and estimate the real state of the system more smoothly in real-time control. Based on the motivation to better predict the VSVD suspension response, a 3-degree

of freedom (DOF) VSVD model described by Newton's second law, was proposed in this thesis.

Using the variable stiffness and damping suspension system to mitigate vibration from its excitation source is an innovative idea. To further improve the potential of the system, an advanced real-time controller is required to control the variable stiffness and damping suspension. The research area of variable stiffness and damping control is still largely unexplored; just few works have been proposed on this topic with the consideration of riding comfort only [12, 13], and most of them are verified by numerical result without experiment. Therefore, an effective variable stiffness and variable damping controller is really needed. Based on this motivation, this thesis developed a TS fuzzy modelling based variable stiffness and damping control algorithm which considering riding comfort and suspension real-time travel simultaneously. Furthermore, the effectiveness of the controller was verified on a quarter-car test-rig.

1.2 Research aim and objectives

This research aims to develop controllable MR devices and the corresponding controllers to improve the overall dynamic performance of vehicle suspension, including developing riding comfort. The aim of the research is achieved through accomplishing the following objectives:

Ⅰ. To analyse and optimize the dynamic characteristic of vehicle suspension, and to develop an MR damper for vehicle suspension with optimization design.

Ⅱ. To develop a state observer based TS modelling controller of MR damper, in order to improve vehicle suspension performance.

Ⅲ. To develop a full-size variable stiffness and damping MR suspension for vehicle; and to propose a 3-DOF mathematic model to predict the dynamic performance of the variable stiffness and damping MR suspension.

Ⅳ. To develop an advanced TS fuzzy modelling based controller for the variable stiffness and variable damping MR suspension to further improve the vibration control ability of a vehicle.

1.3 Thesis outline

This thesis starts with the introduction including background and motivation, aim and objectives, and online. The subsequent chapters are structured as follows.

Chapter 2 provides a literature review of existing adaptive technology for vehicle suspension, including classification of suspension, MR fluid material and its application, control strategies for semi-active suspension, and VSVD suspension and its control strategies. It also identifies relevant research gap in this field.

Chapter 3 presents the theoretical analysis of MR vehicle suspension system, including suspension modelling, MR damper modelling, and multi-objective optimization work. Furthermore, an MR damper with optimization design was fabricated and its contribution to improve suspension performance was investigated experimentally.

Chapter 4 presents a state observer-based Takagi-Sugeno fuzzy controller (SOTSFC), which was designed for a semi-active suspension installed with MR damper. This chapter also provides proof of the effectiveness of the proposed controller by experimental validation.

Chapter 5 presents the design, prototyping, modelling and evaluation of a new MR suspension with capabilities of varying both stiffness and damping. A new 3-DOF phenomenological model was proposed to capture the dynamic characteristics of the

proposed suspension. Numerical results demonstrate that the sprung mass acceleration under VSVD on-off control holds the minimum value, which verified the semi-active VSVD suspension performs the best regarding the vibration attenuation effectiveness.

Chapter 6 focuses on improving the vibration control effectiveness of vehicle installed with the VSVD suspension. To achieve this goal, an advanced control strategy was designed. The TS fuzzy approach was used to model the system where the VSVD suspension was installed. Different algorithms, including skyhook, Short-time Fourier transform (STFT) and state observer method were designed and integrated in the control system to enhance the suspension. The excellent ability of the controller to improve the vibration control ability was experimentally verified.

Chapter 7 summarises the key findings generated from this study and gives recommendations for future research in this field.

2 LITERATRURE REVIEW

Suspension is one of the most important unit to a vehicle that it has a great effect to the performance of a car. For conventional passive vehicle suspension with constant parameter values, it is difficult to get good overall performance under different road disturbance. With the development of auto industry and the increase of customer requirement, the semi-active technology applied on vehicle suspension is becoming wider, epically the application of magneto-rheological (MR) technology. This chapter reviews the studies related to the MR semi-active vehicle suspension system which includes device structure, modelling, and corresponding control strategies.

2.1 Semi-active suspension for passenger vehicles

Vehicle suspension can be classified into three types: passive, active and semi-active suspension. A passive system is quite simple and cost-effective. However, this configuration has significant limitation that the damping force cannot be changed to deal with uncertain disturbances. In addition, an inevitable vibration at frequencies close to the natural resonance frequencies of passive suspension system, which are usually around 2 Hz [14], can be encountered and cannot be reduced.

When the suspension system is controlled by an external active force generated by a controllable energy input component, like hydraulic pump, air pump, and electric motor, it is called active suspension. Active suspension can adjust the damping force between sprung mass and unsprung mass according to the travelling information collected by sensors. Better control performance can be provided by an active suspension in a wide frequency range than its passive counterpart. The controllable frequency bandwidth of this suspension almost covers the resonance frequency of sprung mass and unsprung mass. To meet the high real-time requirement, the active

damper is often equipped with a passive damper in parallel. The power consumption of the whole system can reach about 5-10 kW [15]. Noticeable energy consumption and expensive hardware cost must be considered when designing the controller. However, in terms of the semi-active vehicle suspension, the power consumption of a controllable damper is around 10-20 W at vehicle speed 25 mph [16]. Besides energy consumption, comparing with active suspension system, the semi-active one also has damping force constraint. This energy dissipation characteristic makes a semi-active damper to be a fail-safe device.

In order to compensate for these limitations of the passive and active ones, semi-active vibration control system is utilized. Semi-active system can offer both the reliability of passive system and the effective control performance of active system without high energy injecting.

Comparing with active suspension, the semi-active suspension can provide a similar performance in vibration control with lower energy consumption [17, 18]. It might be considered as the most widely used controllable suspension system [19], although the concept and actual business application of semi-active one is bit late than active one. In 1973, Karnopp et al. [20] firstly proposed the skyhook control and introduced the concept of vehicle semi-active suspension. In 1983, TOYOTA Corp. launched a car, Soarer 280GT, which equipped with the semi-active suspension with three operating conditions. In 1988, based on Supersonic suspension technology, NISSAN Corp. applied semi-active suspension on the car Maximas. Later on, in 1989, FORD Corp. combined semi-active control with active control and apply this control strategy in the car Thunderbird [21]. Currently, the car models applied with semi-active suspension include BMW 7 series, Porsche 911, and Benz S-class, etc. [15]. The most widely used semi-active suspension technology includes the following two types [22]:

Ⅰ. The Continuous Damping Control (CDC) proposed by ZF Sachs Corp., which was firstly applied on the car model, Phaeton, by Volkswagen Corp. This technology is able to change the aperture of the damper to adjust damping continuously in real-time, and the highest response frequency can be 1000 Hz [23]. In the latest Audi A6 all-road Quattro vehicle technique, CDC is combined with air suspension structure; similar adaptive control strategy including Hydractive technology has been proposed by Citroen Corporation. [24].

Ⅱ. MagneRide technology proposed by Delphi Corporation. This technique designed based on MRF is firstly applied by GM Corp. on the car model Cadillac Seville STS in 2002. With about 15 years development, MR damper as a standard component, has been widely used in the mid to top-end car models by GM Corp., Volkswagen, Ferrari, Land Rover Corporation. Delphi [25] declares that the transforming time of MRF can reach millisecond level from low viscosity Newton fluid into high viscosity bingham body. The experiment facility used in this thesis is based on this kind of damper, and the following sections describe the work on its design, optimization, assembly, modelling, and control in detail.

To describe the dynamic characteristics of a vehicle suspension more accurately, many vehicle suspension mathematical models have been presented in existing literature [26-28]. The most widely used vehicle suspension model includes the following two types:

(1). MacPherson suspension model

Considering that the real suspension structure is almost on the basis of MacPherson type suspension, therefore, a MacPherson suspension model that possesses nonlinearity is needed to be built. The classical MacPherson suspension system is constructed out of joint and A-type below transverse arm, in which damper traveller is

also functioned as the kingpin that steering knuckle turns around it. Typical MacPherson suspension structure has been built and studied by much research [29-31], which is shown in Figure 2.1 as follows:

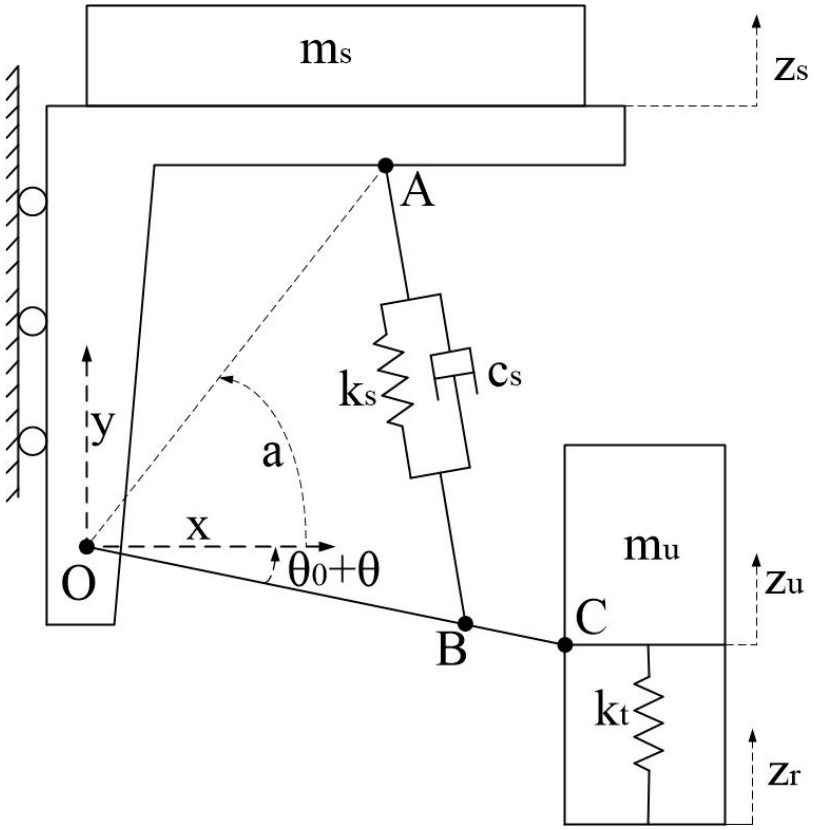

Figure 2.1 MacPherson type suspension model [32].

The 2-DOF of the system are the displacement of spring mass z_s, and the angle of below transverse arm θ. Define the initial position angle between below transverse arm and X-axis is θ_0, the angle to the initial position when below-transverse move in system is θ. Note that counter-clockwise is defined as the forward direction. In order to obtain the system dynamic equation, the Lagrange method [33] should be used to build Lagrange motion equation (see Appendix A for full modelling process).

(2). Linear quarter-car model

A 2-DOF linear quarter car is a simple model to simulate the vertical motion of a chassis and wheel without considering the pitch or roll vibration modes [34, 35]. The model is shown in Figure 2.2 which is widely used for suspension analysis.

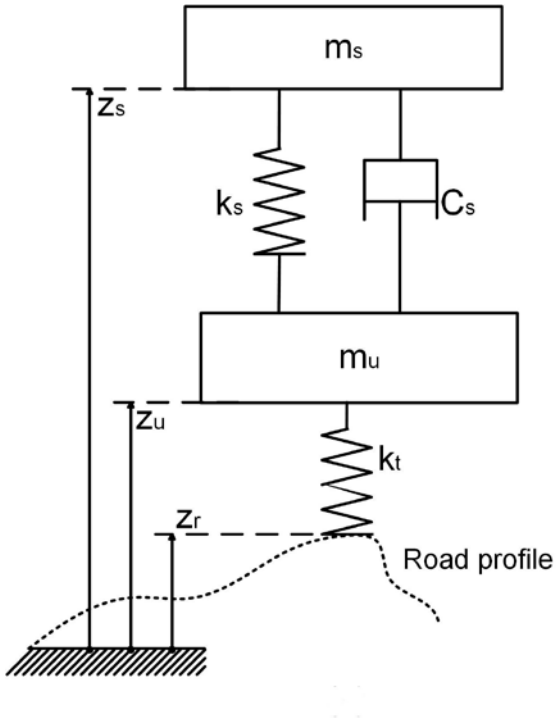

Figure 2.2 Linear 2-DOF quarter car model [34].

In Figure 2.2, m_s stands for a quarter of the suspension mass; m_u is the unsprung mass; z_s and z_u are the displacements of sprung mass and unsprung mass, respectively; and z_r represents the road profile; k_t is the tyre stiffness, whereas k_s is the stiffness of the spring between the tyre and the chassis; c_s is the damping of a passive damper that provides a damping force proportional to the velocity $\dot{z}_s - \dot{z}_u$. Then, the state-space equation of the quarter-car system (see Appendix B for full modelling process) can be represented as a particular case of the McPherson nonlinear model.

2.2 MR fluid material

Dating back to 1948, Jacob Rabinow unravelled an MR fluid (MRF) that can produce a class of smart fluids which yield stress can be controlled when he was working at US National Bureau of Standard. MRF is composed by micron magnetic particles e.g., iron or cobalt particles, and carrier fluid as well, e.g., silicone oil or hydraulic oil [36, 37]. The magnetic particles in MRF can easily move in its carrier fluid when magnetic field is unapplied, as shown in Figure 2.3(a). However, under the application of magnetic field, the magnetic particles would disable to move freely and form a chain-like structure along with the direction of magnetic induction line. In this case, the magnetic particles polarize to each other and further attract one another in magnetic field, as shown in Figure2.3(b). Therefore, MRF is able to change its viscosity and yield stress by changing the structural arrangement of ferromagnetic particles. Comparing to traditional materials, MRF is much more excellent for it can present rheological transition and viscoelastic properties within milliseconds under the application of magnetic field with the help of its soft morphology and controllable rheology.

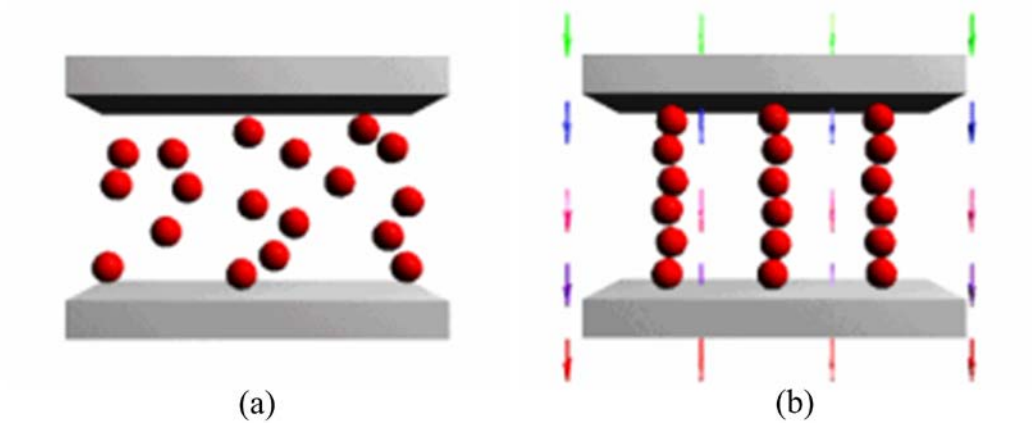

Figure 2.3 State variation of MRF (© 2005 Lord Corporation).

Based on the numerous advantages of MR material, the MR instrument is becoming very attractive in practical application, including controllable linear damper, rotary brakes, etc. Furthermore, the corresponding control has also been generated and developed. Since the nonlinearity characteristic of MRF, it is a real challenge to develop a proper phenomenological model with this property for the control of MR damper. Due to the nonlinear hysteretic feature of MR damper, many classical linear models are hard to improve the accuracy of the instrument response. Therefore, how to choose an effective phenomenological model, which can describe the hysteric behaviour of MR damper to eliminate the response error, is an important beginning of the research in this thesis. The following are some existing dynamic models for MR damper.

2.3 Phenomenological model of MR damper

Due to the high non-linearity of MR damper, it is hard to develop a high-fidelity model which is the basement of this experiment to apply in control system design and analysis. In 1997, Stanway [38] proposed a viscoplastic model, called Bingham model, that is stress-strain which is often applied to describe the behaviour of MR (and ER) fluids. The Bingham model consists of a Coulomb friction element placed in parallel with a viscous damper, as shown in Figure 2.4. Based on this model which described rheological behaviour of MR/ER fluids, Shames [39] later introduced an idealized mechanical model which doesn't cause non-linearity fore-velocity, while the acceleration and velocity exhibit opposite signs or the velocity and the displacement have the same sign from the point view of observed data. Besides, the magnitude of the velocities is also small.

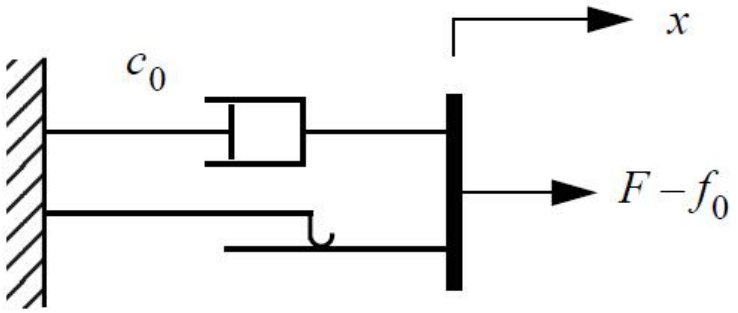

Figure 2.4 Bingham model of MR damper [40].

One model that is numerically tractable and has been used extensively for modelling hysteretic systems is the Bouc-Wen model [41]. The one is extremely versatile and can exhibit a wide variety of hysteretic behaviour. The Bouc-Wen model consists of a linear spring placed in parallel with a viscous damper and a hysteretic module, as shown in Figure 2.5(a).

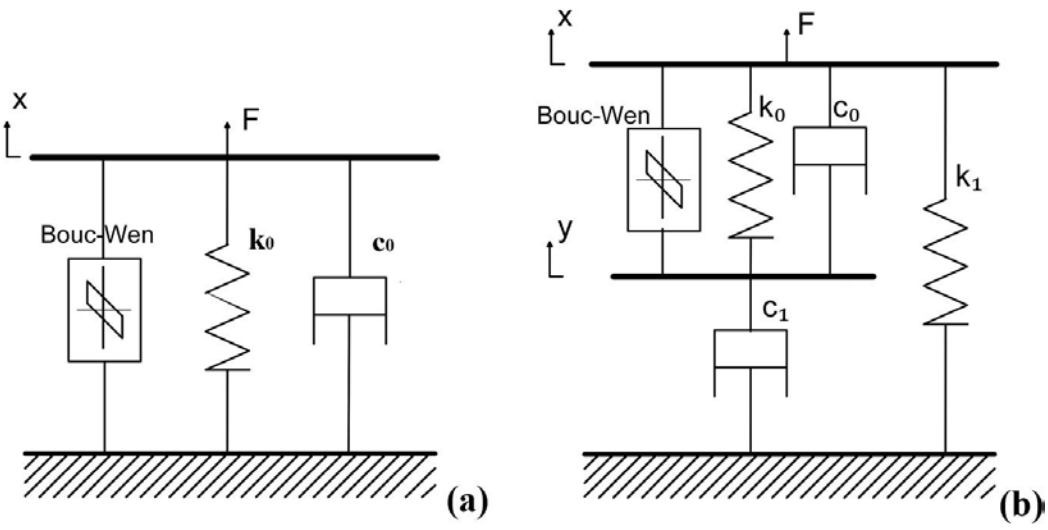

Figure 2.5 The dynamic model of MR damper: (a) Bouc-Wen model; (b) modified Bouc-Wen model.

The Bouc-Wen model can accurately describe the force-displacement curve of damper, and it also approach the real experimental data closer when dealing with force-velocity

behaviour [42]. Nevertheless, just like Bingham's model, its force-velocity response cannot roll off from acceleration region and velocity have opposite signs. Moreover, the magnitude of the velocities is also small. In order to precisely predict MR damper's response, Spencer [40] proposed a modified Bouc-wen model based on the classic one and it is shown in Figure 2.5(b). When only consider the upper section of the modified model to obtain the governing equations, the forces on each side of the rigid bar are equal in value. A comparison between the predicted response based on the modified Bouc-Wen model and the corresponding experimental data has also been provided in [40], which illustrates that the modified Bouc-Wen model predicts the behaviour of damper very well in all region, including in the region where the acceleration and velocity have opposite signs and the magnitude of the velocities are small.

2.4 Optimization design for MR suspension system

Considering conventional passive vehicle suspension with constant parameter value, it is difficult to get good overall performance under different road conditions and vehicle speeds [43]. With the development of semi-active technology, the vehicle suspension installed with MR damper has been widely used. The performance of a semi-active vehicle suspension is very sensitive to the structural parameters of the MR damper and the controlling parameters of the corresponding controller. Therefore, optimizing the parameters has been a very important program in damper and controller design; the research on multi-objective optimization of vehicle suspension parameters has also received much attention.

In the suspension parameter optimization progress of traditional vehicle design, the optimization goal, such as riding comfort, suspension deflection and tyre dynamic loading, is mostly considered separately. To achieve the multi-objective optimization

in MR damper design, Prabakar et al. reported a method to determine the parameter of the damper using non-dominated sorting Genetic Algorithm II [44]. As Figure 2.6 shows, the Pareto front for the modified Bouc-Wen model parameters are obtained using the procedure with the optimizing objects including sprung mass acceleration (SMA), suspension deflection (SD), road holding, and control force. The overall solutions in the front are represented by the symbol '●' and the respective optimal solutions projected on the respective planes are represented by the symbol '×'. In order to further verify the effectiveness of this optimizing method, Prabakar et al. proposed a modified multi-objective optimization technique for a half-car model with MR dampers moving over a random road [45]. The Monte Carlo simulation result proves that the MR damper suspension system with optimal parameters perform better than the passive suspension and closer to the performance of the fully active suspension.

In terms of riding comfort, one of the most popular and fitting ride measures is based on the root-mean-square (RMS) value of vertical acceleration of the sprung mass, typically measured or projected at the driver's or passengers' seat locations. In a field study in 1978 [46], the authors involved 78 passengers in two different vehicles and 18 different road sections to conclude that 'excellent correlation was found to exist between the subjective ride ratings and simple RMS acceleration measurement at either the vehicle floorboard or the passenger interface'. Further refinements of the RMS ride measure are possible through adding the RMS value of the sprung mass jerk (the derivative of acceleration) to the RMS value of sprung mass acceleration. Some literature [47-49] advocates the inclusion of jerk as an added measure that amplifies the contribution from high-frequency disturbances, which are important for noise, vibration and harshness (NVH).

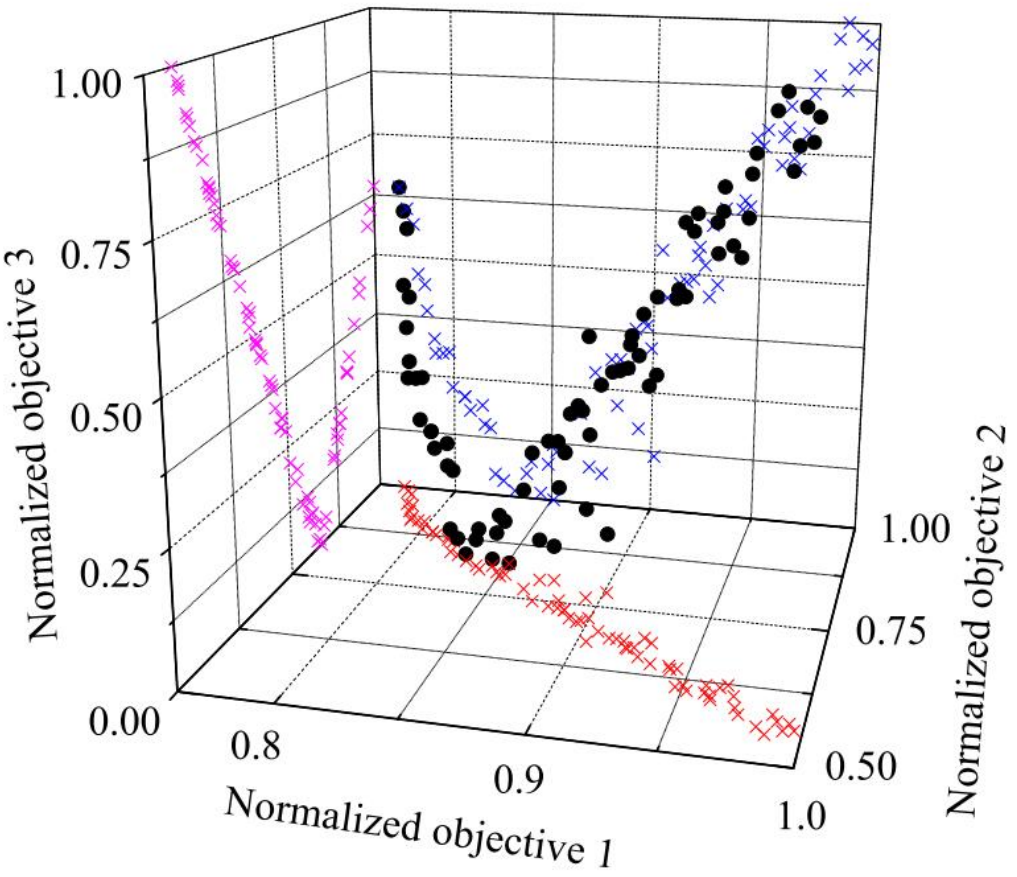

Figure 2.6 Pareto optimal front based on modified Bouc-Wen model [44].

To account for the frequency dependency of human sensitivity to vibrations and the length of time of human exposure, a standard has been developed by the ISO 2631 [50]. It is noted that region of greatest human sensitivity to vertical vibration lies between 4 and 8 Hz, which roughly includes the various resonances of human internal organs. The ISO-based metric can be easily incorporated into the H_2 optimization formulation. The ride metric of choice will depend on the context of its usage. While the more complex ones can reflect more details and differences, the simple one can better focus on the system level and major benefits. In addition, the available suspension displacement or so-called rattle space is limited. The research in [51] includes this constraint by adding the suspension displacement in the performance

index. With the attempt to minimise the corresponding cost, the optimization method effectively ensures the lowest level of the suspension displacement.

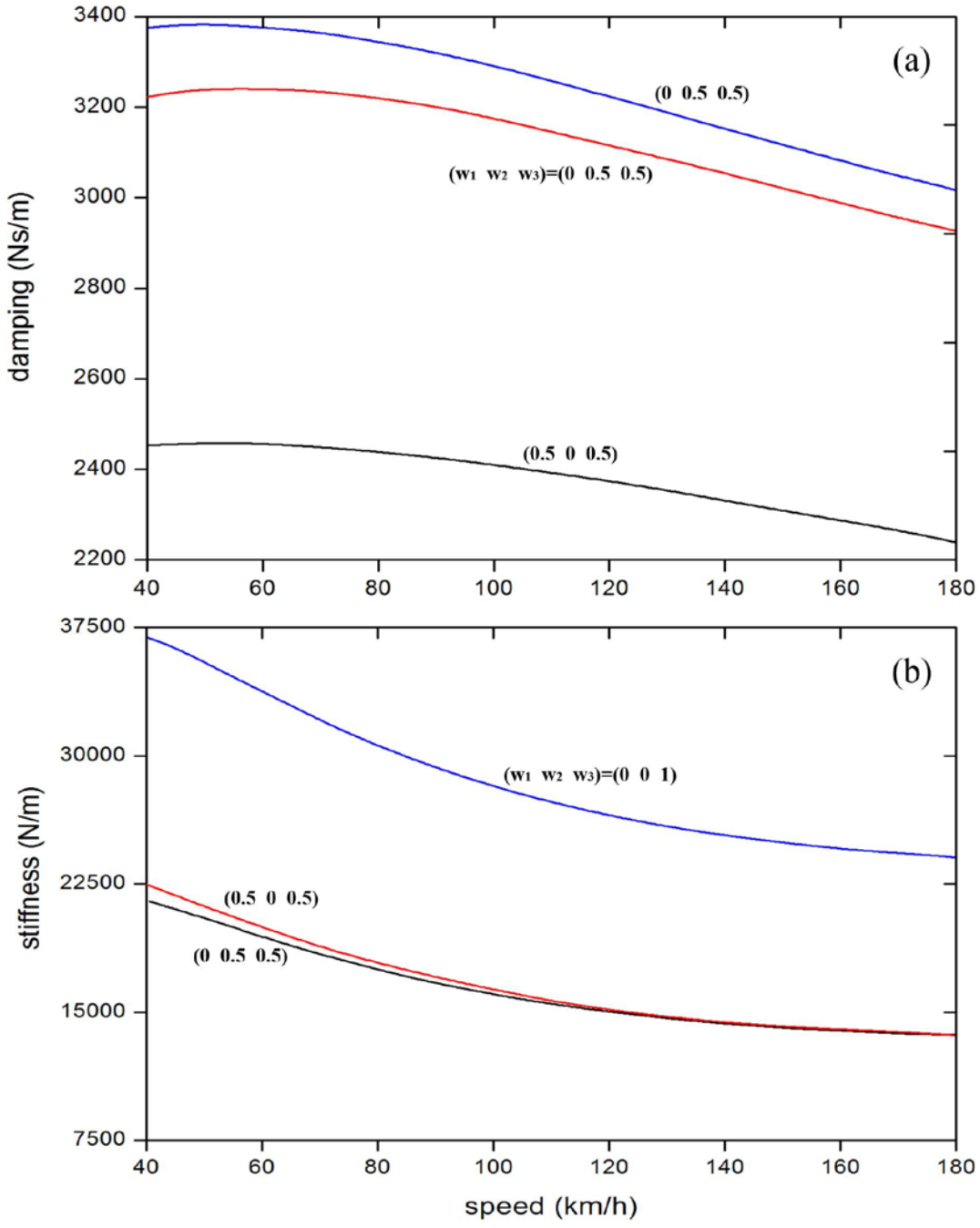

Figure 2.7 Optimum values of (a) the suspension damping coefficient and (b) stiffness coefficient for a linear quarter-car model (w_1 for sprung mass acceleration, w_2 for stroke, and w_3 for tyre load) [52].

Similar to the ride comfort metric, the suspension displacement-related cost can be reflected on the RMS value of suspension displacement especially for random road input. When it comes to performance index for road holding, it is conceivable that a very large variation of tyre deflection (TD) may even lead to a loss of contact with the ground. Therefore, the RMS value of tyre defection variation can be an explicit metric for handling characteristics. Furthermore, the direct relationship between TD and cornering capabilities have been experimentally studied in [53].

Based on the aforementioned discussion, there is no surprise that the most widely used performance index for semi-active suspension study is the combination of the three previously discussed RMS values. That is, using a weighted combination of RMS acceleration of sprung mass, RMS suspension displacement, and RMS tyre deflection variation to represent the performance index for optimization. In recent years, some researchers [54] have begun to consider the factors simultaneously, namely, multi-objective optimization. As these criteria mentioned above are conflicting, a suitable multi-objective method with weighting function should be chosen properly. Verros et al. presented a methodology for optimizing the damping and stiffness parameters of quarter-car models [52]. When considering the linear model case, the optimized parameter value vs. vehicle speed can be described by polynomial curves accurately, as shown in Figure 2.7. However, in the nonlinear model case, the tendency of the optimized damping and stiffness values demonstrate a very strong unpredictability under different vehicle speed, so that the optimal parameters of the nonlinear suspension system are very difficult to be predicted exactly. Nonlinear issue which exists in many control targets, especially MR dampers, should be well optimized.

2.5 Control strategies for MR vehicle suspension

In consideration of the broad scope of research including the uncertainty, nonlinearity, and state constraint of a real suspension system, Nnumerous studies have gone into developing advanced control algorithms for semi-active suspension in the recent 40 years. This section reviews the studies related to the semi-active control strategy.

2.5.1 Classical control algorithms

Nnumerous studies have focused on developing controller design for semi-active suspension systems. Some controllers such as skyhook control [55, 56] and the one with time delay [57] have been successfully applied on vibration control of vehicle system. Skyhook control strategy was first introduced by Karnopp [58] whom suggested the controller can be mounted between the sprung mass and a stationary sky. Skyhook control algorithm could drive the system performance to be as good as that of an active control strategy, though it lowers the cost. Over the last several decades, skyhook control scheme has been widely studied and used by many researchers. Guo [59] implemented the skyhook controller into a vehicle suspension system in which the bi-viscous and hysteretic MR damper model is used. Abramov *et al*. [60] proposed an on-off skyhook and continuous skyhook controller which improved the ride comfort but failed to improve the handling stability of the vehicle.

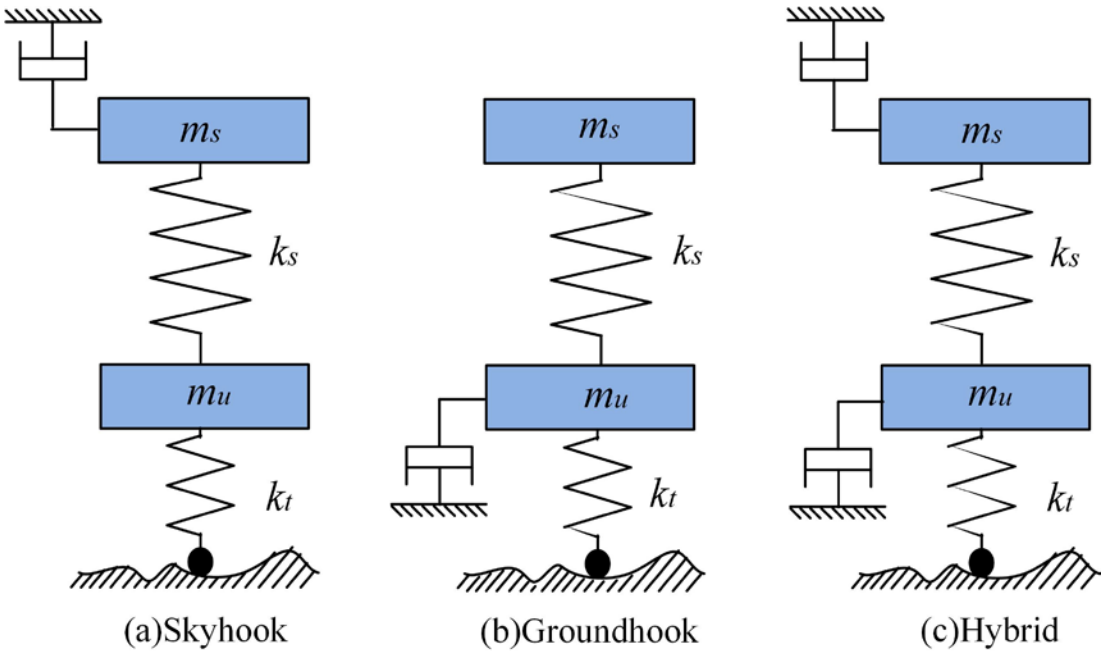

Figure 2.8 Hook group controllers scheme [61].

To overcome the limitations of skyhook control, Valasek [62] added another fictitious damper between the un-sprung mass and the ground which improved the road holding ability of a vehicle. The skyhook controller was then improved using hybrid control approach that was a trade-off between the skyhook control approach and a groundhook control law. The controllers mentioned above are shown in Figure 2.8. Extensive theoretical and experimental studies of the performance of semi-active skyhook, groundhook, and hybrid controller can be found in the literatures [63-65].

Currently, many of the existing skyhook/groundhook control strategies for MR damper aim at designing the desired damping force first, and then use different methods, such as the inverse dynamics model method [66] and the clipped-optimal method [67], to compute the command voltage sent to the MR damper. However, the nonlinearity of MR damper is still not to be taken into consideration, and the command voltage to the MR damper can only be u_{min} and u_{max}.

2.5.2 Modern control strategies

The uncertain and time-varying characteristics have been a challenging problem to automatic control for a long time. To address the hysteresis non-linear behaviour of MR dampers and also some uncertain factors in semi-active suspension system, many nonlinear control strategies including those based on neural networks, fuzzy logic, sliding mode and H_∞ control have received much attention for their use in the controller design of MR suspension system.

In [68], a model-free fuzzy logic controller was presented by Shojaei. the most basic control algorithm was used in this controller, named Heaviside step function method, in which the applied voltage is either zero or a maximum value. Tusset [69] studied a model free fuzzy control strategy for non-linear vehicle suspension with MR damper. The numerical simulations were provided to show the effectiveness of the control performance. Then, Khajavi [70] concerned with a proposed fuzzy logic semi-active system designed for a specific automobile with a passive suspension. A direct adaptive fuzzy controller with feedback control of damping force for MR damper was studied in [71], the test results verify the effectives of the force feedback method. In [72], a fuzzy control strategy was employed in controlling the MR suspension system; the performance of the semi-active system was evaluated experimentally. Since the controller was employed on a real car in this experiment, the input signals, two velocities, were calculated by the acceleration signals collected from the two accelerometers. The accuracy of velocity signal would be decreased by the integral process. Furthermore, Rashid *et al*. [73] developed a hybrid fuzzy logic controller which integrated a proportional-integral-derivative (PID) controller to analyse quarter-car model. A neuro fuzzy control strategy for a quarter-car system was conducted to an experimental evaluation with a semi-active suspension system in [74]. To

effectively estimate the control current for the MR damper, an inverse mapping method which based on neural network and modified back-propagation algorithm was applied in the control system.

The classical fuzzy control strategy is model free and the fuzzy parameters of the controller are totally determined by designer's experience. As an improvement of fuzzy control, the idea of model based fuzzy modelling using the concept of the fuzzy sets theory [75] has been taken into consideration to build a nonlinear system controller. The fuzzy modelling method proposed by Takagi and Sugeno [76] is an effective modelling method for nonlinear system. It is described by fuzzy IF-THEN rules which represents local input-output relations of a nonlinear system. The main feature of a TS fuzzy model is to express the local dynamics of each fuzzy implication by a linear system model. The overall fuzzy model of the nonlinear system can be described by the integration of the linear system models. A classical TS fuzzy system including TS fuzzy modelling and the corresponding control unit is shown in Figure 2.9. A control strategy utilized the TS fuzzy modelling approach was proposed to deal with the nonlinearity of the vehicle suspension installed with an MR damper [77]. Du and Zhang [78] presented a model-based TS fuzzy controller for a building installed with MR damper. The output of the TS fuzzy controller was optimized by GH_2 control and the performance was theoretically validated. A TS fuzzy model for the analysis of a quarter-car with MR damper was presented in [79]. The ride comfort and vehicle road holding ability are both taken into consideration in the controller design. In [80], the TS fuzzy modelling approach is applied to a 4-DOF one-half vehicle suspension to analyse not only vertical vibration but also lateral stability of the system.

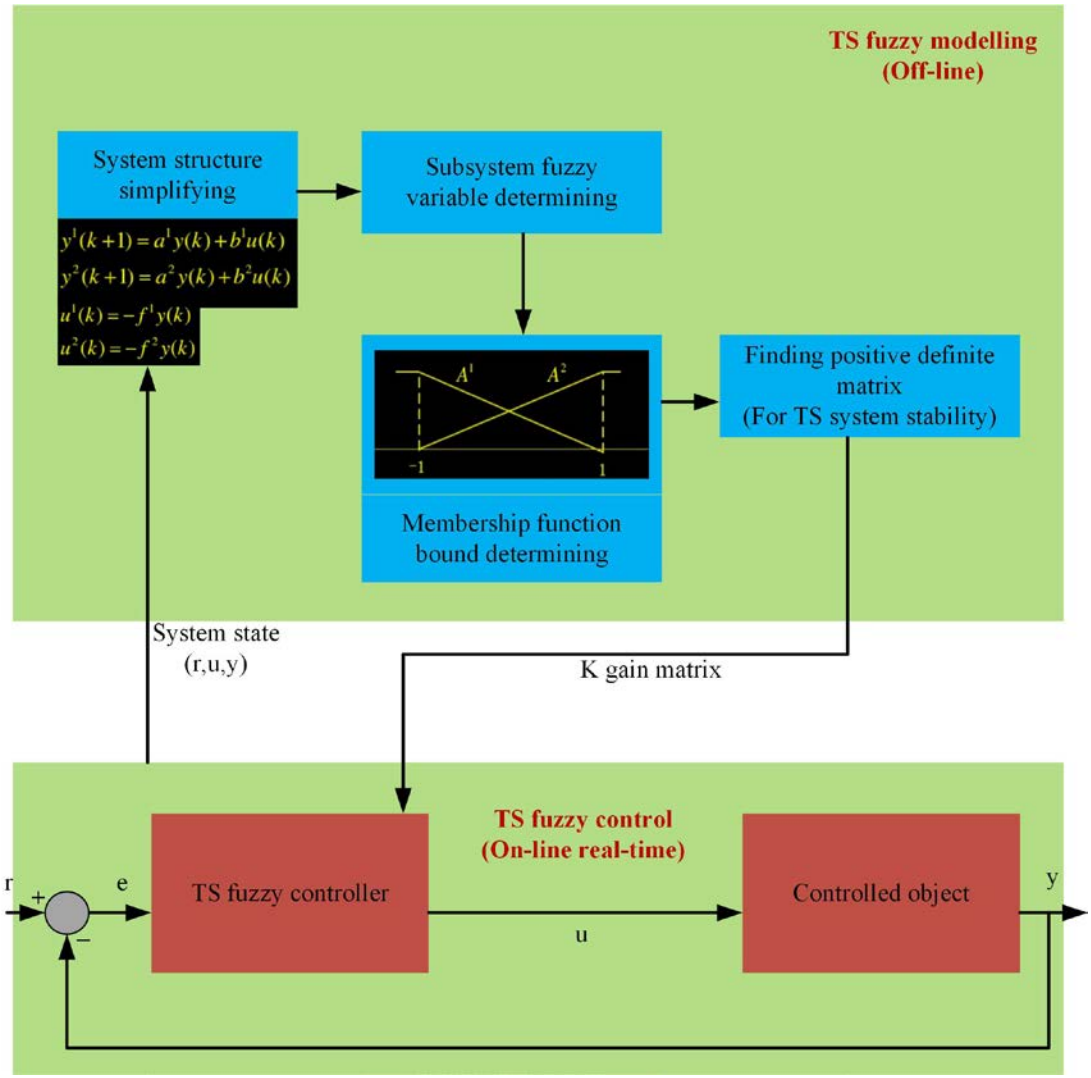

Figure 2.9 Scheme of a TS fuzzy system.

However, with extra DOFs in the nonlinear system, huge work is required to identify the exact TS nonlinearities boundaries, according to disturbances, state, and control signals. These studies indicate that the unwanted vibration from road disturbance can be reduced by using TS fuzzy controller in semi-active suspension. The performance of the TS fuzzy controllers is generally better than classical skyhook controllers and model free fuzzy controllers.

The TS fuzzy approach can handle nonlinearities in modelling nonlinear vehicle suspension by approximating nonlinear terms to any specified accuracy with a family of fuzzy sets and rules. And it is worth noticing that there exist not only nonlinearities

but also the parameter uncertainties of the boundaries of the membership function when modelling the suspension. Based on the type-2 fuzzy set theory [81], an interval type-2 fuzzy logic system can be designed to handle the parameter uncertainties of the fuzzy membership function to make the controller more robust. In [82], an advanced interval type-2 fuzzy-neural network indirect adaptive sliding mode control for a vehicle suspension was presented. In this research, the model was built by interval type-2 fuzzy-neural network to approximate any nonlinearities of membership functions from the MR classical type-1 fuzzy model. Nguyen *et al*. [83] proposed a new adaptive type-2 fuzzy sliding mode controller for an MR damper based railway suspension to partly overcome the unwanted impacting of uncertainty and disturbance while train is operating. In [84], the closed loop control performance of type-1 fuzzy and interval type-2 fuzzy were compared each other. The result shows that the interval type-2 fuzzy control system is better in real-time control performance and more robust against noise and unknown disturbance. However, in interval type-2 fuzzy control, double numbers of nonlinearity boundaries should be determined, which means the control system is more complex and might be slower in real-time control than a type-1 fuzzy controller.

In addition to TS fuzzy modelling method, many other control algorithms have also received attention in controller design for MR suspension system, including neural networks, sliding mode control and H_∞ control, etc. A robust linear controller using H_∞ control for an active suspension was presented in [85], the performance of the controller was also identified by experimental results. A clipped-optimal linear quadratic semi-active suspension system was designed and tested in [86]. To deal with the optimal control problem, a stochastic Hamilton-Jacobi-Bellman equation on a finite horizon was solved. The performance of the controller was demonstrated by

experimental validation. Sliding mode control, has also been proposed to obtain the shock absorption effect of semi-active suspension systems. In [87], a model reference sliding mode controller was proposed which only needs two acceleration sensors and eliminates measuring road signal program. The controller applies an approximate idealized skyhook hook system as the reference model to estimate the state of the real system. In [88], an adaptive sliding mode control based on Lyapunov stability theory was proposed. The simulation work illustrates that the proposed method provides higher adaptation ability and performance than standard sliding mode controllers. A sliding mode controller was proposed in [89] by Zhang. The acquired control damping force is converted to the direct drive current of the MR damper, whose current is calculated by the dynamic errors between the sliding mode surface and the skyhook-based reference model. The adaptive robust performance of the sliding mode controller on dealing with hysteresis nonlinearity and load uncertainty of MR suspension was verified by simulation work.

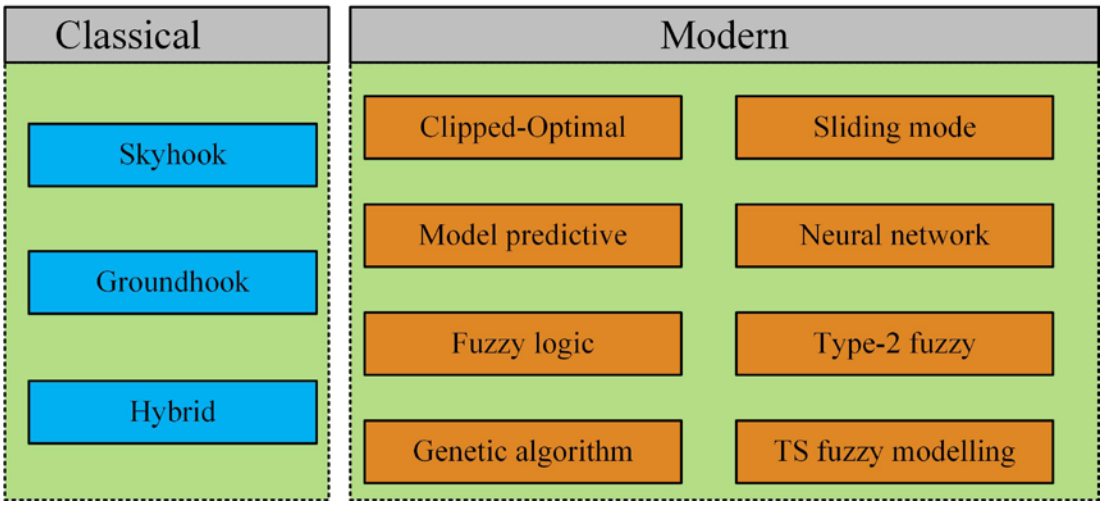

Figure 2.10 The classification of control algorithms.

Meanwhile, integrating multiple control algorithms has also been applied in controller design to amplify the advantages of each control algorithm. In [90], an online adaptive

TS fuzzy-neural modelling has been proposed for uncertain active suspension system. The simulation result illustrates that the displacement tracking of sprung mass based on this model is effective, even when the spring of active suspension system is broken. In order to deal with the problem in an adaptive sliding-mode control that how to guarantee the reachability of the specified switching surface, Li [91] added the TS fuzzy method to the control system to describe the original nonlinear system for the control-design aim. Shin and Choi [92] presented an adaptive type-2 fuzzy controller featuring a combination of H_∞ control and sliding model control. Simulation and experimental results show the proposed controller can provide better vibration control performance than the two independent controllers. The scheme of control algorithms is shown in Figure 2.10.

Whereas, most of the previous methods assume that all state vectors are measurable or require extra sensors to measure vertical velocities and absolute displacements. These variables are difficult to be obtained by the normal instrumentation of a vehicle, which typically only has accelerometers and linear variable differential transformer (LVDT) to be installed. The estimation program that direct integrating acceleration signal to get the velocity information deteriorates the consequence accuracy. Moreover, the absolute displacements, such as the unsprung mass displacement, are nearly unmeasurable while a vehicle is working. Only relative ones, such as the displacement between unsprung mass and road profile, can be directly obtained in practical application by a laser sensor. To deal with this problem in real-time control, a state observer need to be designed to estimate the state of the system. Dinana et al. [93] presented two estimation strategies, an unknown input observer and a robust H_∞ observer, whose schemes are shown in Figure 2.11, to deal with the observability problem attributed by the system state and unknown road profile decoupling. In [94],

fuzzy observers based on the relaxed stability conditions for the TS fuzzy system was proposed. The observer is useful to estimate the real-time state information, which is usually hard to obtained by sensors. However, the time delays of data processing in the observer should be improved. Ren [95] recently reported an adaptive sliding mode controller with a state observer based on unscented Kalman filter. This state observer can estimate the suspension states in real-time for the realization of the controller and make the controller to be adaptive to different road profiles. It can be seen that with adding extra observer, the controller is more feasible for practical application.

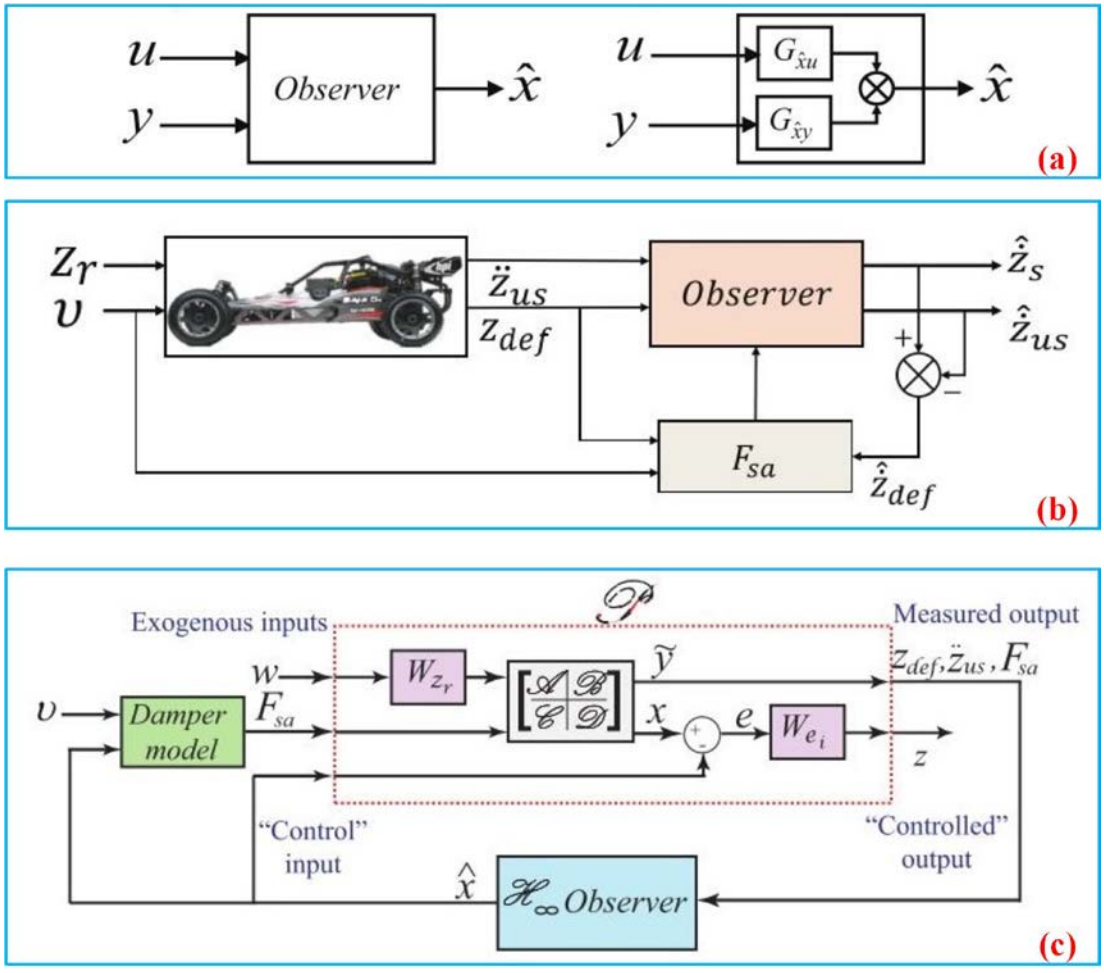

Figure 2.11 The observer design: (a) observer representation; (b) block diagram of the unknown input observer with damper estimation; (c) H_∞ observer design in a quarter-car system [93].

The excellent performance by using the TS fuzzy modelling based control has been verified by much simulation research, but experimental validation of TS fuzzy controller for vehicle suspension have rarely been developed. In addition, the TS fuzzy controller installing with state observer capable of full-state estimating for practical applications has never been proposed.

Based on this motivation, this thesis has developed an advanced state observer based TS fuzzy controller for semi-active MR vehicle suspension, and it is presented in Chapter 4.

2.6 Variable stiffness and damping technology for vibration control

Stiffness and damping are basic characteristic and also two of the most important evaluation for many technical systems. It is also necessary to be controlled so that it can achieve the needed dynamic behaviour and diminish or eliminate any undesired vibration. Inevitably, the reduction of vibration has been deeply planted into the concept of variable damping or variable stiffness, in which “variable” means controllable, real-time and reversibility. As shown in Figure 2.12, with variable stiffness and damping, a single DOF system’s dynamic characteristic is presented. Here, the adjust of damping will change the system’s dissipation degree of vibration energy, and further cause the decrease of resonance magnitude (compare lines A, B, C and lines D, E, F). In addition, the variation of stiffness will induce the change of the system’s nature frequency to further influence the transmission ability of the controlled system (compare lines A and D, B and E, C and F). As we can see from the figure, comparing to a constant damping system, variable damping (shown as blue line) can control vibration better. Specifically, when combined the left part of line C and right part of line A, a lower vibration transmissibility can be achieved. Besides, another

important phenomenon can be found from the figure that after the combining of both variable damping and stiffness, which also means that after combing the left part of line F and right part of line A, a further lower vibration transmissibility can be obtained, which is shown as the red dash line in the figure.

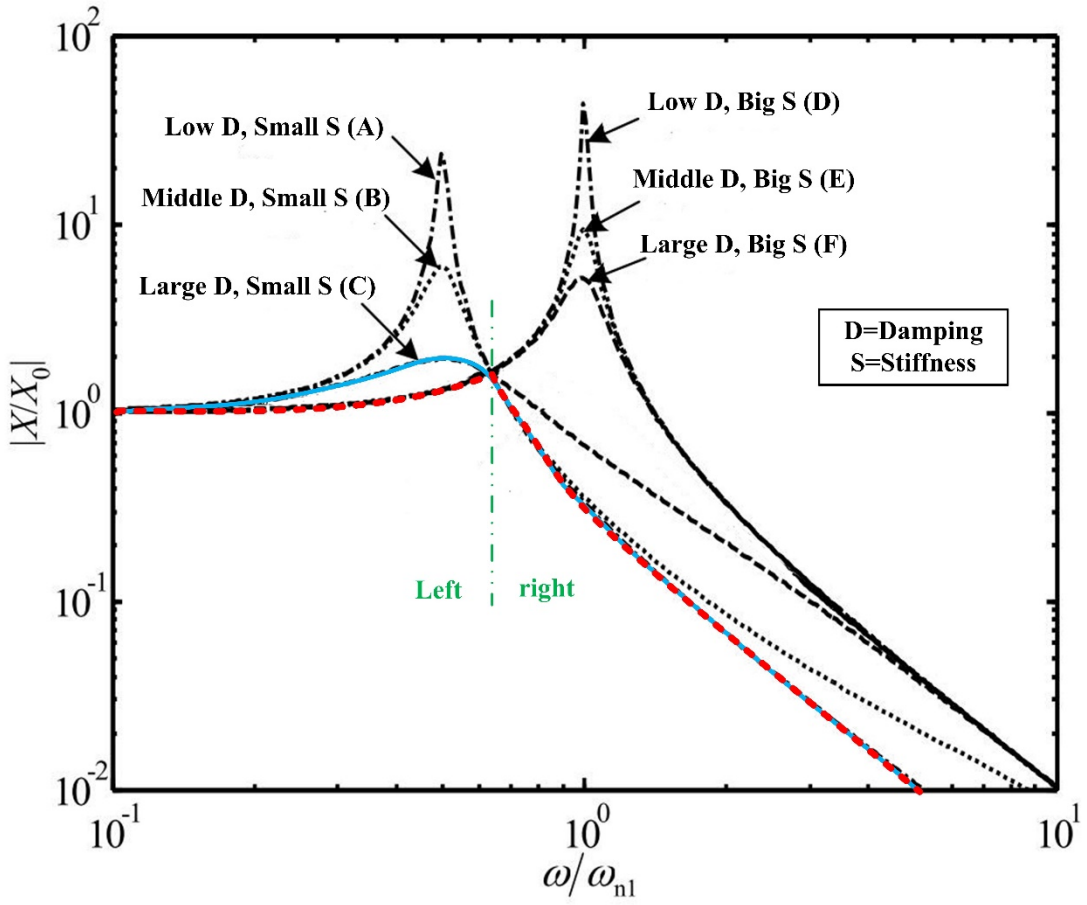

Figure 2.12 The transmissibility of one DOF with different suspension systems [96].

Based on this foundation, many researchers [97-99] have studied the concept of variable stiffness and damping to validate and improve the dual controllability of stiffness and damping. Liao et al. embedded a voice coil motor into an MR elastomer isolator to realise variable stiffness and damping characteristics [100]. In [101, 102], a variable stiffness and damping MR damper was presented by Zhang et al. the damper consists of an air spring, separate films, and MR valve and accumulator. A relative

large range of the stiffness and damping dynamic response was measured in the experimental validation. Following this research, Sun et al. investigated an innovative suspension system for railway vehicles that includes an MRF based variable stiffness air spring and an MR damper, as shown in Figure 2.13 [103]. The research theoretically verified that the variable stiffness and damping suspension suppresses vibration better than suspension with only variable damping or variable stiffness. In [104], a compact variable stiffness and damping isolator structure was purposed by Zhu et al. In this compact design, the MR damper varies the damping of the isolator while the pneumatic spring gives the isolator the variable stiffness capability. Because of the pneumatic spring, mode switching between passive and semi-active vibration control comes stable, flexible, and versatile in practical application.

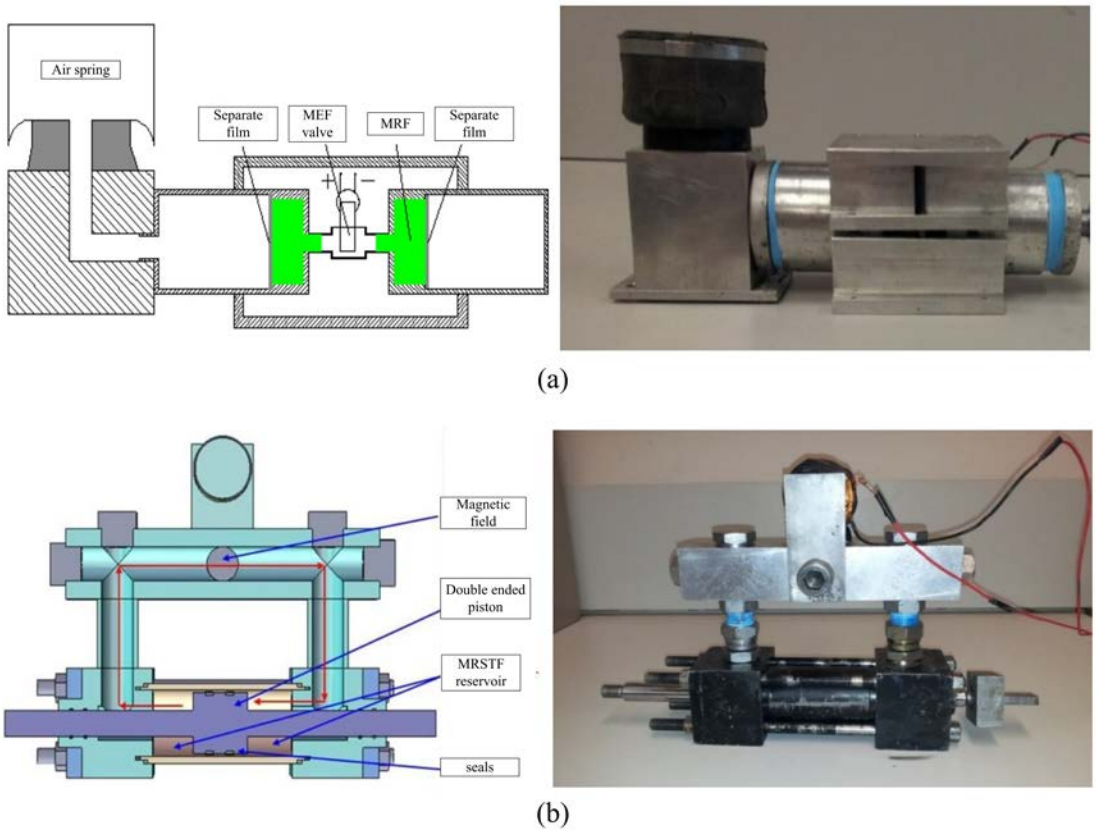

Figure 2.13 The schematic and structure of (a) the bypass MRF damper (b) the stiffness variable air spring [103].

For heavy off-road engineering vehicle, a new variable stiffness and variable damping device which can output maximum force about 10000N was developed by Raja et al. in [105]. However, based on the MRF damper-liquid spring system, the suspension cannot change the stiffness and damping separately in control and its stroke is limited. Greiner-Peter et al. recently reported an unique structure that uses MRF to realise variable stiffness and damping characteristic [106]. This semi-active MRF mechanism offers variable stiffness and damping by utilising two MR valves and two springs. The experimental results prove that the damping of this system is continuously variable but its effective stiffness can only be varied between three different values instead of consecutively.

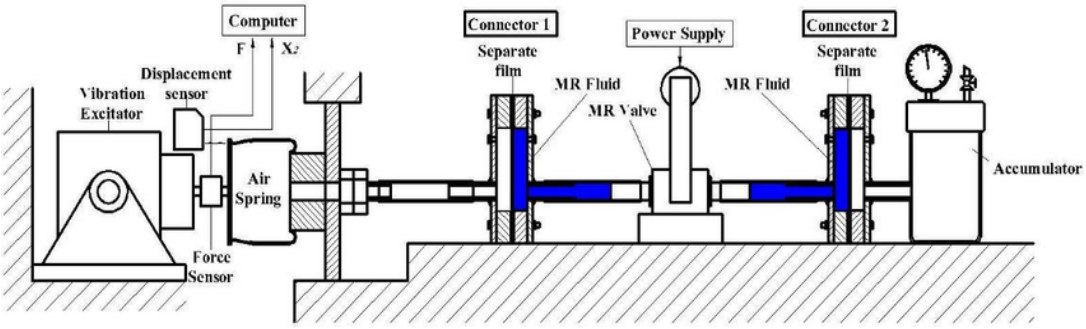

Figure 2.14 Variable stiffness and damping mechanism [107].

In order to verify the effectiveness of a variable stiffness and damping suspension, Liu et al. proposed a structure with two voigt elements (each one consisting of a constant spring and a controllable damper) in series to control variable stiffness and damping [107], as Figure 2.14 shows. In their design, damping and stiffness cannot be controlled independently because the two MR dampers are installed in series. In order to improve the design, Liu and his group then proposed a new structure which can vary its stiffness and damping independent of each other [96]. This new structure also has

two MR dampers. A vibration testing experiment was carried out to evaluate how it performed to isolate vibration. The results show that the suspension with variable stiffness and damping performs best. Despite of the verification of the superiority of the variable stiffness and damping system, compact devices capable of varying both stiffness and damping for practical applications has rarely been developed. Based on this motivation, Sun et al. developed a small scaled compact variable stiffness and damping damper for vehicles [11, 108, 109]. However, the damping variation of the compact device is limited and effectiveness verification needs to be done. Therefore, a full-size VSVD MR suspension for vehicle was developed and the damping variation range was significantly improved in this thesis. The detail is presented in Chapter 5.

Based on the VSVD suspension, an appropriate control strategy is required to verify the effectiveness of the advanced system in real-time vibration control. In [110, 111], Xu et al. proposed a hybrid control strategy for a VSVD suspension to improve vehicle lateral stability. The control strategy composed of a fuzzy controller that the output is wheel slip ratio and a simple on-off controller to improve normal force at tyre. The simulation result verifies their usefulness in enhancing vehicle stability by replacing a passive front suspension system with a hybrid control based variable stiffness and damping structure. In active VSVD system, a control algorithm [112] proposed by Anubi et al. applies the concept of nonlinear energy sink to effectively transfer the vibrational energy in the sprung mass to a control mass. This skyhook based concept can reduce the vibration from road disturbance to car body at a relative lower cost than a traditional variable damping active suspension. In addition, Aunbi et al. recently reported a corresponding semi-active structure for suspension system in [113]. The performance of the controller based on NES concept has been verified by simulation work. In this case, the control algorithm is applied to a horizontal MR damper in a

McPherson suspension structure to adjust the corresponding stiffness value. To improve multi-objective optimization by VSVD structure, an advanced compatible control algorithm using the nonlinear H infinite theory with frequency weighting functions was proposed in [114] by Liu et al. The simulation work demonstrates the proposed control algorithm provides better performance in the whole frequency region than the other different control schemes, as shown in Figure 2.15 (the name of the proposed algorithm is 'DC+SC'). In detail, the variable stiffness is effective to reduce the low frequency responses of sprung mass acceleration; and variable damping is able to reduce the high frequency responses of wheel load fluctuation effectively.

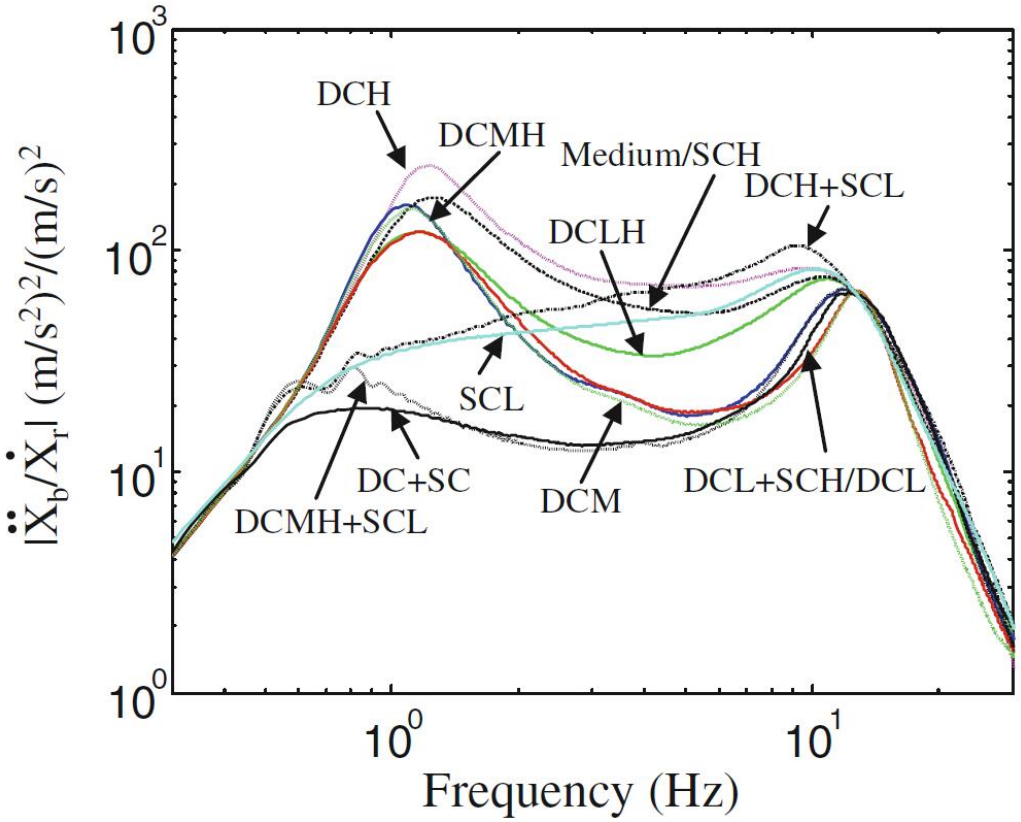

Figure 2.15 Frequency responses of the system with different VSVD control schemes [114].

Furthermore, Spelta et al. developed a new algorithm to control the variable stiffness and damping suspension to further improve the riding comfort of vehicles [115]. The simulation result demonstrates that the variable stiffness and damping suspension controlled by their control algorithm improves vibration isolation better than suspensions with only variable damping. Better performance of variable stiffness and damping control algorithm has been verified by the simulation methods, but the controller's capability for practical applications has rarely been verified. A simple and effective VSVD controller is really needed to be designed and proved by experimental validation. Based on this motivation, this thesis developed an advanced state observer based TS fuzzy variable stiffness and damping control algorithm. The effectiveness of the controller was verified on a quarter-car test rig, and it is presented in Chapter 6.

2.7 Conclusions

This chapter reviewed the semi-active vehicle suspension system and its practical applications, and the semi-active control strategies to improve the dynamic performance of vehicle, including classical model free control strategies and model based control algorithms. The optimized design for damper and controller have also been introduced in this section.

This review has clearly detailed existing gaps in the application of MR technology and corresponding control algorithms onto vehicle suspension. At this stage, the variable stiffness structure to change the resonance frequency of suspension has rarely been investigated; a compact variable stiffness and damping structure suitable for vehicle suspensions has not yet been found; corresponding effective control algorithm for variable stiffness and damping has also been rarely reported. Based on these

motivations, the current research into enhancing vehicle suspension's vibration control effectiveness with semi-active MR technology is presented in the following chapters.

3 ANALYSIS OF VIBRATION CONTROL ON VEHICLE SUSPENSION WITH MR DAMPER

3.1 Introduction

In this chapter, the issues of vibration control of the vehicle suspension are systematically analysed. In order to rightly analyse and design the suspension system with MR damper, the phenomenological model of vehicle suspension and MR damper were established. The road profiles to provide excitation for vehicle system were also calculated. To further improve the system performance, a multi-objective optimization program was presented and used for MR damper and controller design. Based on the optimization results, an optimized MR damper (OMRD) for a vehicle suspension was designed, fabricated, and tested on the INSTRON machine. Furthermore, the dynamic performance of OMRD was validated on the existing quarter-car test rig.

3.2 Mathematical model of suspension system

The quarter-car suspension system is a mechanical system which possess nonlinearity, time-varying, and exists ubiquitous nonlinearity and parameter uncertainty. As for such kind of complicated mechanical system, the more consideration is taken into, the more fidelity it keeps. However, a complex model is also much more difficult to be built and analysed. In addition, an over-complicated model would have significant impact on the responding time in real time control that would further affect the result. An over-simplistic model is easy to analyse, but the reached result wouldn’t be accurate enough. Therefore, the principle to build vehicle model can be described as: to find a balance between accuracy and controlling feasibility. The objectives of modelling program include suspension system and MR damper.

During the modelling program in this thesis, the following assumptions can be applied: (1) The vehicle suspension is a rigid body with a symmetrical structure. (2) The vehicle keeps running at a constant speed. The tyres always keep in contact with road surface. (3) Only vertical vibration should be considered in this case.

3.2.1 Modelling of suspension system

A typical quarter-car suspension system is combined with sprung mass, elastic component, damping component and unsprung mass that all can be vividly presented in a linear quarter-car model. In the meantime, considering that there is nonlinearity which caused by executive component and setup angle of the system, MacPherson suspension model was established to accurately describe the real mechanical structure of vehicle suspension. As for the selection of suspension model, this paper deduced and compared the systematic equivalent variations of linear quarter-car model and MacPherson suspension model, which two were introduced in Chapter 2, on the basis of test rig experiment result. The system of quarter-car test rig is shown in Figure 3.1.

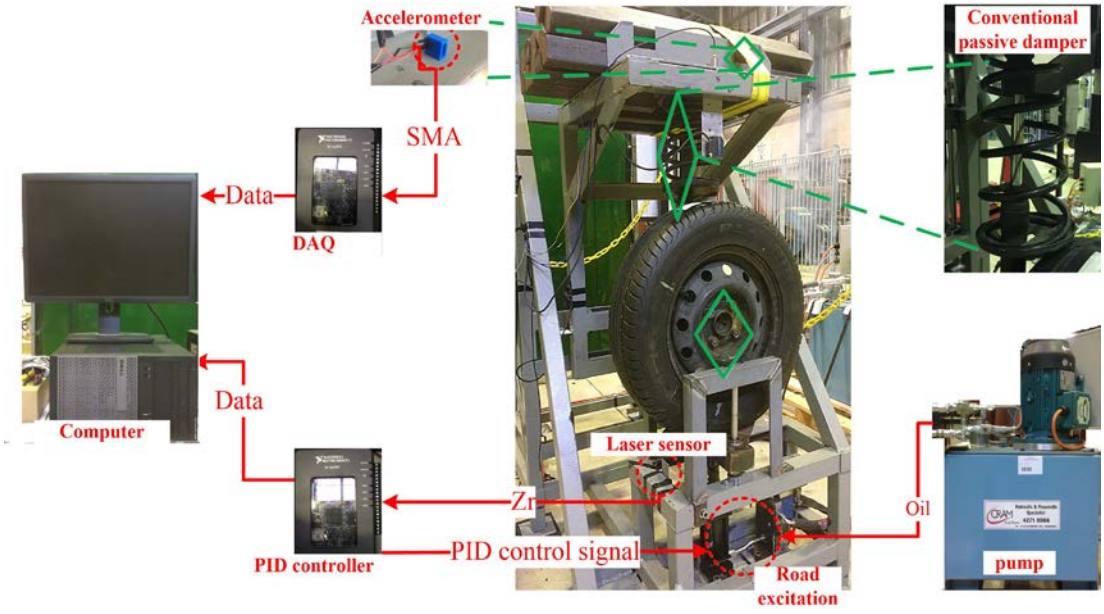

Figure 3.1 The system scheme of the quarter-car test rig.

The measured primary parameters of the quarter-car test rig are $k_s = 18500\ \mathrm{N/m}$, $k_t = 179000\ \mathrm{N/m}$, $m_s = 257.6\ \mathrm{kg}$, $m_u = 33.2\ \mathrm{kg}$, $c_s = 860\ \mathrm{N\,s/m}$. The tyre is excited by a 2Hz, 10mm amplitude standard sine wave signal generated by a hydraulic system, which is controlled by a PID controller. The suspension (Model: 48540-02080, Toyota Corp.) is equipped with a conventional passive damper.

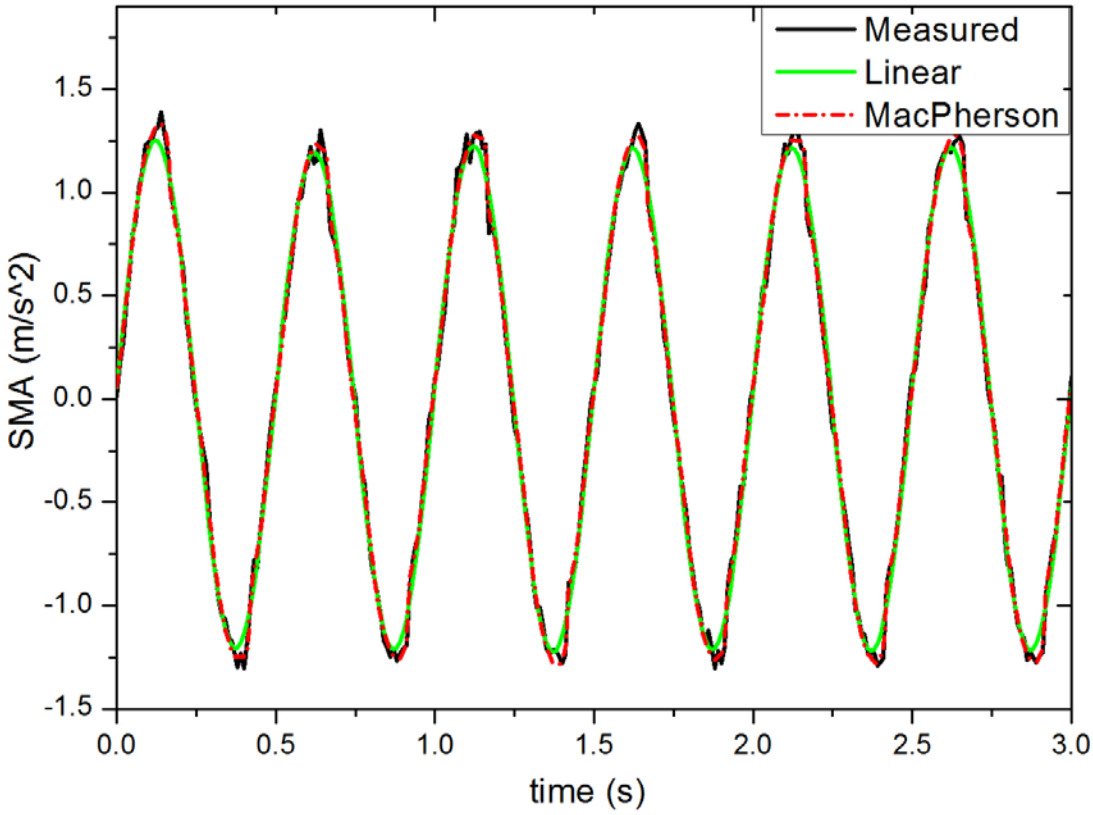

Figure 3.2 The comparison in SMA between measured data and simulation result.

In terms of the simulation results from Simulink® and the experiment result collected from the test rig, the comparison of the two suspension models is drawn as Figure 3.2 shows. As we can see from the chart, both the MacPherson suspension model and quarter-car model which are built in this part can exactly present the accuracy of the suspension's dynamic characteristics. The modelling errors of the two suspensions are

shown in Table 3.1. The cost function value calculated for the linear quarter-car model (1.3589) is close to the one calculated for the MacPherson model considered (1.1022).

Table 3.1 The modelling errors of the two suspension models

Object	Iteration	F-count	Cost function value
Measured	N/A	N/A	N/A
MacPherson	14	28	1.1022
Linear Q-C	9	36	1.3589

In the following chapters, the linear quarter-car model will be used to analyse the dynamic of vehicle suspension for following two considerations:

Ⅰ. There is no obvious result difference between the linear quarter-car model and MacPherson suspension model, and both can present the characteristics of vehicle dynamics.

Ⅱ. Quarter-car vehicle model is easy to be built and with less parameters, which is more convenient to be build and verify in real time control at later work.

3.2.2 Modelling of MR damper

(1) Bouc-Wen model

The Bouc-Wen model that is numerically tractable and has been used extensively for modelling hysteretic systems. The one is extremely versatile and can exhibit a wide variety of hysteretic behaviour.

The phenomenological model is governed by the following five simultaneous equations:

$$
\begin{aligned}
F &= c_0\dot{x} + k_0 x + az, \\
\dot{z} &= -\gamma|\dot{x}|z|z|^{n-1} - \beta\dot{x}|z|^n + A\dot{x}, \\
a &= a(v) = a_a + a_b v, \\
c_0 &= c_0(v) = c_{0a} + c_{0b} v, \\
\dot{v} &= -\eta(v - u).
\end{aligned} \tag{3.1}
$$

In this model, the parameters for adjusting the hysteresis are represented by $\gamma, \beta, \text{and } A$; and a is the evolutionary coefficient; c_0 is the viscous damping observed at high velocities; k_0 is the stiffness at large velocities; v is the output of a first-order filter; and u is the control voltage sent to the MR damper.

(2) The modified Bouc-Wen model

The dynamic characteristic of the modified Bouc-Wen model can be described as

$$c_1\dot{y} = \alpha z + k_0(x - y) + c_0(\dot{x} - \dot{y}), \tag{3.2}$$

where the evolutionary variable z is governed by

$$\dot{z} = -\gamma|\dot{x} - \dot{y}|z|z|^{n-1} - \beta(\dot{x} - \dot{y})|z|^n + A(\dot{x} - \dot{y}). \tag{3.3}$$

By adjusting the parameters of the model γ, β and A, one can control the linearity in the unloading and the smoothness of the transition from the pre-yield to the post-yield region. Solving for $\dot{y}$ results in

$$\dot{y} = \frac{1}{c_0 + c_1} c_0\dot{x} + k_0(x - x_0) + \alpha z. \tag{3.4}$$

The total force generated by the system is then found by summing the forces in the upper and lower sections of the system below

$$F = \alpha z + k_0(x - y) + c_0(\dot{x} - \dot{y}) + k_1(x - x_0). \tag{3.5}$$

From Eq. (3.2), the total force can also be written as

$$F = c_1\dot{y} + k_1(x - x_0). \tag{3.6}$$

Thus, the MR damper system can be added in a quarter-car dynamic equation by replacing $c(\dot{z}_s - \dot{z}_u)$ to F.

(3) Comparison of MR model's dynamic characteristics

With the purpose of comparing the dynamic characteristics of the two kinds of models, a stretch experiment was carried out using a LORD MR damper. The appearance of the LORD MR damper is shown in Figure 3.3.

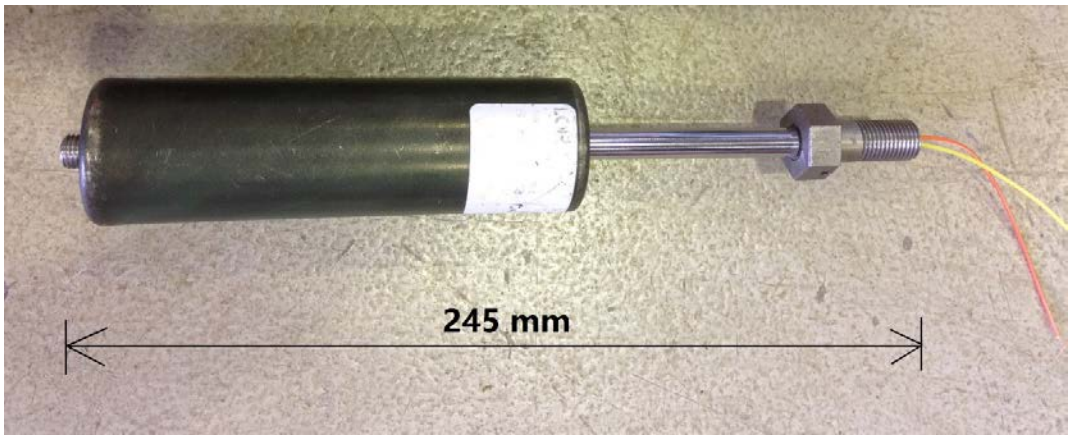

Figure 3.3 Appearance of the LORD MR damper.

After obtaining the force-displacement curve of the damper, the parameters of Bouc-Wen model and modified Bouc-Wen model were identified in Simulink® based on acquired experiment data, in which, the experiment result and simulation result are shown in Figure 3.4.

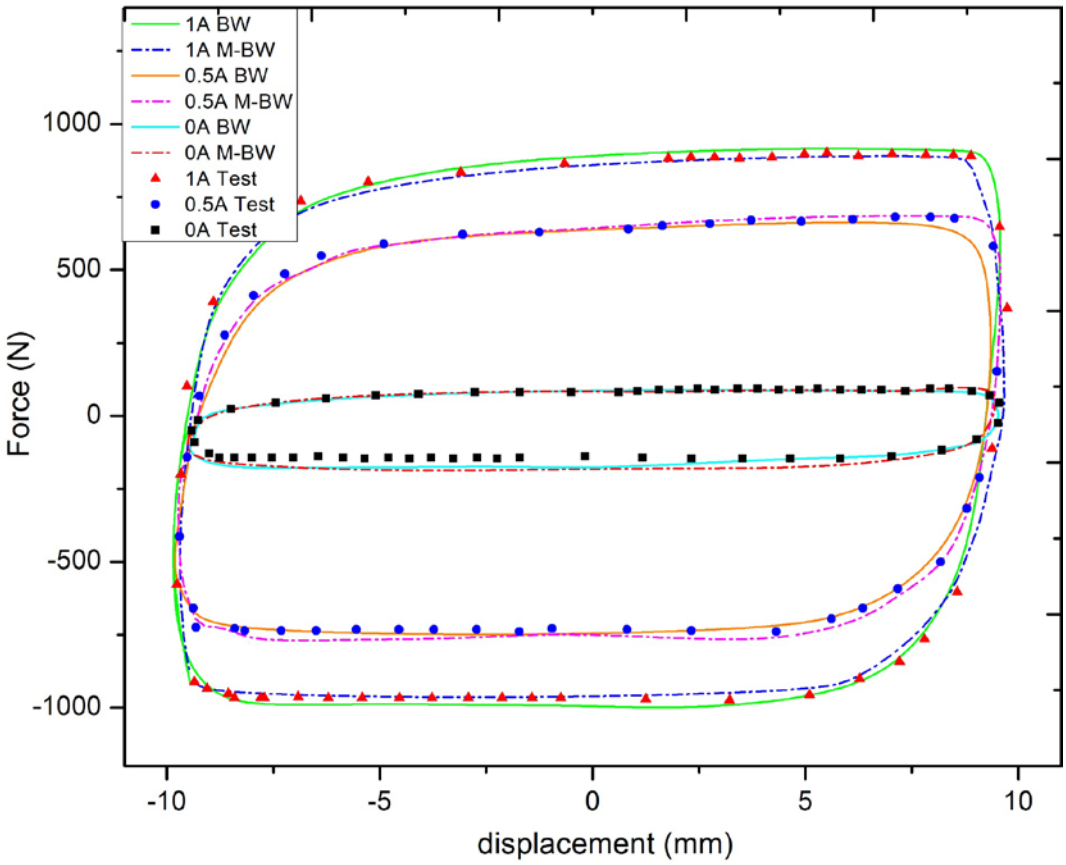

Figure 3.4 The comparison between the identified responses and the measured response

The modelling errors of the two damper models are shown in Table 3.2. In this case, the cost function value calculated for the modified Bouc-Wen model (1.8660) is relatively smaller than the one calculated for the Bouc-Wen model considered (2.1149), which two values are almost close.

Table 3.2 The modelling errors of the two damper models

Object	Iteration	F-count	Cost function value
Measured	N/A	N/A	N/A
Bouc-Wen	5	42	2.1149
Modified B-W	3	28	1.8660

Based on the preliminary simulation result, it can be seen that the shape functions of each model both can comparatively well describe the dynamic characteristic of the MR damper (The cost function value of Bouc-Wen and modified Bouc-Wen are 2.11 and 1.86, respectively, which are close to each other). These two models would be used in the following chapters. Cause 1, the modified Bouc-Wen model performs well in numerical simulation that can precisely describe an MR's dynamic characteristics. Cause 2, the Bouc-Wen model can effectively predict the force-displacement behaviour of an MR damper as well as the modified Bouc-Wen model, but with more concise mathematical expression of MR damper force. For real-time controller design, the Bouc-Wen model can be also adopted here.

3.3 Models of road excitation

Two typical road profiles, bump road and random road, which are often used to evaluate suspension performance in the time domain, were considered in this experiment.

3.3.1 Bump road excitation

A bump input, which is normally used to describe the transient response characteristic, is adopted as the first road excitation. The corresponding road displacement is given by

$$z_r(t) = \begin{cases} \frac{a}{2}\left[1 - \cos\left(\frac{2\pi v_0}{l} t\right)\right], & 0 \le t \le \frac{l}{v_0}, \\ 0, & t > \frac{l}{v_0}, \end{cases} \tag{3.7}$$

where $a = 0.035$ m and $l = 0.8$ m are chosen as the height and the length of the bump, and the vehicle forward velocity is $v_0 = 0.856\, m/s$ [116].

3.3.2 Random road excitation

The second type of road excitation, normally used to evaluate frequency response, is a random road excitation based on the harmony superposition mothed. Most studies have demonstrated that road roughness is a Gaussian probability distribution with zero mean value. It has smooth traversal characteristic if it is transferred to a stochastic process. The road roughness characteristics can be presented by power spectral density (PSD) function $S_q(\Omega)$. Qualitatively, a larger value of exponent n is defined to describe the roughness at longer wavelengths, while a smaller value at shorter wavelengths. For this reason, a spectrum corresponding to the geometrical profile of typical roads can be represented by the following segmented function

$$S_q(\Omega) = \begin{cases} S_q(\Omega_o)(\Omega/\Omega_o)^{-n_1}, \ if \ \Omega \le \Omega_o, \\ S_q(\Omega_o)(\Omega/\Omega_o)^{-n_2}, \ if \ \Omega \ge \Omega_o, \end{cases} \tag{3.8}$$

where, Ω is the spatial frequency, $\Omega_o = 1/2\pi$ is a reference spatial frequency, n is the frequency exponent; generally, $n_1 = 2$ and $n_2 = 1.5$ so that the resulting spectrum exhibits a slope discontinuity at $\Omega = \Omega_o$ in a log-log scale, as shown in Figure 3.5.

Moreover, the value $S_q(\Omega_o)$ is a power spectral density value under the reference spatial frequencies. For a nonlinear quarter-car model, the road excitation can be generated by the spectral representation method [117, 118]. Using the harmonic superposition method, the harmonic component under different frequency are added together to generate random road roughness.

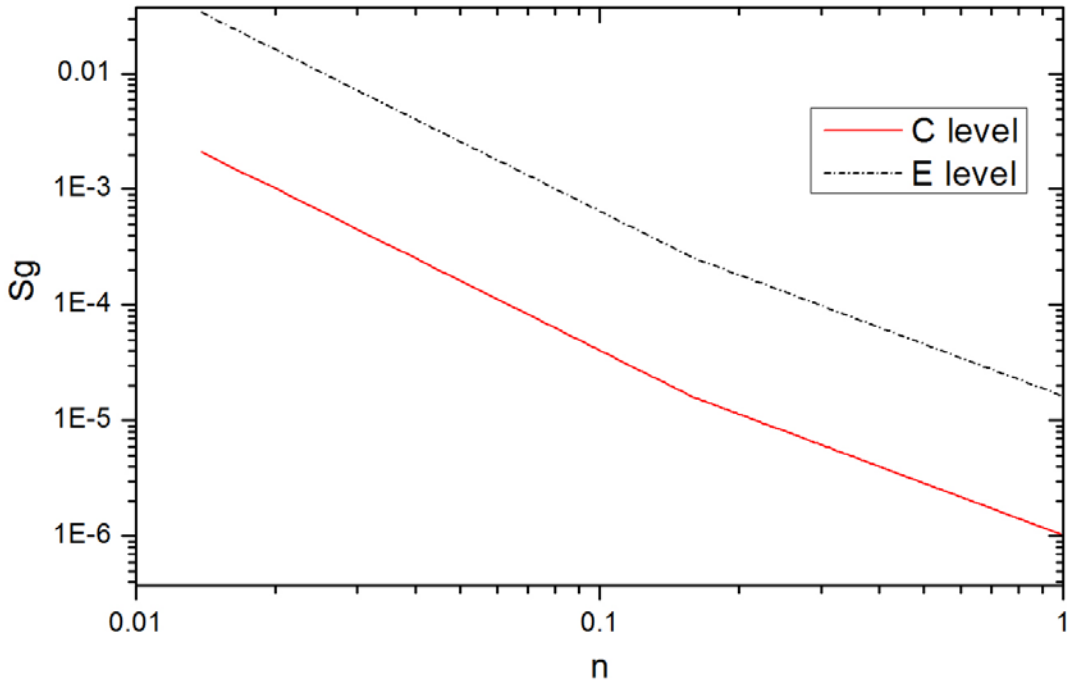

Figure 3.5 The PSD value of typical road profile.

Supposing that a car is traveling on a given road at a constant speed v, the road irregularities can be simulated by the following formula

$$z_r(t) = \sum_{i=1}^{n}\left(\sqrt{2S_q(i\Delta\Omega)\Delta\Omega}\right)\sin(i2\pi\Delta\Omega V_r t + \varphi_i), \quad (3.9)$$

where φ_i is the random numbers distributed uniformly among $[0,2\pi]$, $\Delta\Omega$ is the minimum spatial frequency value we considered, which equals $0.011m^{-1}$.

The random road profile can be simulated by Simulink® under different vehicle speeds, between 10 to 40 m/s. Two specific road profiles with a constant speed $V_r = 10\ \mathrm{m/s}$ over a given road segment with length $L = 100\ \mathrm{m}$ were simulated. They illustrate average-quality case, the C class road profile (ISO 8608) with $S_q(\Omega_o) = 16 \times 10^{-6}\ m^3$, and very poor-quality case, the E class road profile (ISO 8608) with $S_q(\Omega_o) = 256 \times 10^{-6}\ m^3$, vs. time respectively, as shown in Figure 3.6.

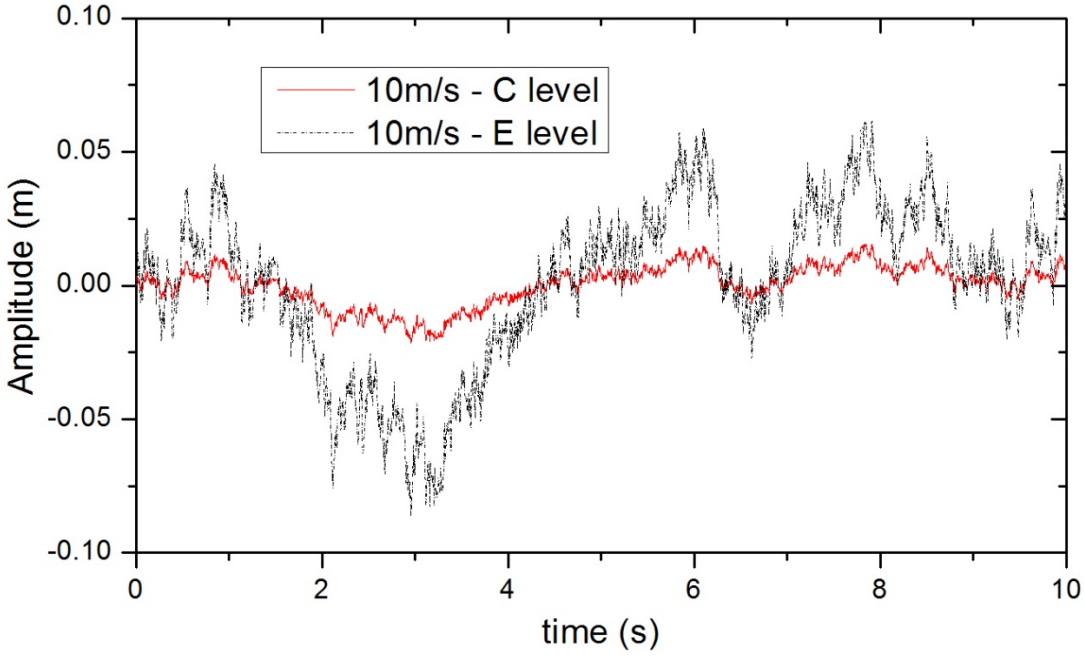

Figure 3.6 Variation of road roughness of rank C & E vs. time.

When driving on complicated terrain or extremely rough landform in the field, vehicle suspension system is required to get more capabilities to provide riding comfort. Thereby, this typical off-road profile is also regarded as an important testing excitation of this thesis.

3.4 Analysis of the suspension parameters with multi-objective optimization

The optimization work of vehicle suspension is extremely sensitive to the factors including the selection of objective function and the driving status like driving speed. This section is to comprehensively consider those factors and then to optimize the parameter of the suspension system based on the characteristic of the existing quarter-car test rig.

3.4.1 Suspension performance objective function

To optimize the parameters of a vehicle suspension, three major factors, riding comfort, tyre loading, and suspension deflection should be considered simultaneous.

Particularly, riding comfort, which can be presented by l_1, can be measured by SMA. In addition, another objective function l_2 can be represented by the displacement between the wheel and the ground, namely TD. The third objective l_3 is the distance $z_s - z_u$ between the wheel subsystem and the car body, which is also known as SD. Then, the three sub-objective functions are combined into a unified objective function J. Considering the random characteristic of the road excitation generated in time domain, the following performance indices can be determined by expectations

$$\begin{aligned} \mathrm{J} &= {w_1 l_1}/{l_{1m}} + {w_2 l_2}/{l_{2m}} + {w_3 l_3}/{l_{3m}}, \\ l_1 &= E\sqrt{\textstyle\sum_{i=1}^{N} \sigma_1 (\ddot{z}_s)^2 / N}, \\ l_2 &= E\sqrt{\textstyle\sum_{i=1}^{N} \sigma_2 (z_u - z_r)^2 / N}, \\ l_3 &= E\sqrt{\textstyle\sum_{i=1}^{N} \sigma_3 (z_u - z_r)^2 / N}, \end{aligned} \tag{3.10}$$

where N is the total sampling points. l_{1m}, l_{2m}, and l_{3m} are the maximum value of each objective function. σ_1, σ_2, and σ_3 are the factors to normalize the magnitude of each performance index. When compare the value of each, there is magnitude difference that lead to the incomparability of each objective function. Hence, a normalization program is needed to be carried out firstly.

By performing direct integration of the equations of motion of the vehicle system with the nominal parameter values, the normalizing factors were determined as $\sigma_1 = 76.92$, $\sigma_2 = 4347.82$, and $\sigma_3 = 0.26$. The constants w_1, w_2, and w_3 denote the weighting coefficients balancing and adjusting the three performance indices. The proportion is determined by the contribution of the individual performance. Four optimization objectives are determined and performed in this test, including J_{MIX}(comprehensive), J_{SMA}(major in sprung mass acceleration), J_{TD}(major in tyre dynamic), and J_{SD} (major

in suspension deflection). The proportion of the weighting coefficients for each objective are shown in Table 3.3.

Table 3.3 The proportion of the weighting coefficients

Object	w_1	w_2	w_3
J_{MIX}	0.6	0.2	0.2
J_{SMA}	0.9	0	0.1
J_{TD}	0.4	0.5	0.1
J_{SD}	0.4	0.1	0.5

3.4.2 Simulation progress of the parameter optimization

The optimization is aimed to find the optimized parameters for different objective functions based on the specific characteristic of the existing quarter-car test rig, in which includes the stiffness of suspension spring and suspension damping. The initial suspension parameter value is taken from the conventional passive suspension (Model: 48540-02080, Toyota Corp.) in Section 3.2.1: $k_t = 179000$ N/m, $m_s = 257.6$ kg , $m_u = 33.2$ kg. In the simulation, the average-quality road profile (C class) was chosen as the road excitation.

(1) Linear model case

For the special case of vehicle model with linear properties, the response of spectral density of the linear dynamic system can be obtained easily in frequency domain by applying road profile spectral density under exact vehicle velocity and the stationary vehicle response matrix through the formula [119]:

$$S_{XX}(\omega) = H_x(\omega)H_x(-\omega)S_{FF}(\omega) = |H_x(\omega)|^2 S_{FF}(\omega). \quad (3.11)$$

In the previous equation, $\omega = 2\pi\Delta\Omega v$ is the temporal frequency, $S_{XX}(\omega)$ and $S_{FF}(\omega)$ represent the spectral density of the response and the excitation, respectively. $H_x(\omega)$ is the frequency response functions of the system [120].

(2) Nonlinear Bouc-Wen model case

Except the linear suspension model presented before, the quarter-car model with MR damper system possesses strong nonlinearities. For this case, Genetic Algorithm (GA), in conjunction with appropriate integration methodologies developed for nonlinear systems [121], is applied to evaluate the suspension response with probabilistic characteristic.

GA belong to the larger class of evolutionary algorithms, which generate solutions to optimization problems using the technology inspired by natural evolution. This global optimization algorithm has a characteristic that it has less possibility to fall into partial optimal solution in the iterative process. For this reason, it has become a powerful tool to calculate complex optimization issues of a nonlinear system. More detailed discussion and description of GA are available such in [122]. In the work presented in this article, GA and Direct Search Toolbox in MATLAB® was applied for parameter optimization. A fixed population size with string length of 50 and the generations of 100 are used, crossover fraction is 0.8, and migration fraction is 0.2.

3.4.3 The numerical results of the parameter optimization

In terms of a linear model, the suspension response with second moment characteristic excitation in Eq. (3.11) is readily obtained by the numerical sum of the corresponding response of the power spectral density function with specific ω. To compare the optimal stiffness value between linear passive model and nonlinear Bouc-Wen model,

the results are depicted in Figure 3.7. A major phenomenon can be observed that by increasing vehicle's speed, the optimized values are getting smaller.

In Figure 3.7, the red curve illustrates the tendency of nonlinear model optimal parameter, and the black line is obtained from the linear model as a reference. Consequently, the trend is observed as the dependence of the linear suspension stiffness to the vehicle horizontal velocity, and the value of the nonlinear one demonstrates relative irregular trend within the velocity range considered. The result presented is attributed by the characteristic of MR damper, which has a strong nonlinearity in the relation between the output force and the cylinder's moving velocity.

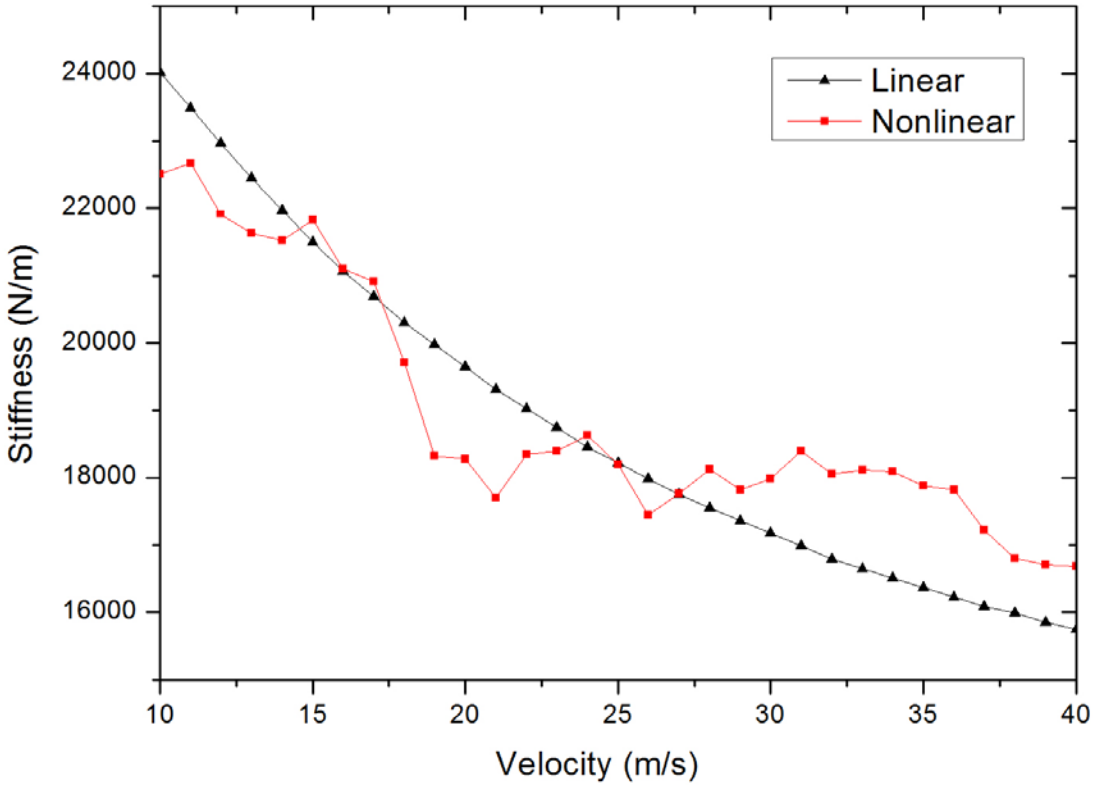

Figure 3.7 Linear and nonlinear system optimal stiffness values vs. velocity under mixed objective function.

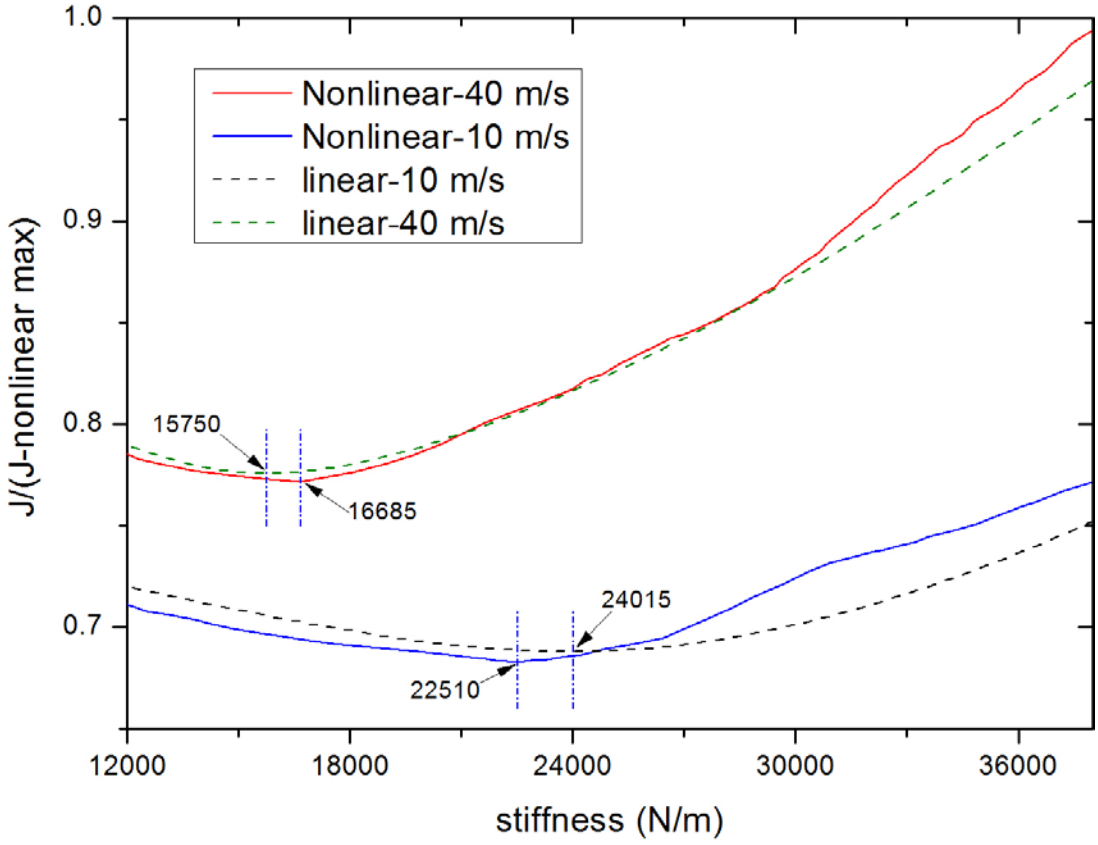

Figure 3.8 Mixed object value vs. stiffness values.

Figure 3.8 illustrates the normalized objective sum value (includes linear and nonlinear) on the suspension stiffness coefficient, for the two extreme values of the velocity spectrum (10 m/s and 40 m/s) considered. Direct comparison indicates that there is a shift in the minimum value of each of these two suspensions as velocity varies. This shift is expected since an increase of the value of vehicle speed led to an increase of the road excitation frequency.

To observe the effect of optimizing stiffness value, verification of the result can be done by analysing the performance index of the system using optimal parameters. The normalized performance indices are drawn in Figures 3.9-3.10.

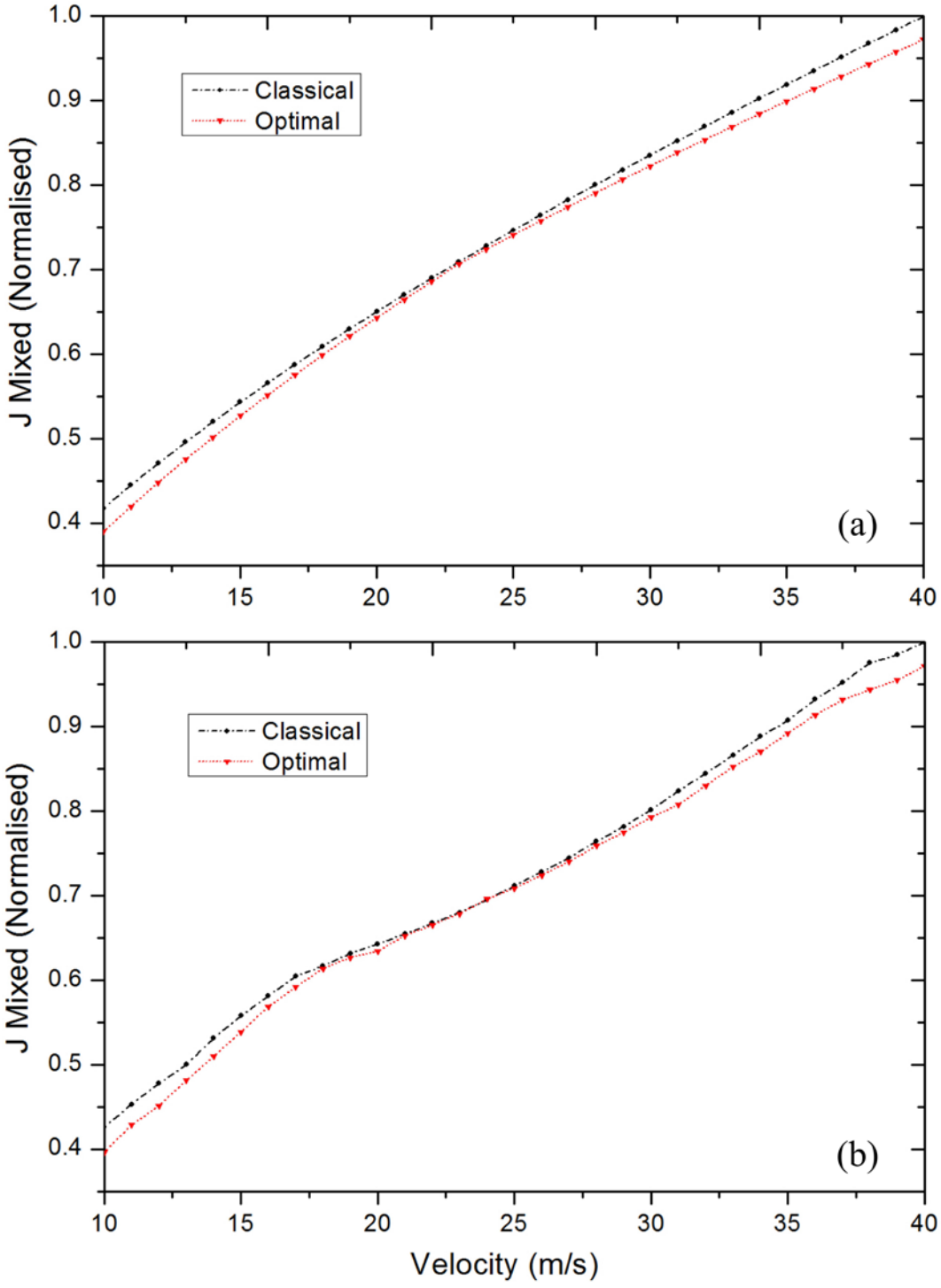

Figure 3.9 Normalized performances of mixed object: (a) linear model; (b) nonlinear model.

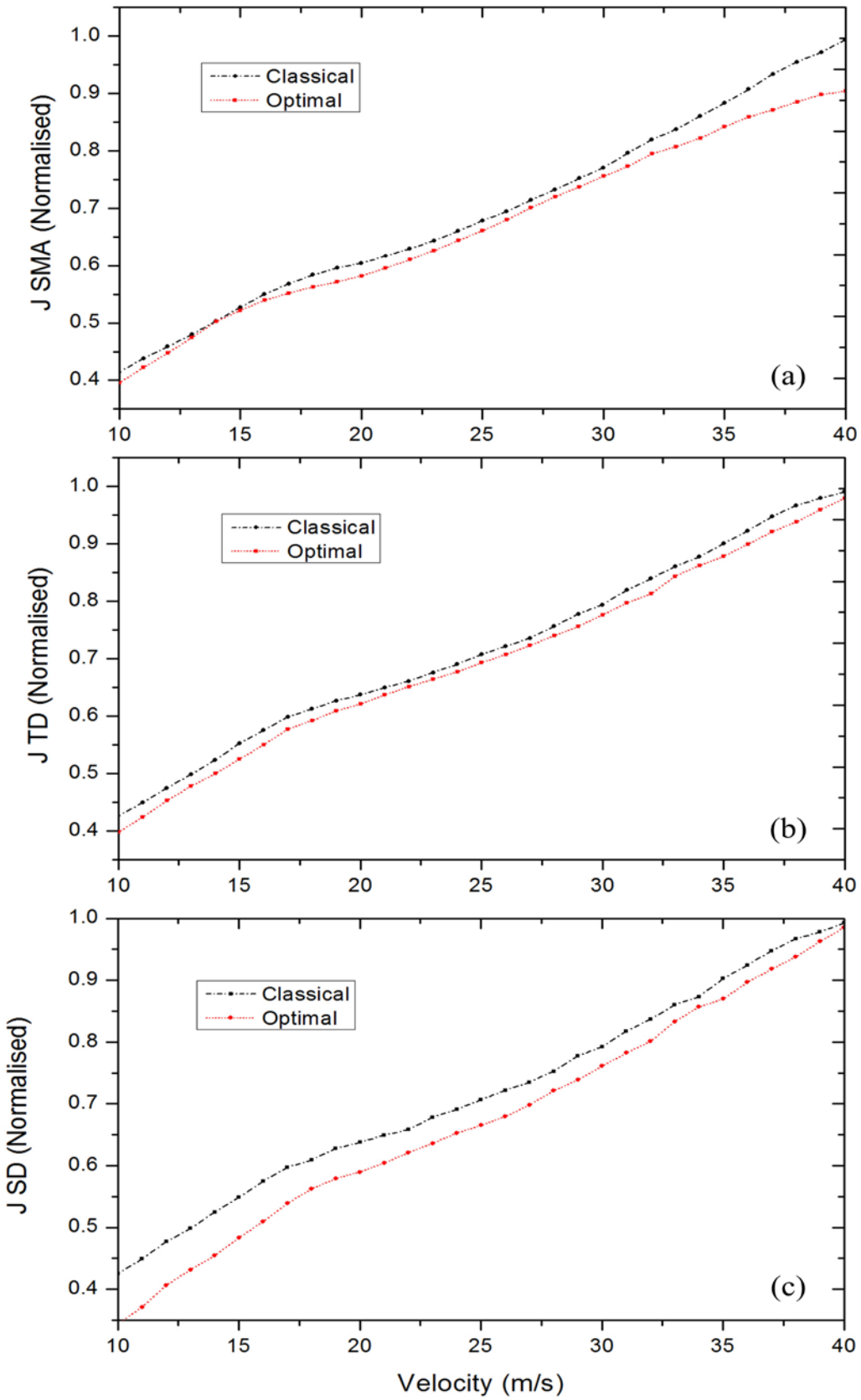

Figure 3.10 Overall performances for nonlinear model: (a) sprung mass acceleration; (b) tyre deflection; (c) suspension deflection.

It can be seen from the figures that, almost at the whole range of vehicle speed considered, the objective function values with optimal stiffness are smaller than the ones with the classic suspension parameter value. It means the suspension system with optimized stiffness value performs better than a normal suspension in vibration control. More specifically, Figure 3.9 demonstrates the overall performances of linear suspension and nonlinear one as a comparison. The associated nonlinear model performance value of sprung mass acceleration, tyre dynamic loading, and suspension deflection are depicted in Figure 3.10. For a single objective optimization shown in Figure 3.10, the overlap of optimal and classic data can be observed under specific vehicle speeds. The overlap effect can be explained after noting that the optimal stiffness value under specific vehicle speeds equals to the classic stiffness value as a reference coincidentally. More specifically, in terms of sprung mass acceleration, overlap is happened in the low vehicle speed region, while the overlap of tyre dynamic loading data can be observed in the medium vehicle speed area. Please note that whether this phenomenon happens or not depends on the reference stiffness value we chosen (The reference stiffness value in this case is 18500 $\mathrm{N}m^{-1}$).

To evaluate the optimization performance, quarter-car model based simulation work was carried out. Time histories of suspensions response in terms of the performance indices, SMA and TD, were recorded and plotted in Figure 3.11 and Figure 3.12. More specifically, by applying stiffness and damping multi-objective optimization onto the suspension, the peaks of acceleration and displacement are decreased effectively than the other two cases. This result clearly shows the large potential benefit of stiffness and damping optimization program in a semi-active suspension design.

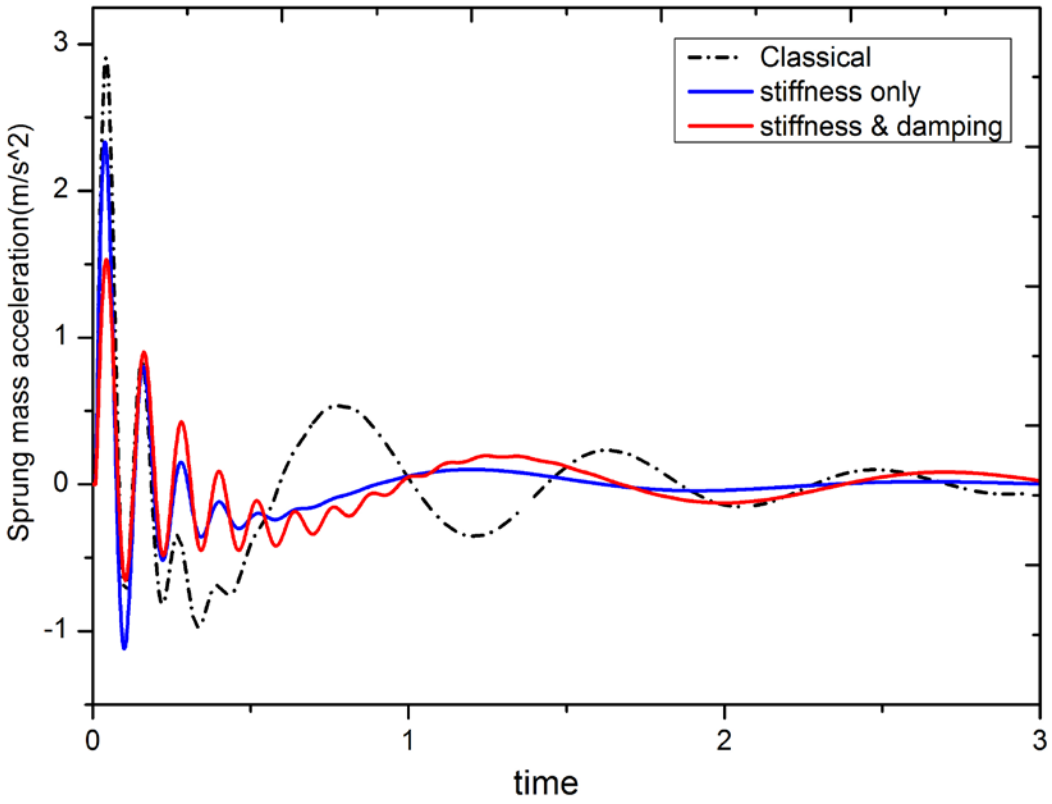

Figure 3.11 The simulation result of SMA.

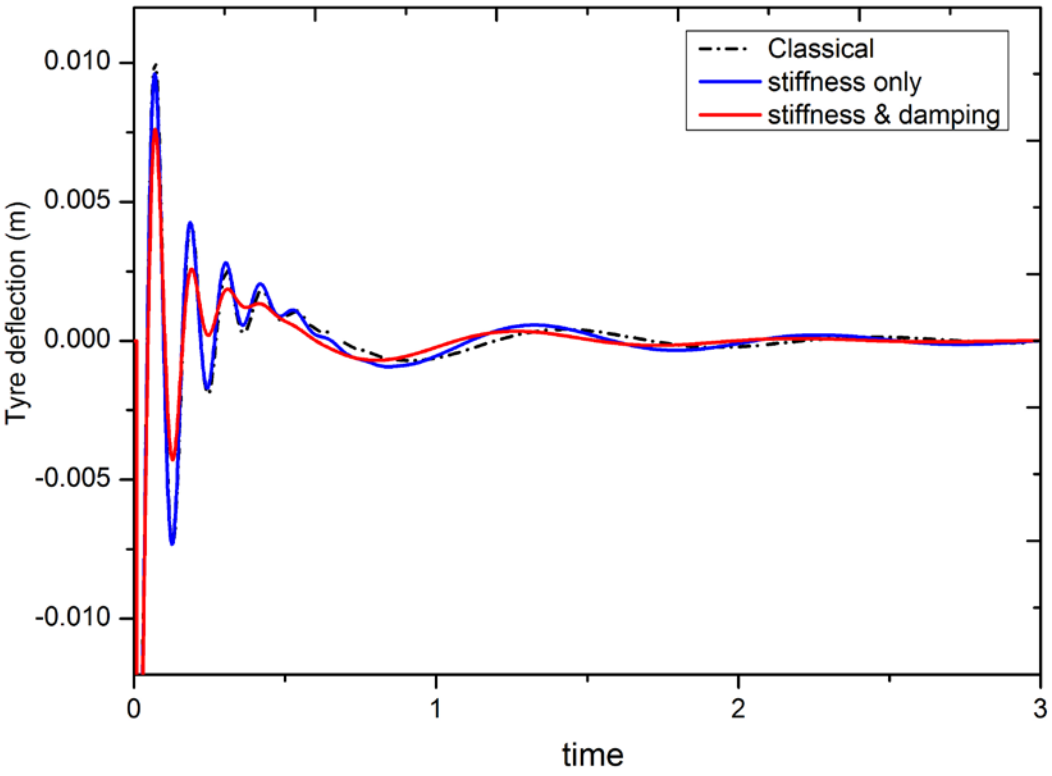

Figure 3.12 The simulation result of TD.

In general, after completing vehicle suspension stiffness optimization process, it can be predicted that the suspension performance can be improved in most traveling conditions. The optimized result of linear one and non-linear one under 10 m/s vehicle speed are shown in Table 3.4 and Table 3.5, respectively. Note that the simulation program of nonlinear case is based on the Bouc-Wen model in Eq. (3.1).

Table 3.4 Optimised linear suspension coefficients

Object	J_{MIX}	J_{SMA}	J_{TD}	J_{SD}
$k_s(\mathrm{N}m^{-1})$	24015	15511	31255	39578
$\mathrm{c}(\mathrm{N}sm^{-1})$	1087	801	1280	1609

Table 3.5 Optimised non-linear Bouc-Wen suspension coefficients

Object	J_{MIX}	J_{SMA}	J_{TD}	J_{SD}
$k_s(\mathrm{N}m^{-1})$	22510	16552	30065	38595
$\alpha(\mathrm{N/m})$	25987	20540	35021	59601
$c_o(N \cdot s/m)$	2300	1901	2511	2546
$k_o(N/m)$	601	198	2001	3750
$\gamma(m^{-2})$	1200254	2605065	1982001	1653240
$\beta(m^{-2})$	895404	2956900	2226580	1959420
A	189	410	85	69

These optimized parameters greatly contributed to a new damper design as well as the determination of the control parameters of its controller. Based on the optimised data, the following section demonstrates the design of the OMRD.

3.5 Design and test of a new MR damper

3.5.1 Design of a new MR damper

A new MR damper was designed in accordance with the specification of a quarter-car test rig. The required damping force range was chosen based on the optimization result in Section 3.4. For the propose to effectively deal with the riding comfort while guarantee small tyre loading and suspension travel, the specific optimized values demonstrated in Table 3.5 were chosen to design an MR damper. More specific, the basic fixed parameters of Bouc-Wen model were determined by the optimized value of J_{SMA}, which is considered as the main optimizing objective. The values are $k_o = 198\ (N/m)$, $\gamma = 2605065\ (m^{-2})$, $\beta = 2956900\ (m^{-2})$, and $A = 410$. When considering the variable damping range, the upper limit was determined by the value of J_{MIX} that $\alpha = 25987\ (\mathrm{N/m})$ and $c_o = 2300\ (N \cdot s/m)$, while the two-thirds point of the damping range was determined by the value of J_{SMA} that $\alpha = 20540\ (\mathrm{N/m})$ and $c_o = 1901\ (N \cdot s/m)$ (for expanding the damping range to enable to get relative small damping for high-frequency vibration control). Therefore, the variation ranges of the two damping control parameters can be determined as α is from $9646\ (\mathrm{N/m})$ to $25987\ (\mathrm{N/m})$ and c_o is from $1103\ (N \cdot s/m)$ to $2300\ (N \cdot s/m)$. Based on the instructional design requirements, the specific dimensions of the device can be determined. Figure 3.13 depicts the schematic configuration of the MR damper designed for this experiment. This MR damper consists of MR fluid, a casing, a spring accumulator, and a piston head in which the magnetic coil is winded.

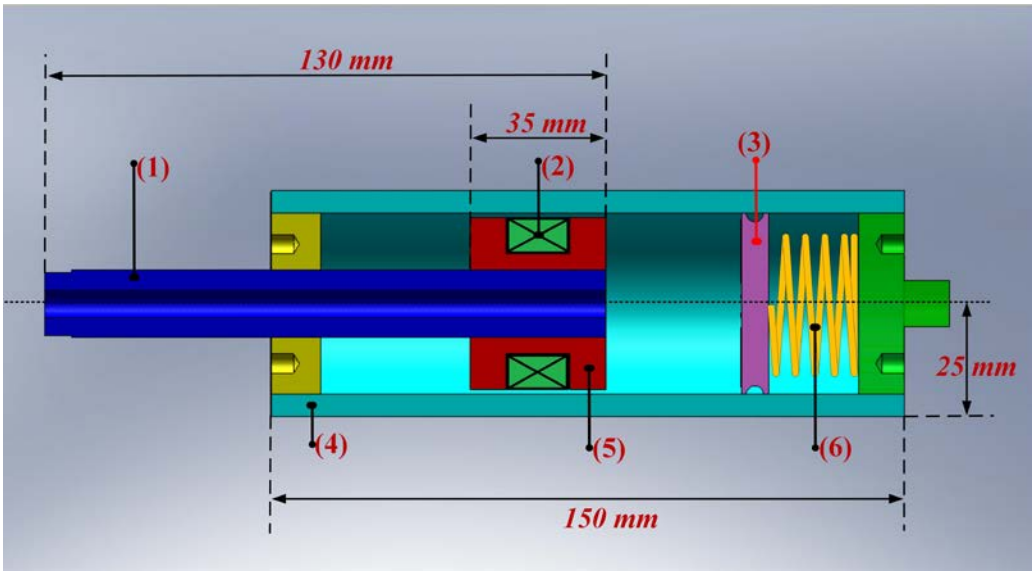

Figure 3.13 Schematic configuration of the MR damper (1) piston rod, (2) coil, (3) floating piston, (4) accumulator spring.

Figure 3.14 Appearances of the MR damper.

The casing and piston head are made of low-carbon steel for preventing magnetic flux leakage phenomenon. The casing is fully filled with MR fluid and divided into upper and lower chambers by the piston head. To compensate for the change of the fluid volume occupied by the piston rod in the chamber, a compression spring is located between the floating piston and the bottom block as an accumulator. The specific parts and the final assembly of the MR damper are shown in Figure 3.14.

3.5.2 Dynamic testing of the MR damper

The phenomenological model of the applied Bouc-Wen model is governed by Eq. (3.1). In this model, the parameters for adjusting the hysteresis are represented by $\gamma, \beta,$ and A; and a is the evolutionary coefficient; c_0 is the viscous damping observed at larger velocities; k_0 is the stiffness at large velocities; v is the output of a first-order filter; and u is the control voltage sent to the MR damper.

Table 3.6 Identified parameters

Parameter	Recommended Value	Identified Value
c_{0a}	N/A	630 $N\,s/m$
c_{0b}	1103 $N\,s/m\,V$	1338 $N\,s/m\,V$
a_a	N/A	3280 N/m
a_b	9646 $N/m\,V$	8026 $N/m\,V$
k_0	198 N/m	220 N/m
A	410	543
β	2956900 m^{-2}	2596078 m^{-2}
γ	2605065 m^{-2}	2766600 m^{-2}

The MR damper was tested by using a 25 kN MTS servo-hydraulic testing system. The force and displacement data were measured and sent to a computer. By analysing the experimental data using the Simulink® parameter estimating function, parameters were determined to fit this model of MR damper. The parameters obtained are shown in Table 3.6. Though there is a high parameter sensitivity to the device's dimensions, the identified parameters are still generally consistent with the instructional optimized parameters. The responses of the MR damper and corresponding simulation results at 1 Hz and 10 mm excitation under 3 different input currents are illustrated in Figure 3.15.

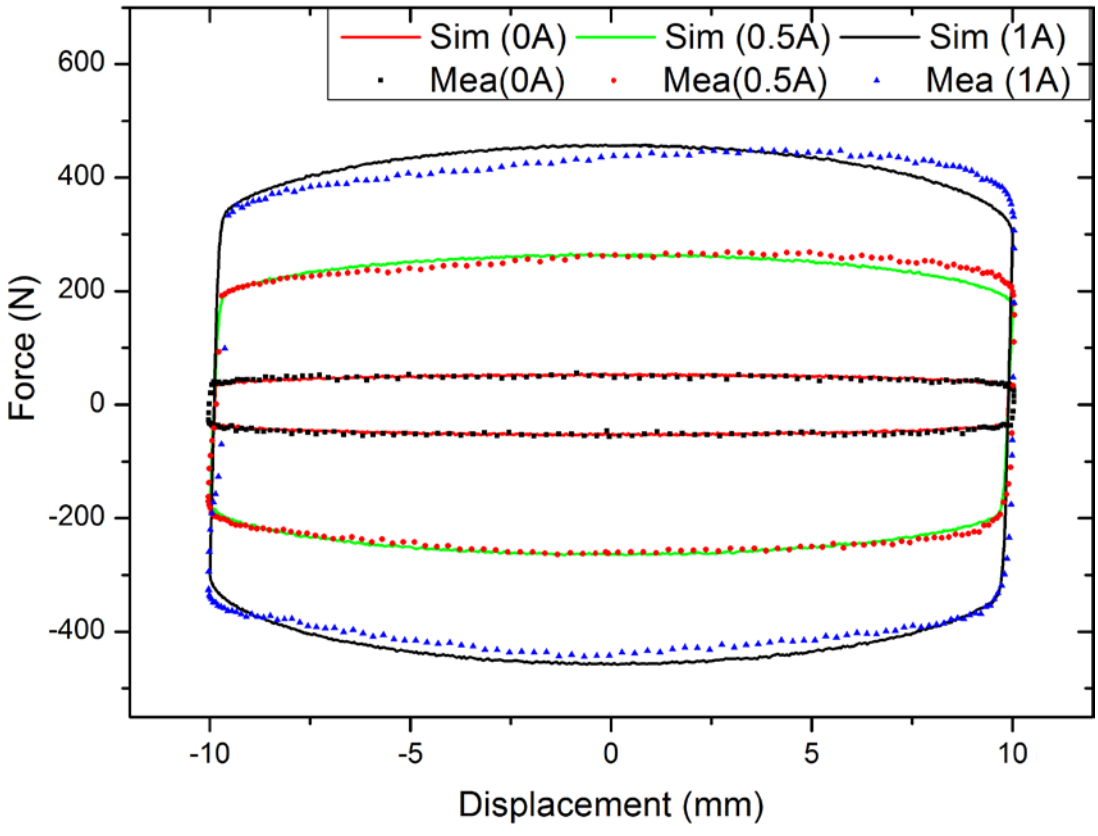

Figure 3.15 Comparison between the identified response and the measured response.

3.6 The experimental research on the optimized MR damper

The simulation of the vehicle suspension parameter optimization demonstrates that the optimized MR damper and spring can enhance the suspension performance. In this section, the passive damper of a vehicle suspension is replaced by the MR dampers, including the LORD MR damper and the OMRD, and then the suspension is tested on the quarter-car test rig to verify the performance of the damper.

3.6.1 Setup of experiment system

The quarter-car test rig was used to do the experimental investigation in this part. Two MR dampers, the standard LORD MR damper and the OMRD as shown in Figure 3.16, were tested in this experiment to investigate the effect of parameter optimization of the damper. The MR dampers were installed between the sprung mass and tyre with a spring. A power amplifier, MR damper controller, and an accelerometer were also included to run this experiment. The composition of the semi-active control loop is shown in Figure 3.17.

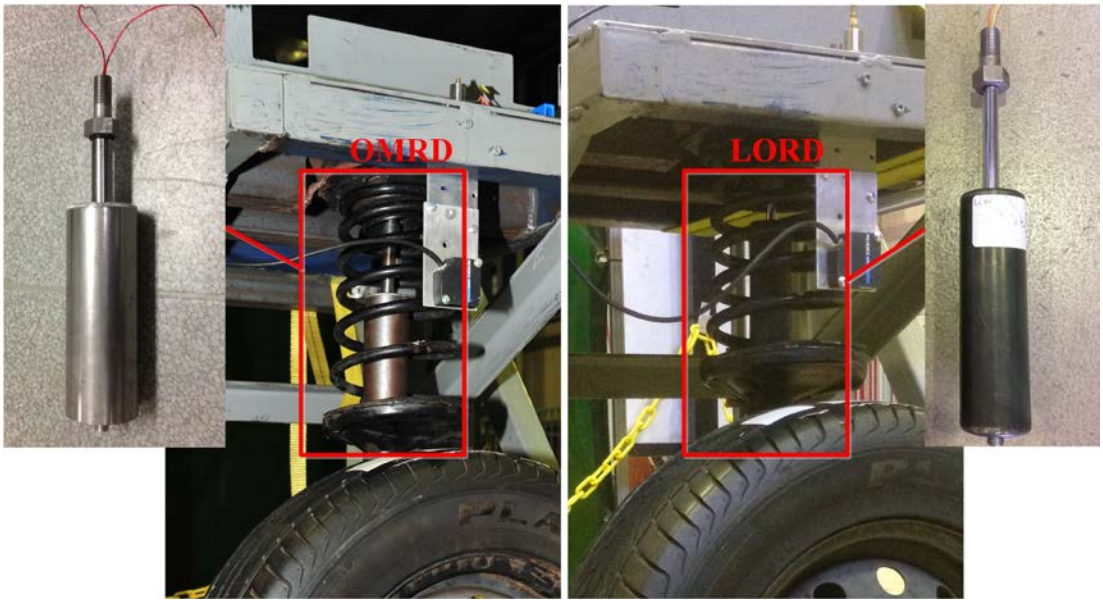

Figure 3.16 The applied dampers in the experiment.

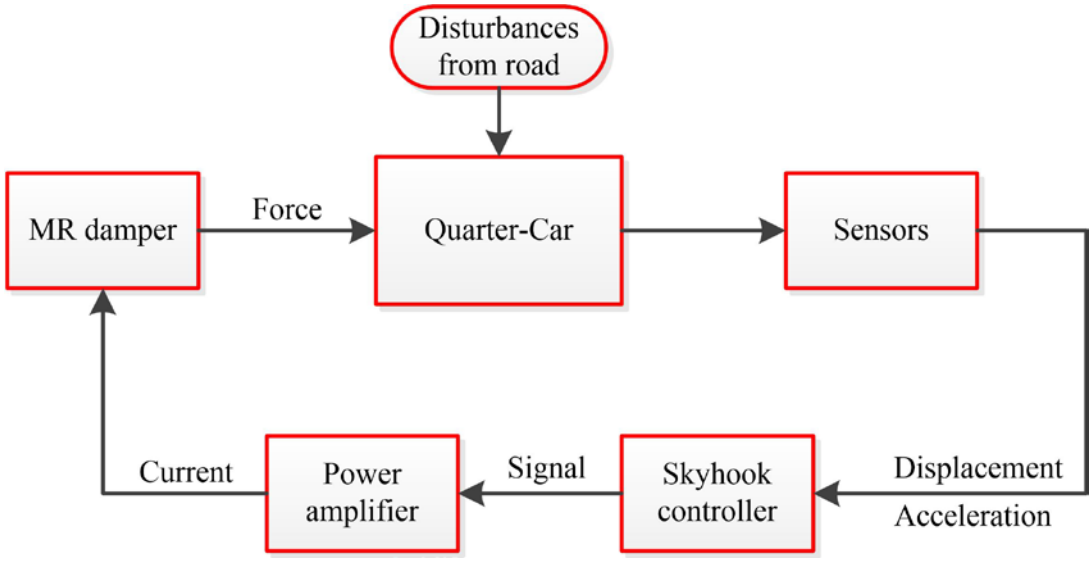

Figure 3.17 Composition of semi-active control loop.

3.6.2 Results of experiment

In this test, control current was changed from 0A to 0.67A. A sinusoidal wave with the frequency of 2Hz was set as the experiment excitation.

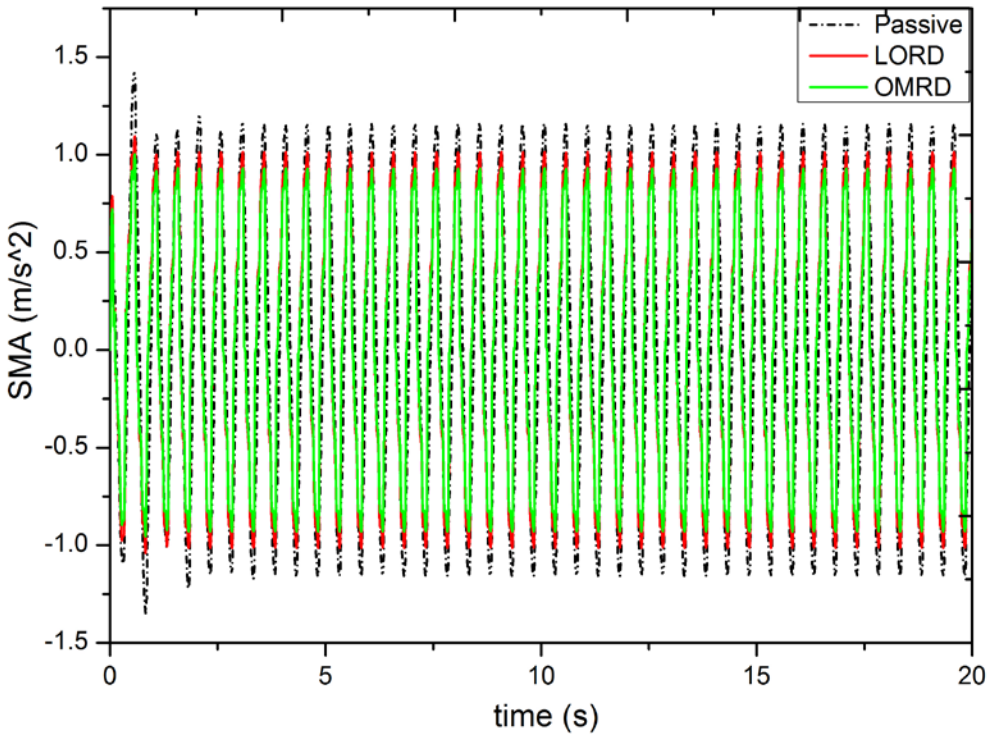

Figure 3.18 Time history of SMA response.

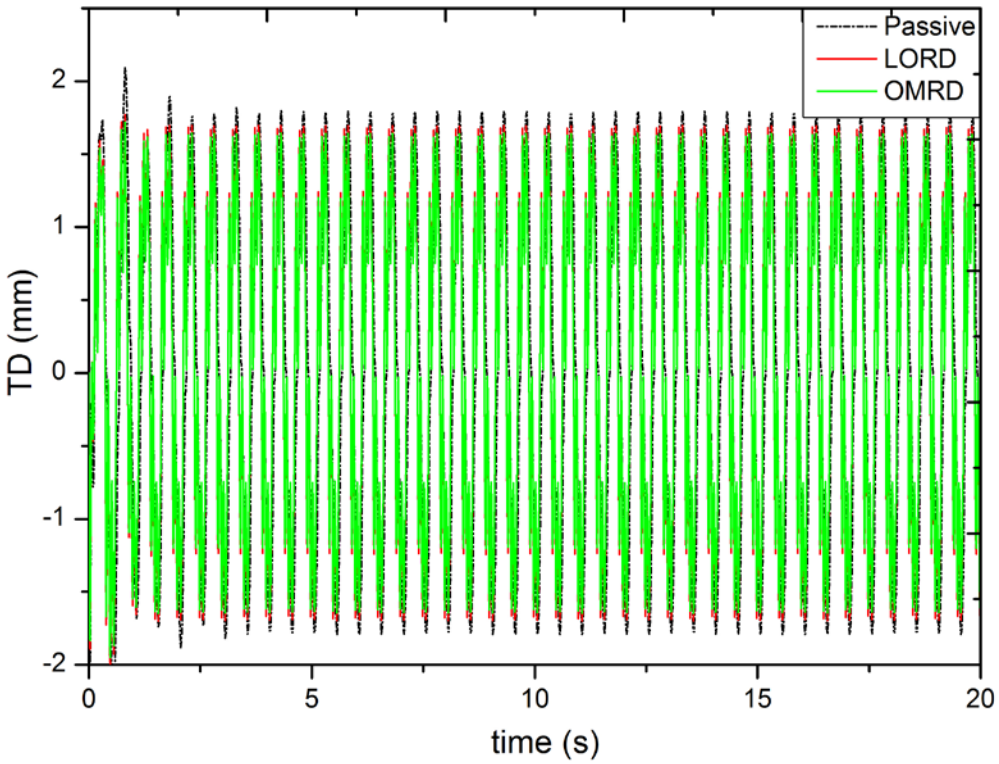

Figure 3.19 Time history of TD response.

Figures 3.18 and 3.19 present the SMA and TD time history of the conventional passive, standard LORD, and OMRD, respectively.

The experimental results in time domain were compared by average peak-to-peak value in Table 3.7. Peak-to-peak value was measured from the top of the waveform, called the crest, all the way down to the bottom of the waveform, called the trough. The improvement ratios compared to the passive damper are also given in Table 3.7. Considering the results of this experiment that there is slight deviation between each peak-to-peak value, the method that to calculate average value is used for analysis purpose. In terms of the object SMA, the RMS one of the OMRD decreases 20% from the one of the passive damper and the corresponding RMS value of the standard LORD damper is just 13%.

Table 3.7 Average peak-to-peak values

Object	Passive damper	LORD damper	Optimized damper
SMA (m/s^2)	2.388	2.079	1.906
%	N/A	-12.93	-20.19
TD (mm)	3.52	3.345	3.271
%	N/A	-4.96	-7.06

For another object TD, the performance of the OMRD and the LORD® damper are similar, which are 7% and 5%, respectively. Based on the specific characteristic of the existing quarter-car test rig, the OMRD performs better which means it is more adoptable to the test rig for experimental validation than a general damper.

3.7 Conclusion

The mathematical model of vehicle suspension and MR damper were established in this chapter. The road excitations to simulate the different driving condition were also designed. To improve the MR system's control performance, an optimization program was conducted for MR damper and controller design. In the program, suspension equivalent damping and stiffness were carefully analysed and optimized; a multi-objective method was used to deal with the driver's demand of a vehicle suspension under different driving status. Based on the optimization results, An MR damper, OMRD, for a quarter-car suspension was designed, fabricated. It was tested comparing with a standard LORD MR damper and a conventional passive damper. The test results show the OMRD performs better than the other dampers based on the existing quarter-car test rig.

4 TS FUZZY CONTROL FOR SEMI-ACTIVE VEHICLE SUSPENSION WITH AN MR DAMPER

4.1 Introduction

This chapter investigates a state observer-based Takagi-Sugeno fuzzy controller (SOTSFC) designed for a semi-active quarter-car suspension installed with an MR damper and provides proof of the effectiveness of the proposed controller. To conduct the test, a quarter-car test rig and control system hardware were used. Then, the TS fuzzy modelling approach was used on the quarter-car system installed with the OMRD. A state observer was built based on the TS fuzzy model. After that, the SOTSFC for the quarter-car test rig was developed. Finally, several tests were conducted on the quarter-car suspension in order to investigate the real effect of the SOTSFC. It was then compared with the use of a skyhook controller to demonstrate its benefits.

4.2 Design of the TS fuzzy control system

4.2.1 TS Fuzzy modelling of the quarter-car with MR damper

A 2-DOF linear quarter-car model is shown in Figure 4.1(a). This is the one, which is widely used for suspension analysis. In the figure, m_s stands for a quarter of the suspension mass; m_u is the unsprung mass; z_s and z_u are the displacements of sprung mass and unsprung mass, respectively; and z_r represents the road profile; k_t is the tyre stiffness, whereas k_s is the stiffness of the spring between the tyre and the chassis; c_s is the damping of a passive damper that provides a damping force proportional to the velocity $\dot{z}_s - \dot{z}_u$.

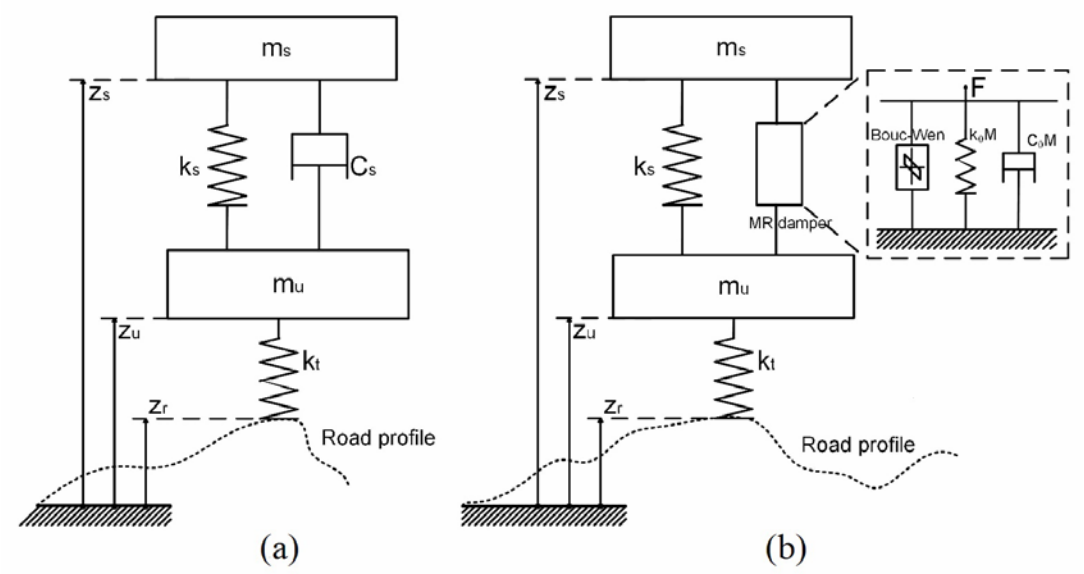

Figure 4.1 Quarter-car suspension systems: (a) linear suspension model; (b) nonlinear suspension model with MR damper [123].

The dynamic model of a quarter-car can be described by the following equations [124]:

$$\begin{aligned} &m_s\ddot{z}_s + c_s(\dot{z}_s - \dot{z}_u) + k_s(z_s - z_u) = 0, \\ &m_u\ddot{z}_u + k_t(z_u - z_r) - c_s(\dot{z}_s - \dot{z}_u) - k_s(z_s - z_u) = 0. \end{aligned} \tag{4.1}$$

The idea is to substitute the linear passive damper with the MR damper to provide variable damping in real-time. Therefore, the linear damper model is replaced by the Bouc-Wen MR damper model mentioned above. The suspension model with the damper replacement is shown in Figure 4.1(b).

Replacing Eq. (4.1) with the Bouc-Wen model Eq. (3.1) gives the dynamic description of the suspension with the MR damper as follows:

$$
\begin{aligned}
m_s\ddot{z}_s &= -k_s(z_s - z_u) - c_0(\dot{z}_s - \dot{z}_u) \\
&\quad -k_0(z_s - z_u) - az, \\
m_u\ddot{z}_u &= -k_s(z_u - z_s) - k_t(z_u - z_r) + c_0(\dot{z}_s - \dot{z}_u) \\
&\quad +k_0(z_s - z_u) + az, \\
\dot{z} &= -\gamma|\dot{z}_s - \dot{z}_u|z|z|^{n-1} - \beta(\dot{z}_s - \dot{z}_u)|z|^n \\
&\quad +A(\dot{z}_s - \dot{z}_u), \\
a &= a_a + a_b v, \\
c_0 &= c_{0a} + c_{0b} v, \\
\dot{v} &= -\eta(v - u),
\end{aligned}
\tag{4.2}
$$

where

$$
|z| = z\,\mathrm{sign}(z). \tag{4.3}
$$

It should be noted that the parameter x in Eq. (3.1) is equivalent to $z_s - z_u$ in Eq. (4.2).

The state variables for the quarter-car suspension are defined as

$$
\begin{aligned}
&x_1 = z_s - z_u, \quad x_2 = z_u - z_r, \quad x_3 = \dot{z}_s, \\
&x_4 = \dot{z}_u, \qquad x_5 = z_d, \qquad x_6 = v.
\end{aligned}
\tag{4.4}
$$

Then, the state-space equation of the semi-active quarter-car system can be represented as

$$
\dot{x} = Ax + B_1 w + B_2 u, \tag{4.5}
$$

where $x = [x_1 \quad x_2 \quad x_3 \quad x_4 \quad x_5 \quad x_6]^T$ is the state vector, the control voltage u is the input, $w = \dot{z}_r$ is the disturbance.

Substituting Eq. (4.4) into Eq. (4.2) with consideration of the nonlinear characteristic of the MR damper, the system motion equations can be rewritten as follows:

$$
\begin{aligned}
m_s\dot{x}_3 &= -k_s x_1 - c_{0a}(x_3 - x_4) - k_0 x_1 \\
&\quad -a_a x_5 - f_1 x_6, \\
m_u\dot{x}_4 &= k_s x_1 - k_t x_2 + c_{0a}(x_3 - x_4) \\
&\quad +k_0 x_1 + a_a x_5 + f_1 x_6, \\
\dot{x}_5 &= A(x_3 - x_4) + f_2 x_5, \\
\dot{x}_6 &= -\eta(x_6 - u),
\end{aligned}
\tag{4.6}
$$

where

$$
\begin{aligned}
f_1 &= c_{0b}(x_3 - x_4) + a_b x_5, \\
f_2 &= -|x_5|[\gamma|x_3 - x_4| - \beta(x_3 - x_4)\,\mathrm{sign}(x_5)].
\end{aligned}
\tag{4.7}
$$

As f_1, f_2 in Eq. (4.6) are bounded due to the bounded suspension relative velocity in practice, to deal with the nonlinear terms $f_1 x_6$ and $f_2 x_5$ in Eq. (4.6), f_1 and f_2 in Eq. (4.7) can be replaced by linear subsystems through the TS fuzzy modelling and represented as follows:

$$
\begin{aligned}
f_1 &= M_1 f_{1max} + M_2 f_{1min}, \\
f_2 &= N_1 f_{2max} + N_2 f_{2min},
\end{aligned}
\tag{4.8}
$$

where M_1, M_2, N_1 and N_2 are fuzzy membership functions, and $M_1 + M_2 = 1$, $N_1 + N_2 = 1$. f_{max} represents the upper bound of the nonlinearity f; and f_{min} is the lower bound. The four membership functions are defined as

$$
\begin{aligned}
M_1 &= (c_{0b}(x_3 - x_4) + a_b x_5 - f_{1min})/(f_{1max} - f_{1min}), \\
M_2 &= 1 - M_1, \\
N_1 &= \{-|x_5|[\gamma|x_3 - x_4| - \beta(x_3 - x_4)\,\mathrm{sign}(x_5)] - f_{2min}\} \\
&\quad /(f_{2max} - f_{2min}), \\
N_2 &= 1 - N_1.
\end{aligned}
\tag{4.9}
$$

Then, the original system can be described by the four linear subsystems mentioned in Eq. (4.9); and each subsystem has the model rule with form IF…THEN…. Then, the nonlinear suspension model Eq. (4.5) can be represented by the following four models:

$$\begin{aligned}
&\text{IF } f_1 \text{ is } M_1 \text{ and } f_2 \text{ is } N_1 \text{ THEN } \dot{x} = \mathrm{A}_{(1)}\mathrm{x} + B_1 w + B_2 u,\\
&\text{IF } f_1 \text{ is } M_1 \text{ and } f_2 \text{ is } N_2 \text{ THEN } \dot{x} = \mathrm{A}_{(2)}\mathrm{x} + B_1 w + B_2 u,\\
&\text{IF } f_1 \text{ is } M_2 \text{ and } f_2 \text{ is } N_1 \text{ THEN } \dot{x} = \mathrm{A}_{(3)}\mathrm{x} + B_1 w + B_2 u,\\
&\text{IF } f_1 \text{ is } M_2 \text{ and } f_2 \text{ is } N_2 \text{ THEN } \dot{x} = \mathrm{A}_{(4)}\mathrm{x} + B_1 w + B_2 u.
\end{aligned} \tag{4.10}$$

After applying the TS approach in [123], the system can be put together in the following description

$$\begin{aligned}
\dot{x} &= \textstyle\sum_{i=1}^{4} h_i \left[A_{(i)} x + B_1 w + B_2 u\right]\\
&= A_h x + B_1 w + B_2 u,
\end{aligned} \tag{4.11}$$

where h_i, i =1-4, are defined as: $h_1 = M_1 N_1$, $h_2 = M_1 N_2$, $h_3 = M_2 N_1$, $h_4 = M_2 N_2$ with the constraints that $h_i \geq 0$, and $\sum_{i=1}^{4} h_i = 1$,

$$A_h = \textstyle\sum_{i=1}^{4} h_i A_{(i)},$$

$$\mathrm{A}_{(i)} = \begin{bmatrix}
0 & 0 & 1 & -1 & 0 & 0\\
0 & 0 & 0 & 1 & 0 & 0\\
\frac{-k_s}{m_s} + \frac{-k_0}{m_s} & 0 & \frac{-c_{0a}}{m_s} & \frac{c_{0a}}{m_s} & \frac{-a_a}{m_s} & \frac{-f_{1(i)}}{m_s}\\
\frac{k_s}{m_u} + \frac{k_0}{m_u} & \frac{k_t}{m_u} & \frac{c_{0a}}{m_u} & \frac{-c_{0a}}{m_u} & \frac{a_a}{m_u} & \frac{f_{1(i)}}{m_u}\\
0 & 0 & A_d & -A_d & f_{2(i)} & 0\\
0 & 0 & 0 & 0 & 0 & -\eta
\end{bmatrix},$$

$$B_1 = [0 \quad -1 \quad 0 \quad 0 \quad 0 \quad 0]^T,$$

$$B_2 = [0 \quad 0 \quad 0 \quad 0 \quad 0 \quad \eta]^T,$$

where the values of $f_{1(1)}$ and $f_{1(2)}$ are f_{1max}; the ones of $f_{1(3)}$ and $f_{1(4)}$ are f_{1min}; $f_{2(1)}$ and $f_{2(3)}$ correspond to f_{2max}; and $f_{2(2)}$ and $f_{2(4)}$ correspond to f_{2min}, respectively.

4.2.2 State observer design

In terms of the quarter-car test rig, both the TD, $z_u - z_r$, and the SD, $z_s - z_u$, can be measured by laser displacement sensors; the SMA, $\ddot{z}_s$, and the unsprung mass acceleration (UMA), $\ddot{z}_u$, also can be measured by accelerometers. Therefore, the observer measurement is defined as

$$\begin{aligned} \mathrm{Y} &= [z_s - z_u \quad z_u - z_r \quad \ddot{z}_s \quad \ddot{z}_u]^T \\ &= \textstyle\sum_{i=1}^{4} h_i C_{1(i)} x \\ &= C_{1h} x, \end{aligned} \tag{4.12}$$

where

$$\mathrm{C}_{1(i)} = \begin{bmatrix} 1 & 0 & 0 & 0 & 0 & 0 \\ 0 & 1 & 0 & 0 & 0 & 0 \\ \frac{-k_s}{m_s} + \frac{-k_0}{m_s} & 0 & \frac{-c_{0a}}{m_s} & \frac{c_{0a}}{m_s} & \frac{-a_a}{m_s} & \frac{-f_{1(i)}}{m_s} \\ \frac{k_s}{m_u} + \frac{k_0}{m_u} & \frac{k_t}{m_u} & \frac{c_{0a}}{m_u} & \frac{-c_{0a}}{m_u} & \frac{a_a}{m_u} & \frac{f_{1(i)}}{m_u} \end{bmatrix}.$$

To effectively estimate the state by using the easily measured signals, the estimation error can be defined based on the observer measurement as

$$e = x - \hat{x}. \tag{4.13}$$

So, the state observer can be designed as

$$\begin{aligned} \dot{\hat{x}} &= \textstyle\sum_{i=1}^{4} h_i \left[A_{(i)} \hat{x} + L_{(i)} \left(Y - \hat{Y} \right) + B_2 u \right] \\ &= A_h \hat{x} + L_h \left(Y - \hat{Y} \right) + B_2 u, \end{aligned} \tag{4.14}$$

where $L_{(i)}$ are the state observer gains to be designed. Re-arrangement of Eq. (4.14) gives

$$\dot{\hat{x}} = (A_h - L_h C_{1h})\hat{x} + L_h Y + B_2 u. \tag{4.15}$$

By differentiating Eq. (4.13), we get the dynamic equation of the state estimation error

$$\begin{aligned} \dot{e} &= \dot{x} - \dot{\hat{x}} \\ &= (A_h - L_h C_{1h})e + B_1 w. \end{aligned} \tag{4.16}$$

4.2.3 TS fuzzy controller design

By applying the parallel distributed compensation scheme [125], the observer-based controller can be represented as

$$u = \sum_{i=1}^{4} h_i K_{(i)} \hat{x} = K_h \hat{x}, \tag{4.17}$$

where $K_{(i)}$ are the state feedback gains to be designed.

Now consider the augmented state vector as

$$\bar{x} = [x \quad e]^T. \tag{4.18}$$

After manipulation, the augmented system can be expressed as the following form:

$$\begin{aligned} \dot{\bar{x}} &= \sum_{i=1}^{4} h_i \left(\bar{G}_{(i)} \bar{x} + \bar{B}_1 w \right) \\ &= \bar{G}_h \bar{x} + \bar{B}_1 w, \end{aligned} \tag{4.19}$$

where

$$\bar{G}_h = \begin{bmatrix} A_h + B_2 K_h & -B_2 K_h \\ 0 & A_h - L_h C_{1h} \end{bmatrix},$$

$$\bar{B}_1 = [B_1^T \quad B_1^T]^T.$$

In order to improve the specific performances of the suspension, including ride comfort, suspension deflection and road holding ability, the controlled output s can

be composed of $\ddot{z}_s$, $z_s - z_u$, and $z_u - z_r$. Therefore, the controlled output is defined as

$$\begin{aligned} s &= [\sigma_1 \ddot{z}_s \quad \sigma_2(z_s - z_u) \quad \sigma_3(z_u - z_r)]^T \\ &= \sum_{i=1}^{4} h_i \bar{C}_{2(i)} \bar{x} \\ &= \bar{C}_{2h} \bar{x}, \end{aligned} \tag{4.20}$$

where

$$\bar{C}_{2(i)} = \begin{bmatrix} \frac{-\sigma_1 k_s}{m_s} + \frac{-\sigma_1 k_0}{m_s} & 0 & \frac{-\sigma_1 c_{0a}}{m_s} & \frac{\sigma_1 c_{0a}}{m_s} & \frac{-\sigma_1 a_a}{m_s} & \frac{-\sigma_1 f_{1(i)}}{m_s} & 0_{1\times 6} \\ \sigma_2 & 0 & 0 & 0 & 0 & 0 & 0_{1\times 6} \\ 0 & \sigma_3 & 0 & 0 & 0 & 0 & 0_{1\times 6} \end{bmatrix}.$$

In order to give the controller adequate response performance under different vibration situations, the H_∞ norm is chosen as the performance measure. The L_2 gain of the system Eq. (4.19) with Eq. (4.20) is defined as

$$\|T_{sw}\|_\infty = \sup_{\|w\|_2 \neq 0} \frac{\|s\|_2}{\|w\|_2}, \tag{4.21}$$

where $\|s\|_2^2 = \int_0^\infty s^T(t)s(t) \cdot dt$ and $\|w\|_2^2 = \int_0^\infty w^T(t)w(t) \cdot dt$. The aim of the work is to design a fuzzy controller Eq. (4.17) such that the closed-loop fuzzy system Eq. (4.19) is quadratically stable. A Lyapunov function for the system Eq. (4.19) is defined as

$$\Pi(x) = \bar{x}^T P \bar{x}, \tag{4.22}$$

where P is a positive definite matrix and $P = P^T$. By differentiating Eq. (4.22), we obtain

$$\dot{\Pi}(x) = \dot{\bar{x}}^T P \bar{x} + \bar{x}^T P \dot{\bar{x}}. \tag{4.23}$$

Adding $s^T s - \gamma^2 w^T w$ to the two sides of Eq. (4.23) yields

$$\dot{\Pi}(x) + s^T \mathrm{s} - \gamma^2 w^T w = \dot{\bar{x}}^T P\bar{x} + \bar{x}^T P\dot{\bar{x}} + s^T \mathrm{s} - \gamma^2 w^T w. \tag{4.24}$$

Substituting Eq. (4.19) and Eq. (4.20) into Eq. (4.24) gives

$$\dot{\Pi}(x) + s^T \mathrm{s} - \gamma^2 w^T w = (\bar{G}_h\bar{x} + \bar{B}_1 w)^T P\bar{x} + \bar{x}^T P(\bar{G}_h\bar{x} + \bar{B}_1 w) + (\bar{C}_{2h}\bar{x})^T(\bar{C}_{2h}\bar{x}) - \gamma^2 w^T w. \tag{4.25}$$

Re-arrangement of Eq. (4.25) gives

$$\dot{\Pi}(x) + s^T \mathrm{s} - \gamma^2 w^T w = \begin{bmatrix}\bar{x}^T \\ w^T\end{bmatrix}^T \begin{bmatrix}\bar{G}_h{}^T P + P\bar{G}_h + \bar{C}_{2h}^T\bar{C}_{2h} & P\bar{B}_1 \\ * & -\gamma^2\end{bmatrix}\begin{bmatrix}\bar{x} \\ w\end{bmatrix}. \tag{4.26}$$

Considering

$$\Psi = \begin{bmatrix}\bar{G}_h{}^T P + P\bar{G}_h + \bar{C}_{2h}^T\bar{C}_{2h} & P\bar{B}_1 \\ * & -\gamma^2\end{bmatrix}, \tag{4.27}$$

when the disturbance is zero, that is, $w = 0$, it can be inferred from Eq. (4.26) and Eq. (4.27) that if $\Psi < 0$, then $\dot{\Pi}(x) < 0$, and the closed-loop fuzzy system Eq. (4.19) is quadratically stable. By considering Schur complement equivalence [126], Eq. (4.27) can be further re-arranged to linear matrix inequalities (LMI), as given below:

$$\Psi = \begin{bmatrix}\bar{G}_h{}^T P + P\bar{G}_h & \bar{C}_{2h}^T & P\bar{B}_1 \\ * & -\mathrm{I} & 0 \\ * & * & -\gamma^2\end{bmatrix} < 0. \tag{4.28}$$

By solving the LMIs using MATLAB® software, the state feedback $\mathrm{K}_{(i)}$ gains and the observer gains $L_{(i)}$ of the SOTSFC are determined.

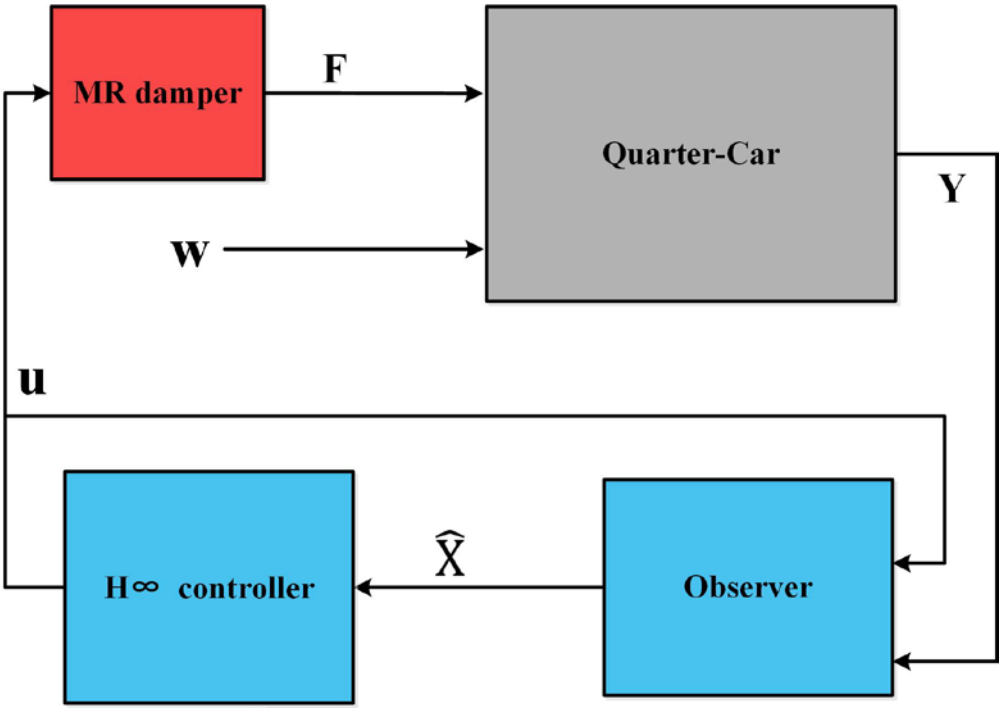

Figure 4.2 Components of semi-active suspension control system model.

After constructing the controller, the TS fuzzy model is left aside in the experiment and the closed-loop system is shown in Figure 4.2.

4.2.4 Numerical application of the controller

In this section, we will validate the effectiveness of the designed controller in simulation. To validate the performance of the SOTSFC, the skyhook controller and the groundhook controller [127, 128] are adopted for a comparison. Skyhook control and groundhook control are often regarded as benchmark control strategies and used to validate any new control strategies for vehicle suspension with MR damper. The skyhook controller defines the desired damping force as

$$F_{sky} = \begin{cases} c_{sky}\dot{z}_s, & \dot{z}_s(\dot{z}_s - \dot{z}_u) \geq 0, \\ c_{min}\dot{z}_s, & \dot{z}_s(\dot{z}_s - \dot{z}_u) < 0, \end{cases} \tag{4.29}$$

where c_{sky}, c_{min} are the maximum and minimum skyhook gains, which correspond to the command voltages u_{sky} and u_{min}, respectively. The groundhook controller defines the desired damping force as

$$F_{ground} = \begin{cases} c_{ground}\dot{z}_s, & -\dot{z}_u(\dot{z}_s - \dot{z}_u) \geq 0, \\ c_{min}\dot{z}_s, & -\dot{z}_u(\dot{z}_s - \dot{z}_u) < 0, \end{cases} \tag{4.30}$$

where c_{ground} is the groundhook gain. In this experiment, the specific skyhook force and groundhook force are expressed as the MR damper force with the control output voltage, $u_{sky} = 2.5$ V or 0 V and $u_{ground} = 2.7$ V or 0 V.

In order to directly evaluate the SOTSFC performance with respect to ride comfort, suspension deflection, and road holding, the evaluation of the suspension is based on the sprung mass acceleration, the suspension deflection, and the dynamic tyre deflection under 2.25 Hz sinusoidal excitation with 0.01m amplitude. The suspension responses in time domain are shown in Figures 4.3-4.5.

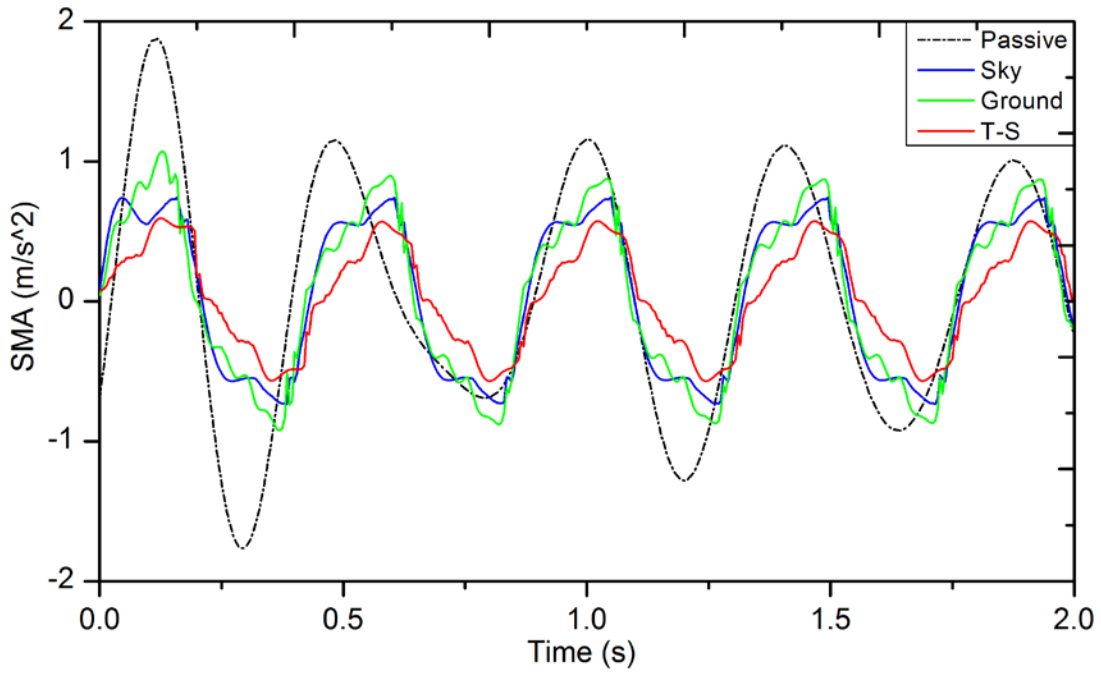

Figure 4.3 Sprung mass acceleration response at 2.25 Hz in time domain.

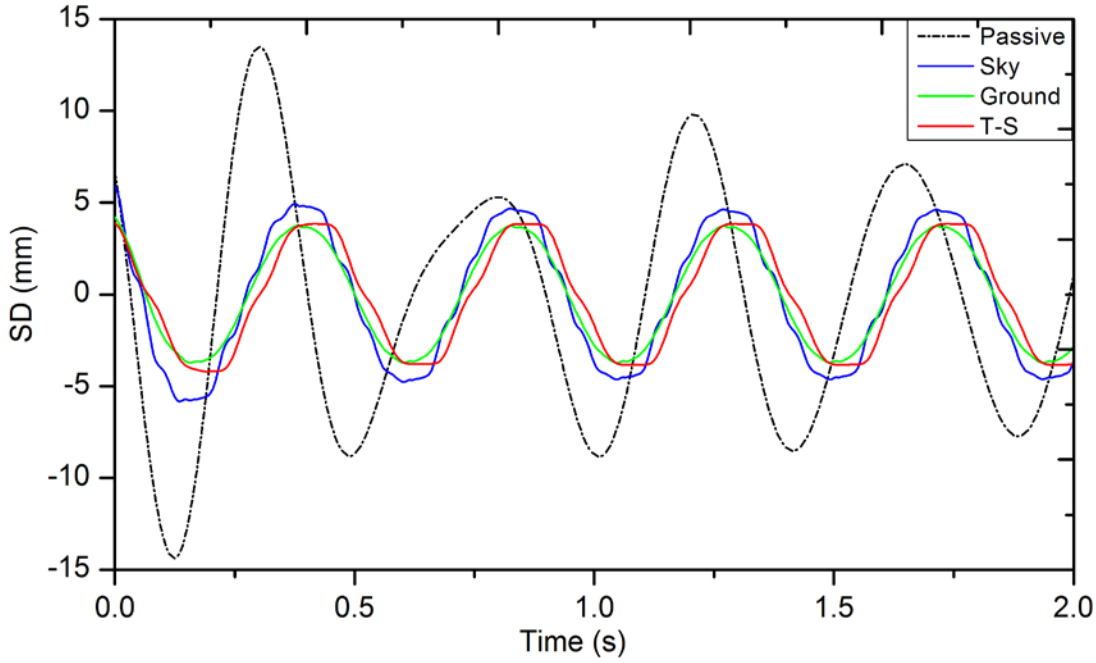

Figure 4.4 Suspension deflection at 2.25 Hz in time domain.

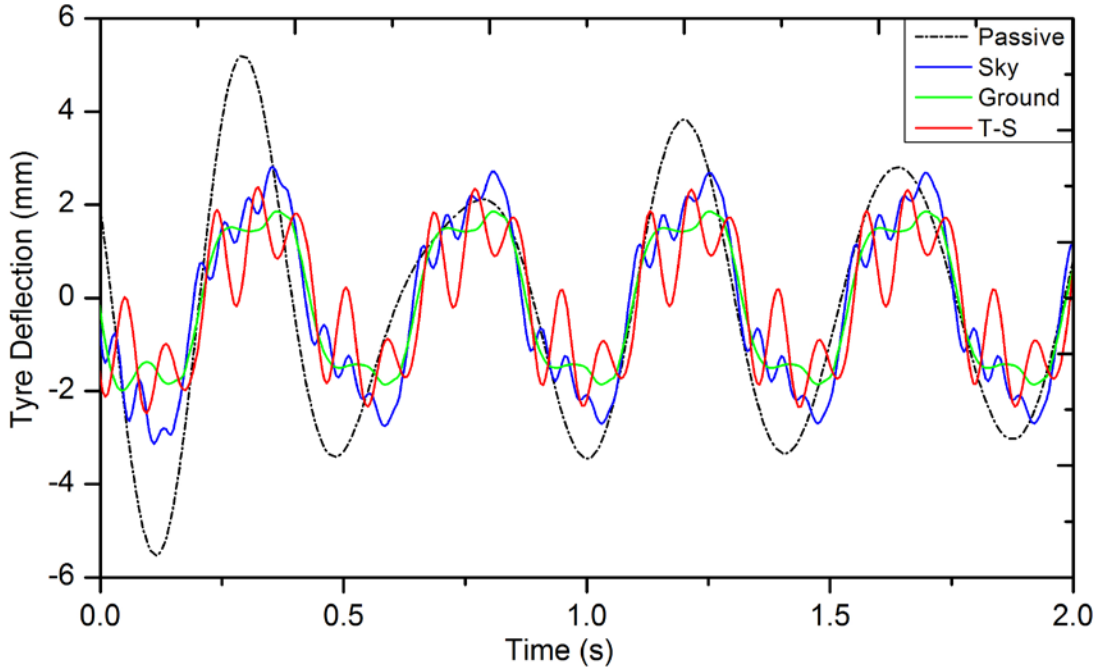

Figure 4.5 Tyre deflection at 2.25 Hz in time domain.

Figure 4.3 presents the SMA value obtained by applying the specific sinusoidal excitations with the PTP amplitude of 0.01m at frequency 2.25 Hz. From the time history of the acceleration shown in the figure, it can be seen that the object reduction performed by the TS fuzzy control is the best one among the other three, passive, groundhook, and skyhook control. The performance of TS fuzzy controller in suspension deflection is as good as the one of groundhook controller, which is shown in Figure 4.4. The same result in regard to tyre deflection can be obtained in Figure 4.5, that the TD amplitude of TS fuzzy is similar to the value of groundhook control but with bigger variance.

4.3 The test system setup

The MR damper used in this research was tested on a 2-DOF quarter-car test rig. The structure of the test rig is shown in Figure 4.6. The measured primary parameters of the quarter-car test rig are $k_s = 16905\ \mathrm{N/m}$, $k_t = 179000\ \mathrm{N/m}$, $m_s = 257.6\ \mathrm{kg}$, $m_u = 33.2\ \mathrm{kg}$, $c_s = 800\ \mathrm{N\,s/m}$. The tyre is excited by a vertical road profile generated by a hydraulic system manufactured by the CRAM Corporation. The hydraulic actuator is controlled by the real-time control board (Model: myRio-1900, NI Corp.) with a PID controller. Acting as the external disturbance of the system, the imposed road profile displacement z_r is measured by a laser displacement sensor (Model: LB-11, Keyence Corp.) and sent to the PID controller for the close-loop control.

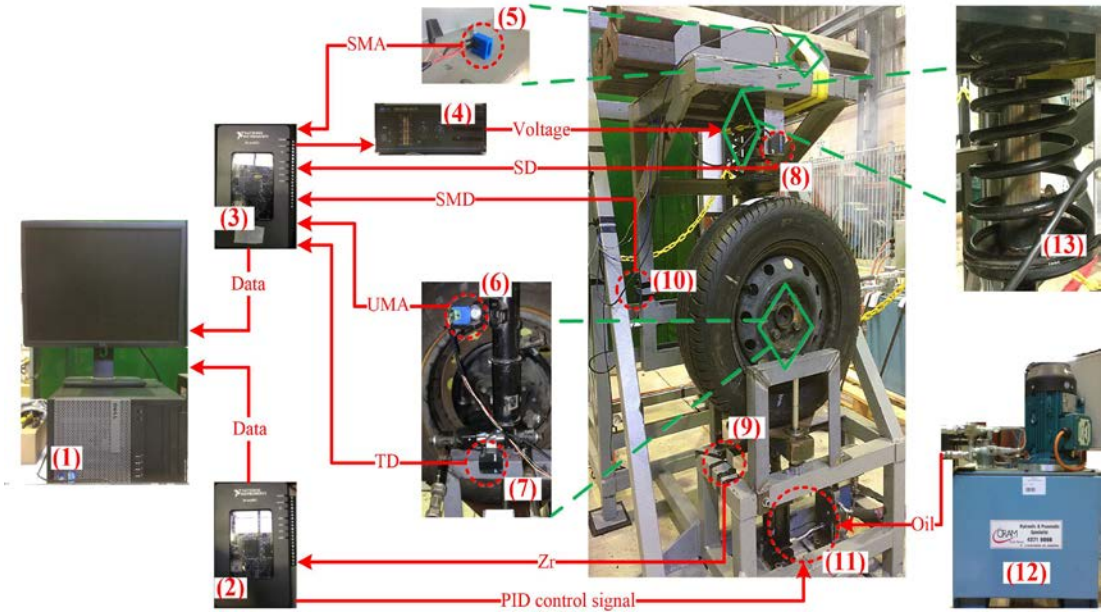

Figure 4.6 Test rig setup (1) computer, (2) NI real-time control board Ⅰ, (3) NI real-time control board Ⅱ, (4) power amplifier, (5,6) accelerometer, (7-10) laser sensors, (11) hydraulic actuator, (12) hydraulic station, (13) the suspension with OMRD.

Regarding the MR damper control, it is a multi-input-single-output (MISO) system. Specifically, three displacement input signals, the sprung mass displacement (SMD), the TD, and the SD, are measured by the three laser sensors (Model: LB-01, Keyence Corp.); and two acceleration input signals, the SMA and the UMA, are measured by the two accelerometers (Model: ADXL327, Analog Devices Corp.). Please note that the signals TD, SD, SMA, and UMA are the inputs of the TS fuzzy controller; the SD and the absolute displacement SMD are the inputs of the digital differentiator to generate the velocities for the referenced skyhook controller. By running the control algorithm based on these inputs, the real-time control board Ⅱ (Model: myRio-1900, NI Corp.) calculates the command voltage and sends it to a power amplifier. After amplifying the power, the voltage u considered as the system output will be sent to the MR damper.

In the first stage of the experiment, a constant amplitude sinusoidal excitation (0.01 m peak to peak amplitude of the harmonic motion) in the frequency range 0.5-2.75 Hz, which contains the sprung mass resonant frequency, with 0.25 Hz step is applied. To verify the performance of the SOTSFC, the SMA transmissibility is measured. The vertical vibration transmissibility of sprung mass is taken as the ratio of $\ddot{z}_s$ to $\ddot{z}_r$ at each excitation frequency. Then, two typical road profiles are considered in the experiment. A bump input, which is normally used to describe the transient response characteristic, is adopted as the first road excitation. The corresponding road displacement is given by

$$z_r(t) = \begin{cases} \frac{a}{2}\left[1 - \cos\left(\frac{2\pi v_0}{l}t\right)\right], & 0 \le t \le \frac{l}{v_0}, \\ 0, & t > \frac{l}{v_0}, \end{cases} \tag{4.31}$$

where $a = 0.035$ m and $l = 0.8$ m are chosen as the height and length of the bump, and the vehicle forward velocity as $v_0 = 0.856\, m/s$.

The second type of road excitation, normally used to evaluate frequency response, is a random road excitation. The standard C class road profile (ISO 8608), with $S_q(\Omega_o) = 4 \times 10^{-6}\ m^3$, is generated with a sinusoidal approximation method [129]. The road irregularities can be described by the following equation

$$z_r(t) = \sum_{i=1}^{n}\left(\sqrt{2S_q(i\Delta\Omega)\Delta\Omega}\right)\sin(i2\pi\Delta\Omega v_r t + \varphi_i), \tag{4.32}$$

where φ_i is the random numbers distributed uniformly among $[0,2\pi]$, $\Delta\Omega$ is the minimum spatial frequency value we considered, which equals to $0.011m^{-1}$. In this experiment, the vehicle is assumed to travel with a constant speed $v_r = 10$ m/s over a given road segment.

For the design of a vehicle suspension, ride comfort, suspension deflection and road holding ability are often regarded as the main optimizing goal in a controller design

[54]. In this test, the weighting parameters of the controlled outputs are set as $\sigma_1 = 0.7, \sigma_2 = 0.1, \sigma_3 = 0.2$ with suitable trade-off.

4.4 Experimental results

By applying the three kinds of road profiles to the tyre, the responses of the conventional passive suspension (Model: 48540-02080, Toyota Corp.), the MR suspension with skyhook controlled and the MR suspension with the SOTSFC controlled are evaluated.

4.4.1 Sinusoidal excitation case

Figure 4.7 presents the transmissibility of the passive suspension and TS fuzzy controlled one under sinusoidal frequency swept excitation. It can be seen that the transmissibility measured on the passive suspension shows a peak at 2.25 Hz, which is the resonance frequency of the sprung mass. The passive suspension acts as a low-pass filter which means that reducing the acceleration transmissibility around the sprung mass resonance frequency is difficult. However, the semi-active one exhibits more than 60% lower vibration transmissibility than the conventional suspension, as shown in Figure 4.7. Specifically, when the excitation frequency is close to the resonance frequency, the SOTSFC has a better performance than the skyhook control strategy for SMA transmissibility.

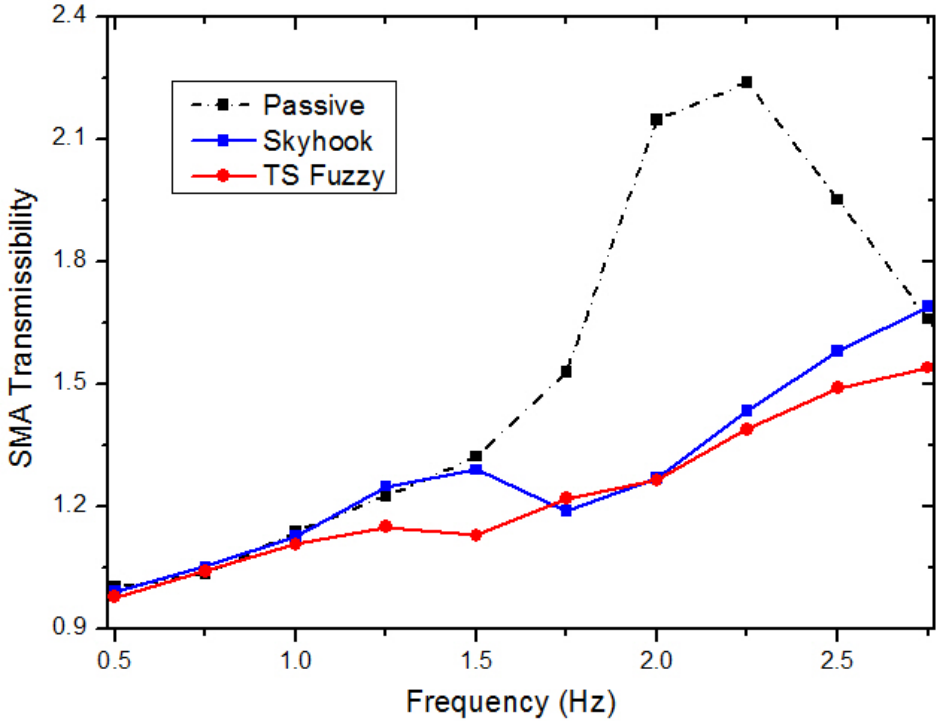

Figure 4.7 Acceleration transmissibility in frequency domain.

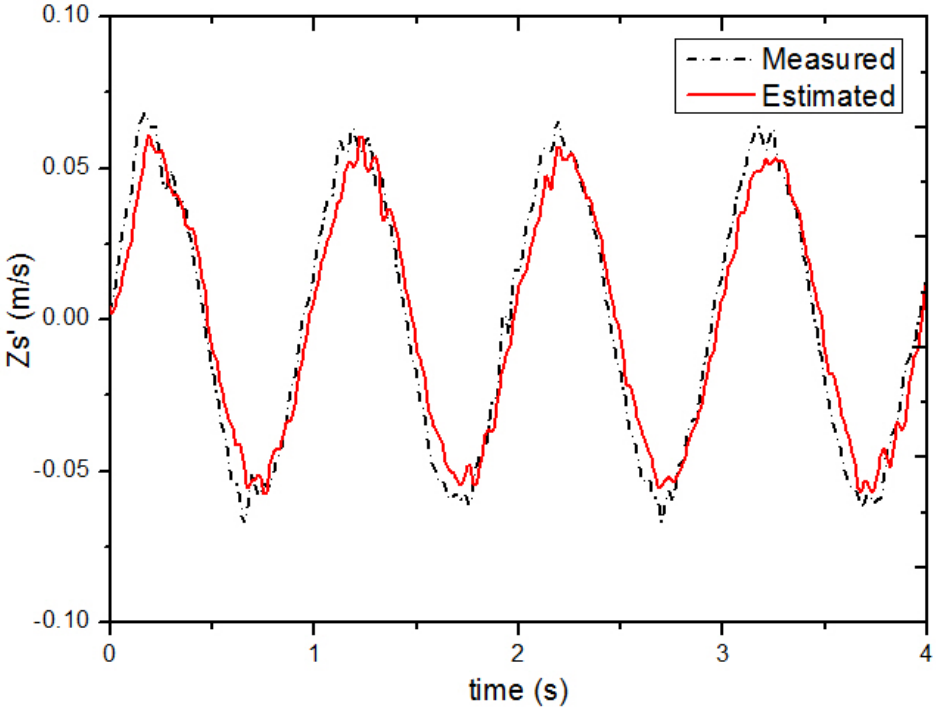

Figure 4.8 Observer estimation result under 2 Hz sinusoidal excitation.

The estimation result of the sprung mass velocity, $\dot{z}_s$, is plotted in Figure 4.8. From the estimation result, it can be illustrated that the state observer could estimate the

waveform of the suspension state precisely but with a signal time delay which is about 0.05s.

4.4.2 Bump road case

In the second stage of the experiment, bump road is carried out to evaluate the systems. Time histories of the test rig response in terms of the three performance criteria are plotted in Figure 4.9.

The input voltages for the two controlled systems are compared in Figure 4.10. The control voltage calculated by the skyhook controller can only be 0 and u_{max}. However, the one computed by the SOTSFC can vary continuously between 0 andu_{max}.

In order to illustrate the experimental results more clearly, the response of the three suspensions were compared in terms of the peak-to-peak (PTP) values and the results are shown in Table 4.1. The improved percentages are compared to the conventional passive suspension. It can be seen from Table 4.1 that the two controlled MR suspensions perform similar effects on peak values for SMA, and the responses of skyhook and SOTSFC are similar and much outstanding smaller than that of conventional suspension. Regarding the time response shown in Figure 4.9(c), the PTP value of tyre load fluctuation of SOTSFC is smaller than those of passive and skyhook by approximately 15% and 14%, respectively. To further show the improved suspension performance, another comparison is indirectly made with the results obtained by a published observer-based semi-active suspension control system. In [130], a state observer-based sliding mode controller was designed for a hydro-pneumatic semi-active suspension, where the reductions on the PTP values of SMA, SD, and TD under bump road excitation were achieved by 4%, 19%, and 4%, respectively, comparing to the passive system.

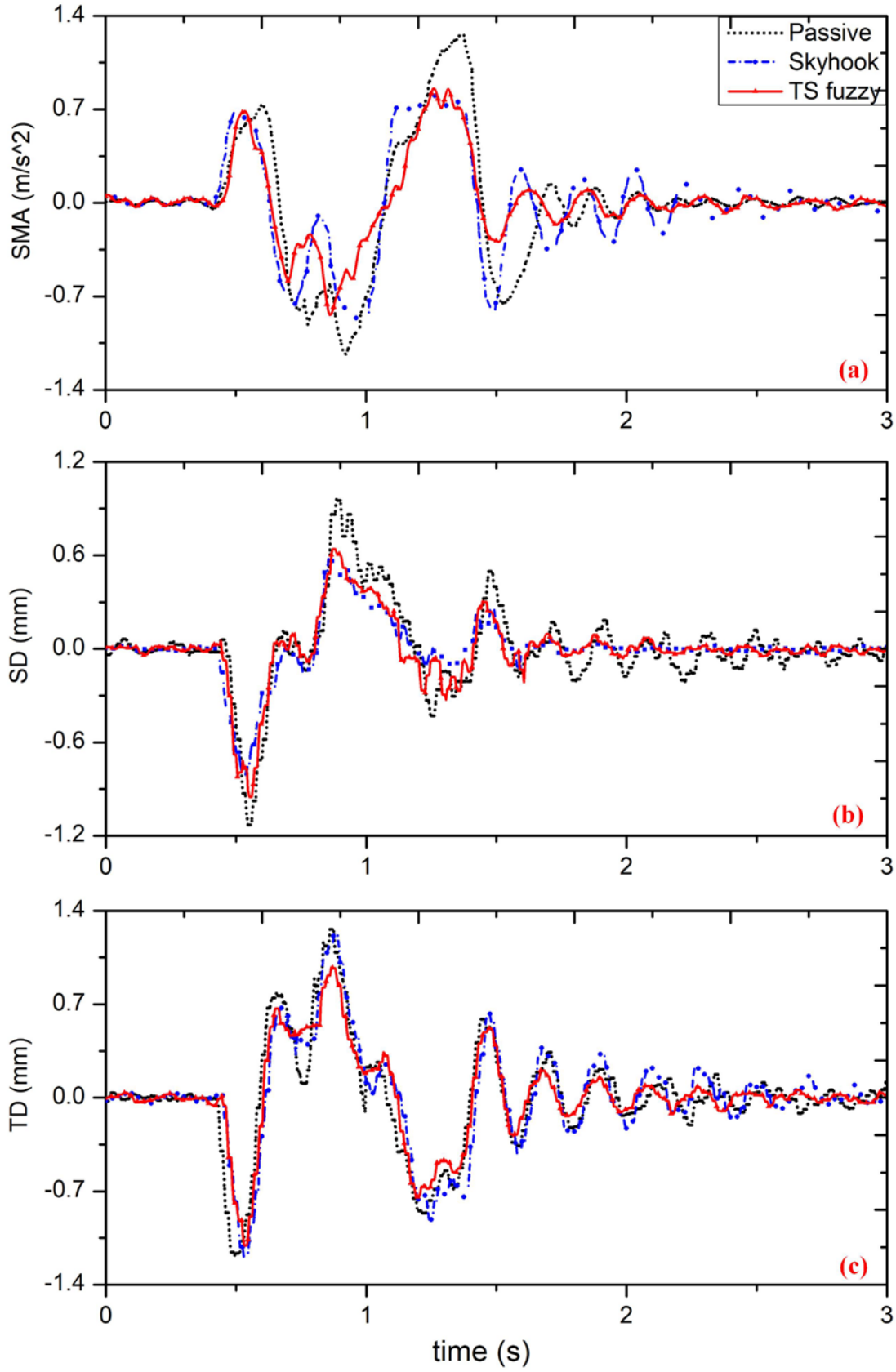

Figure 4.9 Response under bump road excitation: (a) response of SMA; (b) response of SD; (c) response of TD.

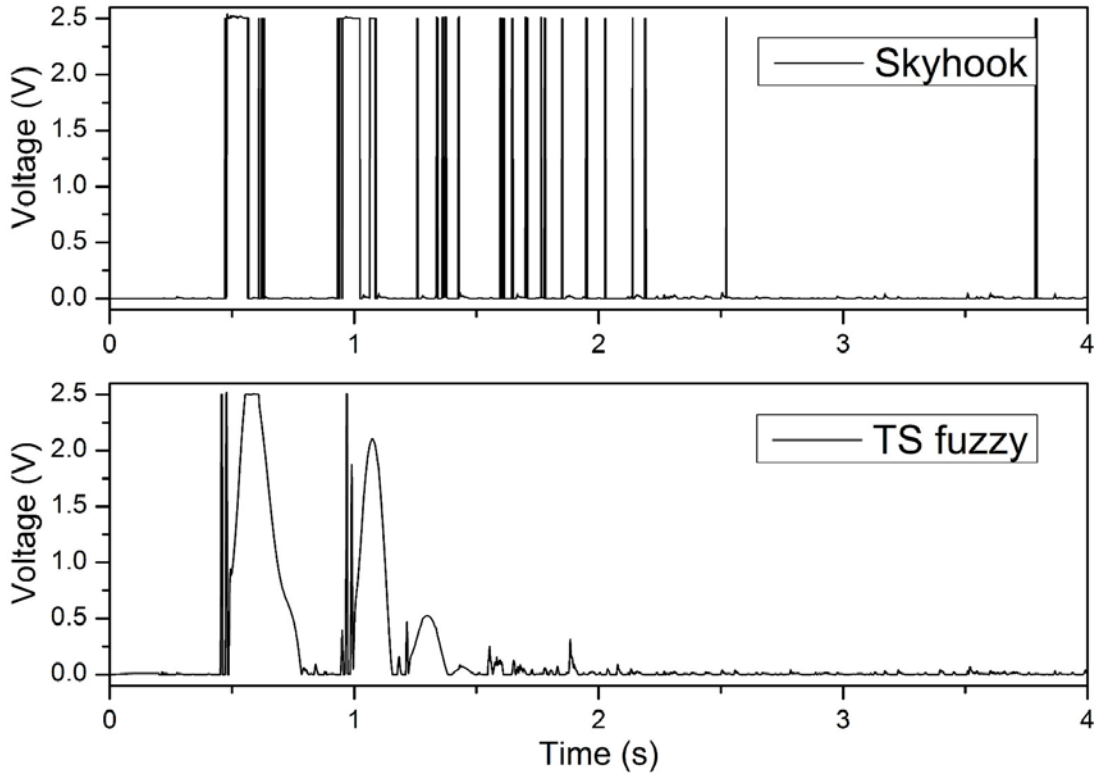

Figure 4.10 Input voltages under bump road excitation.

Regarding the proposed SOTSFC, the reductions on the three objectives are about 28%, 23%, and 14% compared to the passive system, respectively. The results confirm that the improved bump responses are achieved by the TS fuzzy control approach.

Table 4.1 PTP value of the response under bump road excitation

Object	Passive	Skyhook	TS Fuzzy
SMA (m/s^2)	2.388	1.673	1.696
%	N/A	-29.93	-28.99
SD (mm)	2.087	1.389	1.590
%	N/A	-33.41	-23.79
TD (mm)	2.443	2.419	2.079
%	N/A	-0.97	-14.86

4.4.3 Random road case

Time histories of the test rig response to random road excitation are plotted in Figure 4.11, where only the results of passive suspension and the one controlled by TS fuzzy are shown in the figure for clarity. The SOTSFC has limited the objectives and inhibited their variation. The applied voltage to MR damper by different controllers is plotted in Figure 4.12 for comparison.

The RMS values of the system responses are summarized in Table 4.2 and it can be seen that the controlled MR suspension with the SOTSFC has lower RMS value of the SMA. In particular, the semi-active suspension controlled by the TS fuzzy controller can reduce the RMS values for SMA, SD, and TD by about 14%, 30%, and 10%, respectively, compared with the conventional passive suspension. The SMA and TD reductions (-13.58% and -10.70%) of TS fuzzy control are much more effective than the ones of the typical skyhook control (-5.68% and +5.10%), of which TD even fails than the passive suspension.

Table 4.2 RMS value of the response under random road excitation

Object	Passive	Skyhook	TS Fuzzy
SMA (m/s^2)	3.415	3.221	2.951
%	N/A	-5.68	-13.58
SD (mm)	1.143	0.668	0.799
%	N/A	-33.18	-30.15
TD (mm)	1.153	1.212	1.029
%	N/A	+5.10	-10.70

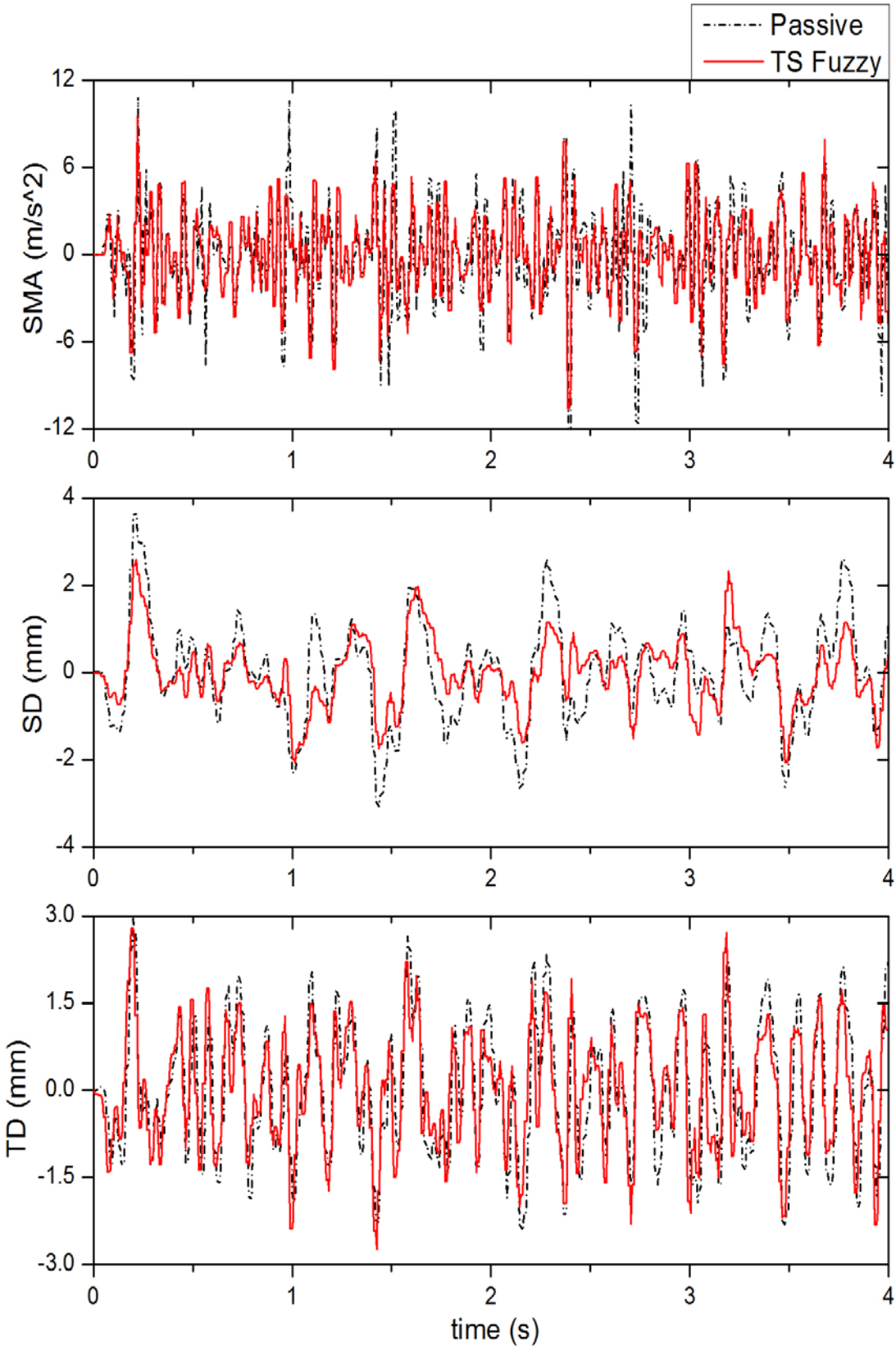

Figure 4.11 Response under random road excitation: (a) response of SMA; (b) response of SD; (c) response of TD.

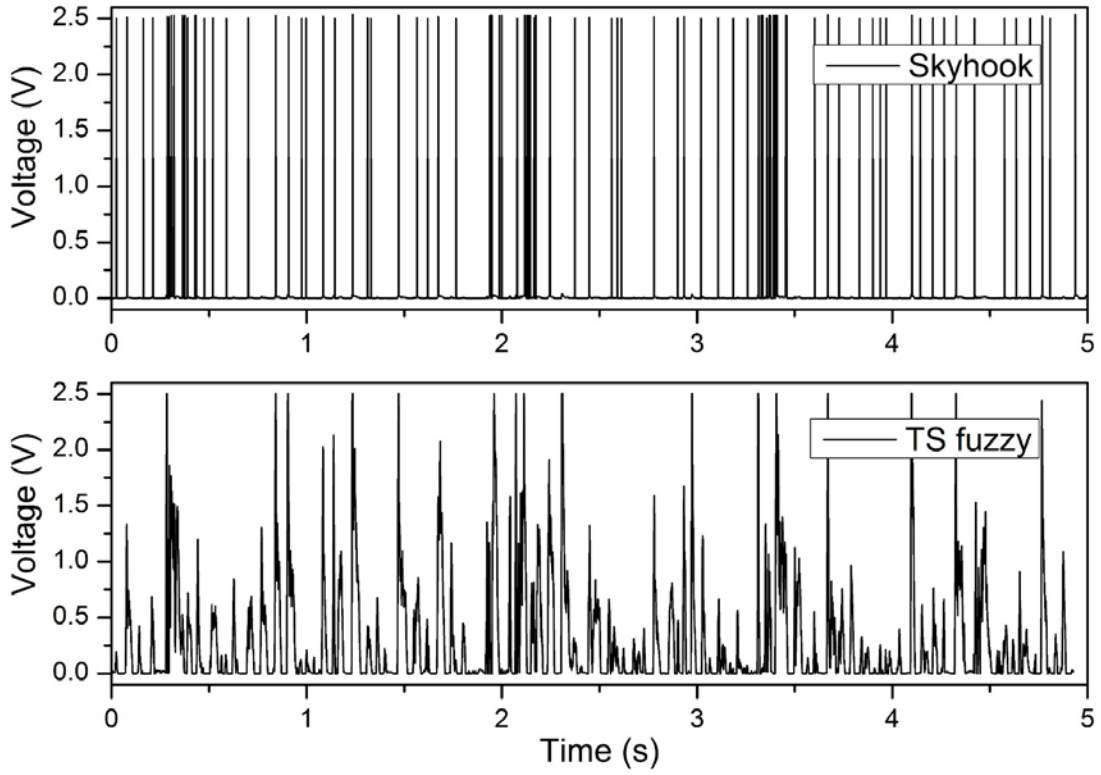

Figure 4.12 Input voltages under random road excitation

The indistinctive effect of skyhook control might be attributed by its nature that it can provide a remarkable attenuation benefit around the body resonance frequency (located at about 2 Hz); whereas beyond that frequency, the filtering performance of the skyhook control strategy are similar to, or even worse than those of the conventional passive suspensions [127]. On the other hand, the TS fuzzy controller can have a better performance than the traditional skyhook semi-active control in a wider frequency range. Therefore, it could present a better performance under excitation with multi-frequency components. In [72], a robust fuzzy logic controller was designed and verified by road testing on a real vehicle with MR suspension. The experimental results showed that the semi-active suspension controlled by the fuzzy logic controller can reduce the RMS value of SMA under random road excitation by about 6% compared to the passive system, which is not as effective as the one of the

proposed controller (13%). By comparing the results, it is further confirmed that good random response is achieved by the TS fuzzy control approach.

4.5 Conclusion

In this chapter, a state observer-based TS fuzzy controller was designed and investigated experimentally. To build the controller, a TS fuzzy model of the quarter-car semi-active suspension was proposed and applied Considering practical application, a state observer was established to estimate the system state in real-time. A quarter-car test rig equipped with the OMRD was constructed for the test. Experimental results under different road excitations were measured. The results demonstrate that the state observer-based TS fuzzy controller outperforms the other control algorithms.

5 A NEW VARIABLE STIFFNESS AND VARIABLE DAMPING VEHICLE SUSPENSION BASED ON MR DAMPERS

5.1 Introduction

The previous chapter focus on improving the performance of vehicle suspension by changing damping with MR technology. In order to further enhance the vibration reduction performance of the vehicle, an innovative compact variable sampling and stiffness damper was designed by our research group [11]. However, small variation range of damping limits the prototype to be used onto a real car.

In order to verify the effectiveness of this structure on a real vehicle structure, a full-size VSVD suspension was further designed, fabricated, and tested in this chapter. The advanced suspension can be easily installed into a vehicle suspension system without any change to the original configuration. the specific contents of this chapter are introduced as following. The structure and design of the full-size VSVD suspension will be presented. The property test of the prototype will be conducted and analysed in Sections 5.3 and 5.4. Section 5.6 presents A new 3-DOF phenomenological model to further accurately describe the dynamic characteristic of the VSVD suspension. The performance of quarter-car with variable stiffness and damping suspension will be evaluated numerically in Section 5.6. The conclusion is drawn in Section 5.7.

5.2 Design of the suspension

5.2.1 Structure design

A schematic view of the hybrid suspension shown in Figure 5.1 indicates that it consists of two parts: an MR variable stiffness unit and an MR variable damping unit. The advanced MR suspension mainly consists of two coaxial damping cylinders and

two springs with different stiffness. The damping cylinder (cylinder 1) is composed of a piston, electromagnetic coils, floating piston and an accumulator spring.

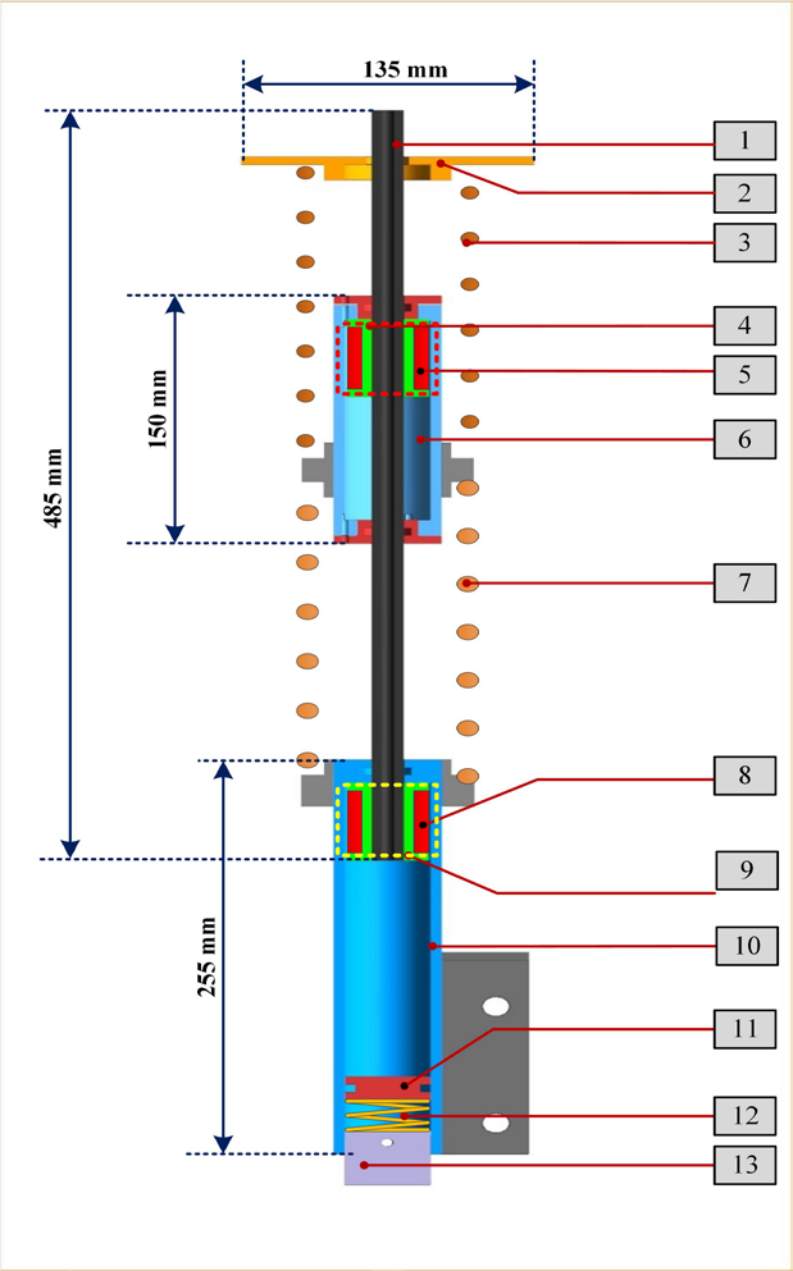

Figure 5.1 Schematic of VSVD suspension (1) shaft, (2) top cover, (3) spring 1, (4) upper piston, (5) coil for stiffness, (6) cylinder 2, (7) spring 2, (8) coil for damping, (9) cylinder 1, (10) lower piston, (11) floating piston, (12) accumulator spring, (13) bottom block.

The stiffness cylinder is composed of the upper piston, wired with electromagnetic coils, the cylinder 2, which connects the top and bottom sealing block, and the fixed block 2, which links the upper and lower springs. Both two cylinders are filled with MRF. The electromagnetic coils extend generally coaxially around the piston. The red dash lines in Figure 5.1 illustrate the magnetic circuit generated by the coils in the stiffness cylinder 2. The damping force of the cylinder is controlled by the applied magnetic field on the basis of MRF properties. The lower damping cylinder 1 is more like to a classic MR damper. Its magnetic circuits are shown by the yellow dash lines in the figure. The two cylinders may have relative sliding motions under the external excitations.

5.2.2 Working principle

The working principle of the variable stiffness and damping suspension can be demonstrated by Figure 5.2, where three different connection modes of this device are shown. When the current I_2 applied to the upper stiffness cylinder 2 is small enough, the cylinder's damping force will allow the relative motion between the shaft and cylinder 2. In this case, the VSVD suspension is working in connection mode 1 where the spring k_1 and the spring k_2 work in series because both springs deform when the cylinder 2 slides along the shaft. When the current I_2 becomes bigger, the device will work in connection mode 2. In this working mode, the larger damping force makes the sliding motion between the cylinder 2 and shaft harder and slower. It is equivalent to the growth of stiffness value of the spring k_2. Furthermore, when the upper cylinder's damping force is large enough to prevent the relative motion between the cylinder and the centre shaft, the VSVD suspension is working in connection mode 3, because only spring k_1 will have a deformation in response to the external force. The

determination of connection mode is controlled by the magnitude of the upper damping force, which is determined by the amount of the input current I_2. The stiffness variability, therefore, is realised by the switch between the connection modes.

The damping variability is realized by adjusting the current I_1 applied to the lower damping cylinder 1. As shown in Figure 5.2, no matter which connection mode the VSVD suspension is, the overall equivalent damping is represented by the damping c_1. c_1 increases as the current I_1 applied to the cylinder 1 increases. In summary, the effective stiffness of the proposed VSVD suspension is controlled by current I_2 and the equivalent damping is controlled independently by current I_1.

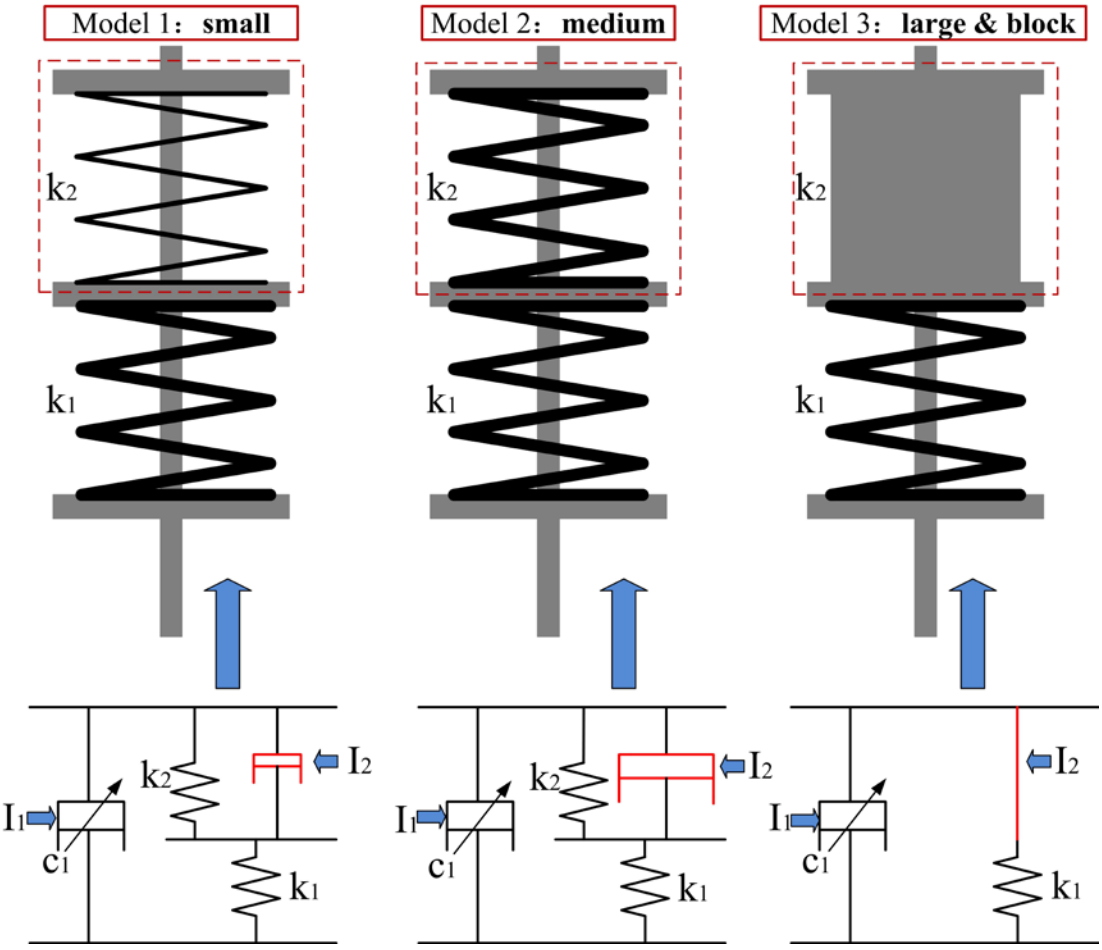

Figure 5.2 Scheme of the VSVD suspension connection mode.

5.3 Prototype and test of the dynamic performance

5.3.1 Prototype of the VSVD suspension

The first step in the assembly of the VSVD suspension was to prepare two sets of electromagnetic coils for two damping cylinders, respectively. MRF (MRF-132DG, LORD Corporation) was then poured into the reserve of the cylinder 1 after the shaft was inserted into the cylinder. Then, a floating piston and a small spring serving as the accumulator with approximately 280N preload was mounted between the piston rod and the bottom block in order to provide enough pre-pressure on the MRF inside the cylinder 2. As follow up, MRF was also poured into the reserve of the cylinder 2. The two sealing blocks were added onto the top and bottom of the cylinder 2 for sealing the MRF inside a closed reserve. In the last step, two fixed blocks were added on the two cylinders surface. Spring 2 was then mounted connecting the cylinder 1 and cylinder 2; Spring 1 was mounted connecting the cylinder 2 and the top cover. Table 5.1 shows the details of the two springs whose parameters were designed based on the optimization result in Chapter 3. the assembled VSVD suspension is shown in Figure 5.3.

Table 5.1 Parameters of the two springs

Parameter	Spring 1	Spring 2
Stiffness (N/m)	29976	38500
No. of active coils	5	6
Free Length (mm)	190	190
Inside Diameter (mm)	60	60
Outside Diameter (mm)	76	80

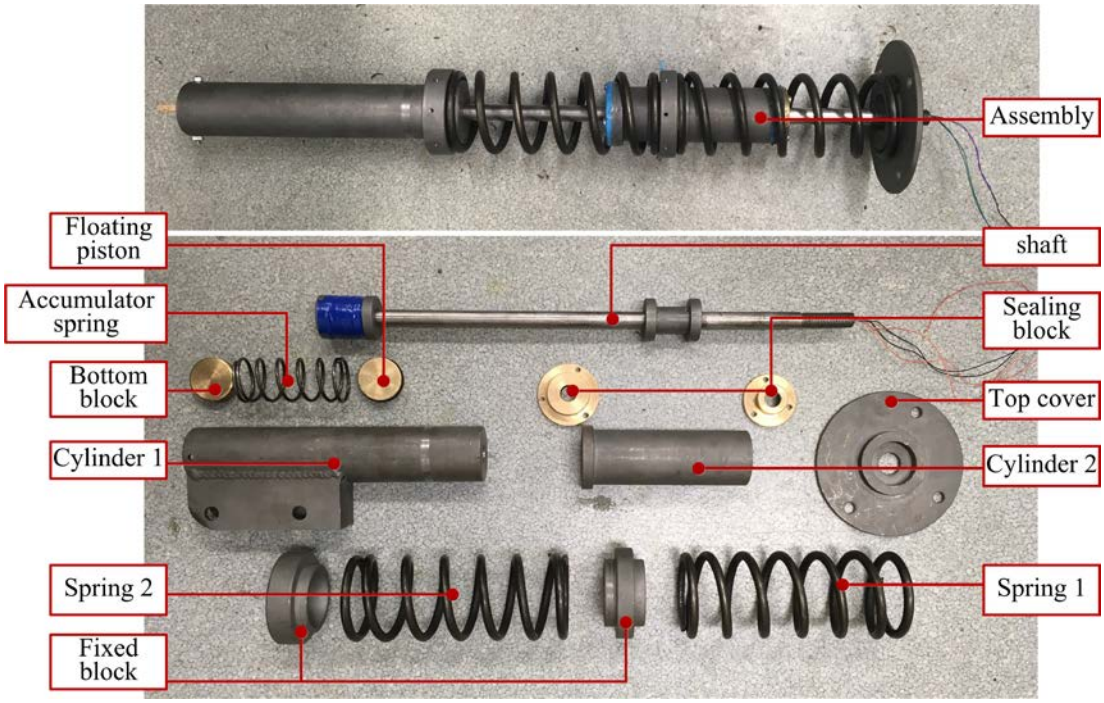

Figure 5.3 Photo of the VSVD suspension prototype.

5.3.2 Test setup for the tensile experiment

As shown in Figure 5.4, a computer-controlled INSTRON machine was used to test the dynamic performance of the VSVD suspension. The INSTRON machine has upper and lower head with grippers that can hold the device in place. The upper head is fixed to the top base and the lower head, which is excited by the hydraulic cylinder, can move up and down at different speeds. A LVDT was also integrated in the lower hydraulic actuator. Furthermore, a Force transducer was mounted over the lower head to measure the force generated by the VSVD suspension. Once the VSVD suspension was mounted on the INSTRON machine using two ends connectors, a predefined routine was programmed into the control software in order to maintain consistency in the testing. Sufficient cycles were measured for each single loading case to ensure the performance stability and uniformity. In summary, the Hydraulic actuator obtained the excitation signal from the software to activate the lower head. The excitation path was

programmed in the software and the force signal generated by the VSVD suspension was measured through the force transducer and then transferred to the computer for recording via a data acquisition board.

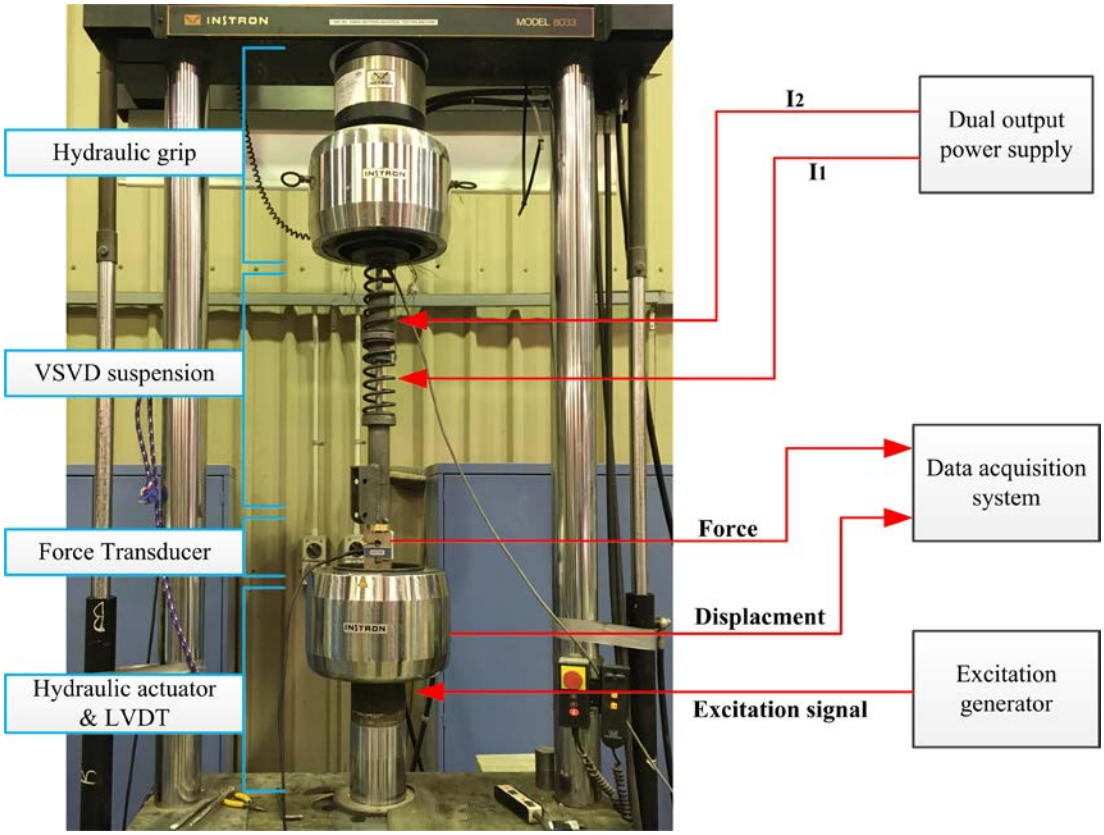

Figure 5.4 Lab-testing rig for tensile experiment.

The properties of stiffness variability and damping variability were tested separately. The excitation signal chosen was a sinusoidal wave with a single frequency of 0.3 Hz and amplitude of 13.75 mm. To obtain the performance in terms of the variable stiffness of the device, the current I_2 applied to the cylinder 2 was varied from 0 to 0.4 A with a step of 0.2 A, while the damping control current I_1 applied to the cylinder 1 was set as 0 A. On the other hand, the current I_1 applied to the cylinder 1 was set to 0, 0.5, 1 A, respectively, with the external current maintained as a constant of 0.25 A to demonstrate the performance of variable damping. In addition to studying the

field-dependent properties, the effectiveness of changing frequency on the device performance is also investigated. In this test, the loading frequency was set to 0.1, 0.3, and 0.5 Hz, respectively.

5.4 Results and discussion

5.4.1 Stiffness variability testing

Figure 5.5 shows a series of stable force-displacement loop under the condition of $I_1 = 0$ A and $I_2 =$ 0 A, 0.2 A, and 0.4 A, respectively. For each case, one cycle was provided to show the device performance for brevity. The test results in the figure show that the output force is a piecewise curve vs. the input displacement in a clockwise direction. In order to analyse the meaning of the force-displacement loop shape and the corresponding working state of the instrument, the dynamic response under the excitation current of $I_1 = 0$ A and $I_2 = 0.2$ A was taken as an example, which is shown by the red line in the figure. Meanwhile, six red letters are placed clockwise at the inflection point of the curve.

For the reason that there exists an initial damping force from the cylinder 2 although on current applied to it, an external force large enough to overcome the internal damping force so as to allow the relative motion between the shaft and the cylinder 1 is requested, which explains segment AB where the displacement is nearly unchanged even though the absolute force continues to grow. Cylinder 2 has the same working principle, which means that the relative motion between the cylinders 2 and the shaft with happen only if the external pressure is large enough to overcome the internal damping force generated by cylinder 2. As the external force increases to overcome the internal damping force, the piston rod begins to move through into the cylinder 1 and spring 1 begins to be compressed, generating an elastic force applied to outside.

During this moving process there is no movement between the shaft and cylinder 2, thus, only spring 1 works and spring 2 remains undeformed. It implies that the effective stiffness of the whole system in this process can be expressed by only the stiffness k_1, which is indicated by segment BC in Figure 5.5. The elastic force increases as spring 1 is more compressed until it is large enough to overcome the external force, which is indicated by the critical inflection C. After point C, the cylinder 2 begins to have a relative movement to the shaft, which indicates that spring 2 also starts to compress and store potential energy. In this stage, spring 1 and 2 can be regarded as working in series, and the system effective stiffness can be expressed by the formula $k_1k_2/(k_1 + k_2)$, and this process is described by segment CD. The effective stiffness of two springs working in series must be less than the stiffness of any one of these two springs. That is why the slope of segment CD is much smaller than that of segment BC.

Regarding to the segment DE, the absolute force decreases but the displacement remained unchanged. This phenomenon is attributed to that the suspension starts to stretch. As shown by segment DE, when the piston rod intends to move in a different direction, the internal damping force prohibits its movement. The segment EF illustrates that the compressed spring 1 begins to restore as the shaft starts to move away from the cylinder 1. In this case, only spring 1 is working and the effective stiffness of the instrument can be presented by the stiffness k_1 because only spring 1 is working. As spring 1 rebounds, the elastic force generated by it gets smaller. When it reaches the critical point at which the elastic force of spring 1 plus the damping force generated by cylinder 2 is not big enough to resist the elastic force generated by spring 2, cylinder 2 begins to slide along the shaft in the opposite direction and spring 2 begins to restore as well. This process can be described by the segment FA, whose two springs

works in series again. From the figure we can see that the segments AB, BC, and CD are parallel to segments DE, EF, and FA, respectively. This phenomenon is consistent with the analysis presented above, and it also means that the dynamic characteristic of this instrument has symmetry expressed in force-displacement relationship. Accordingly, the overall effective stiffness of the VSVD suspension can be evaluated as the slope of the line connecting points B and D.

The force-displacement response under $I_1 = 0$ A and $I_2 = 0.4$ A is shown as a parallelogram. This is because the damping force generated by cylinder 2 under $I_2 = 0.4$ A is large enough to overcome the elastic force generated by spring 1 and spring 2 remains undeformed during this whole test.

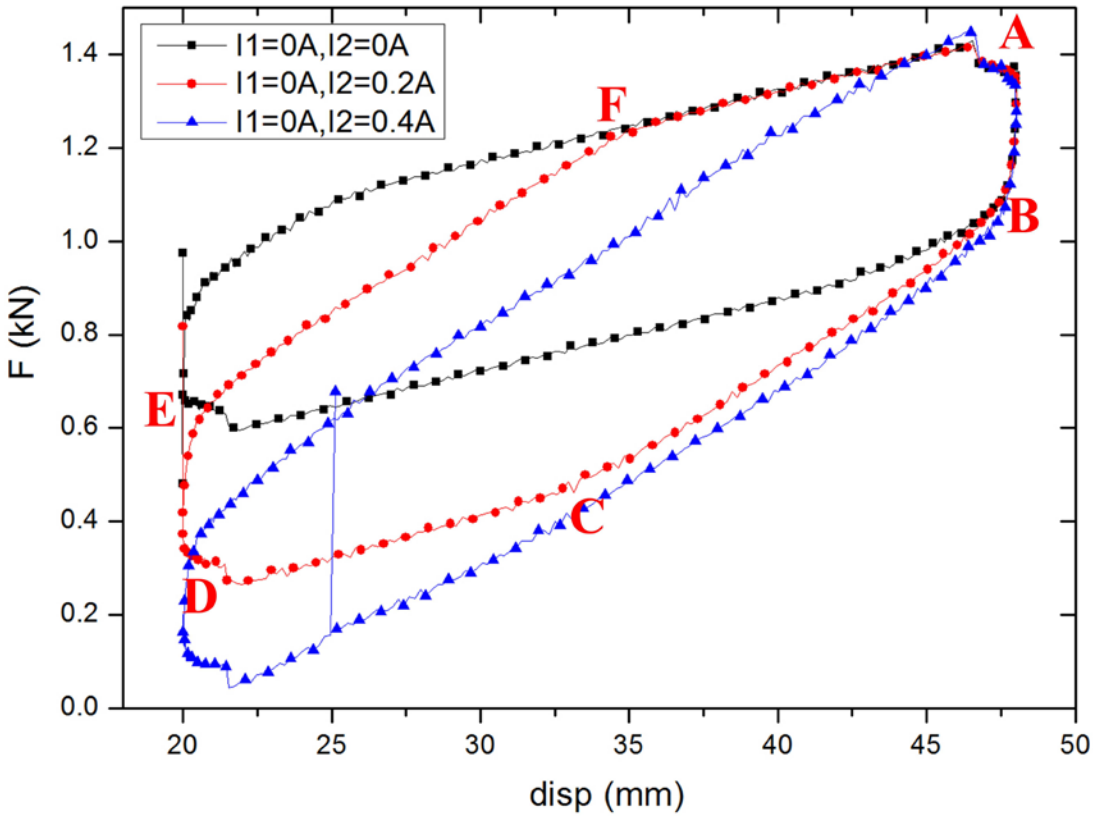

Figure 5.5 Variable stiffness performance under various currents.

Despite of the difference, it can still be seen that the corresponding segments in the different curves are parallel. It is worth noting that the overall effective stiffness increases as the current I_2 applied to the cylinder 2 increases. The effective stiffness versus I_2 is shown in Figure 5.6, which illustrates that the increase of I_2 from 0 to 0.4 A enhances the stiffness from 18.2 kN/m to 38.5 kN/m.

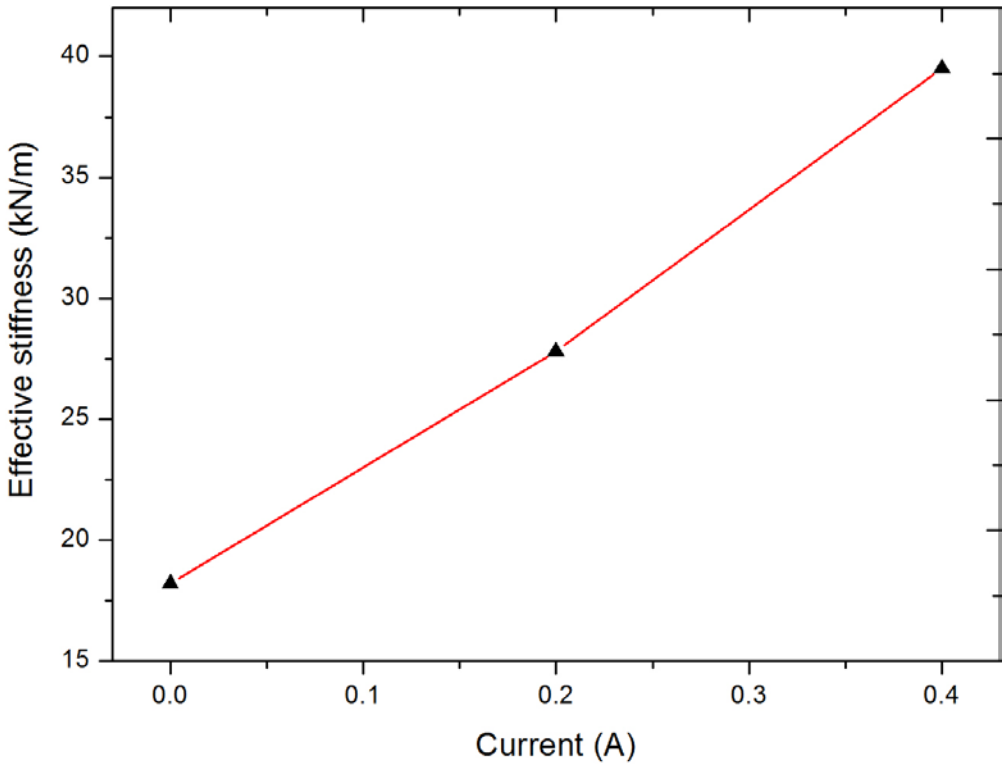

Figure 5.6 Effective stiffness as a function of the current applied to the upper damper.

5.4.2 Damping variability testing

Figure 5.7 shows the variable damping characteristic of the VSVD suspension under different currents of I_1 =0 A, 0.5 A, and 1 A, respectively. It is seen that the enclosed area of the force-displacement loops increases with the increase of current I_1. This means that the increasing I_1 leads to the increase of the equivalent damping of the VSVD suspension, which can be evidenced by Figure 5.8, where the equivalent

damping coefficient c is shown. The equivalent damping coefficient was calculated by Eq. (5.1) and Eq. (5.2) reported in [131].

The equivalent damping coefficient

$$c = E/(\pi\omega X_0^2), \tag{5.1}$$

where X_0 is the displacement amplitude and ω is the excitation frequency. The energy dissipated by the VSVD suspension in one cycle, E, is represented by the area enclosed within the hysteresis loop, which is given as

$$E = \int_0^{2\pi/\omega} F\dot{z}dt, \tag{5.2}$$

where F is the force generated by the VSVD suspension and z is the piston displacement.

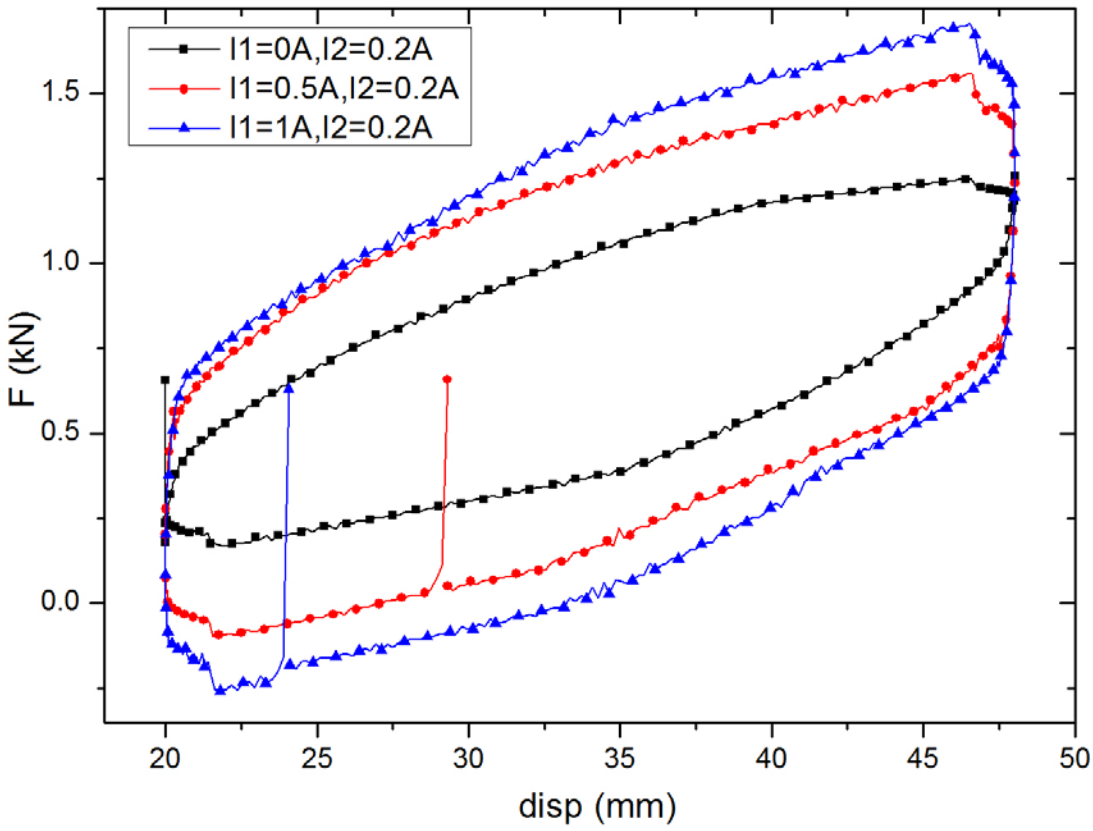

Figure 5.7 Variable damping performance under various currents.

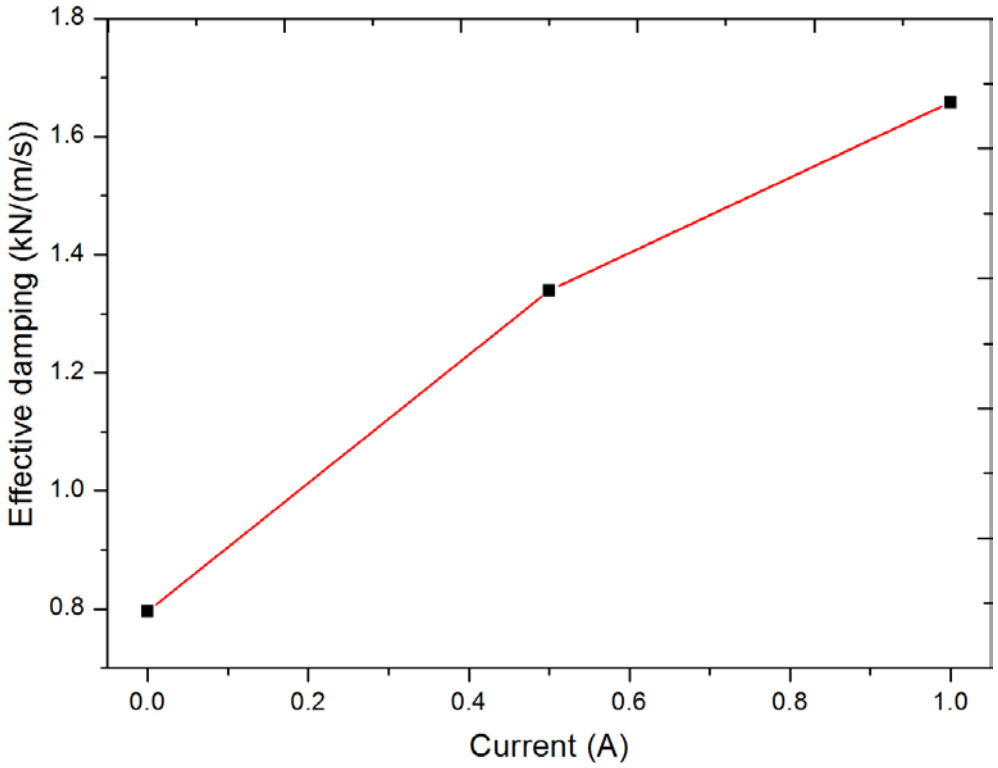

Figure 5.8 Effective damping as a function of the applied currents to the lower damper.

It can be clearly seen from Figure 5.8 that the increase in current I_1 from 0 to 1 A leads to the equivalent damping coefficient being increased from approximately 796 to 1658 $\mathrm{kN/(m/s)}$.

5.4.3 Frequency-dependent response

The part gives an analysis of the effectiveness of changing the loading frequency on the VSVD suspension performance, as shown in Figure 5.9. In this test, the loading frequency was chosen as 0.1, 0.3, and 0.5 Hz, respectively. It is seen that the force generated by the suspension increases slightly though the loading frequency increases, and that the effective stiffness and equivalent damping are almost independent of the loading frequency. The loop shape, tends to stay the same as the frequency grows.

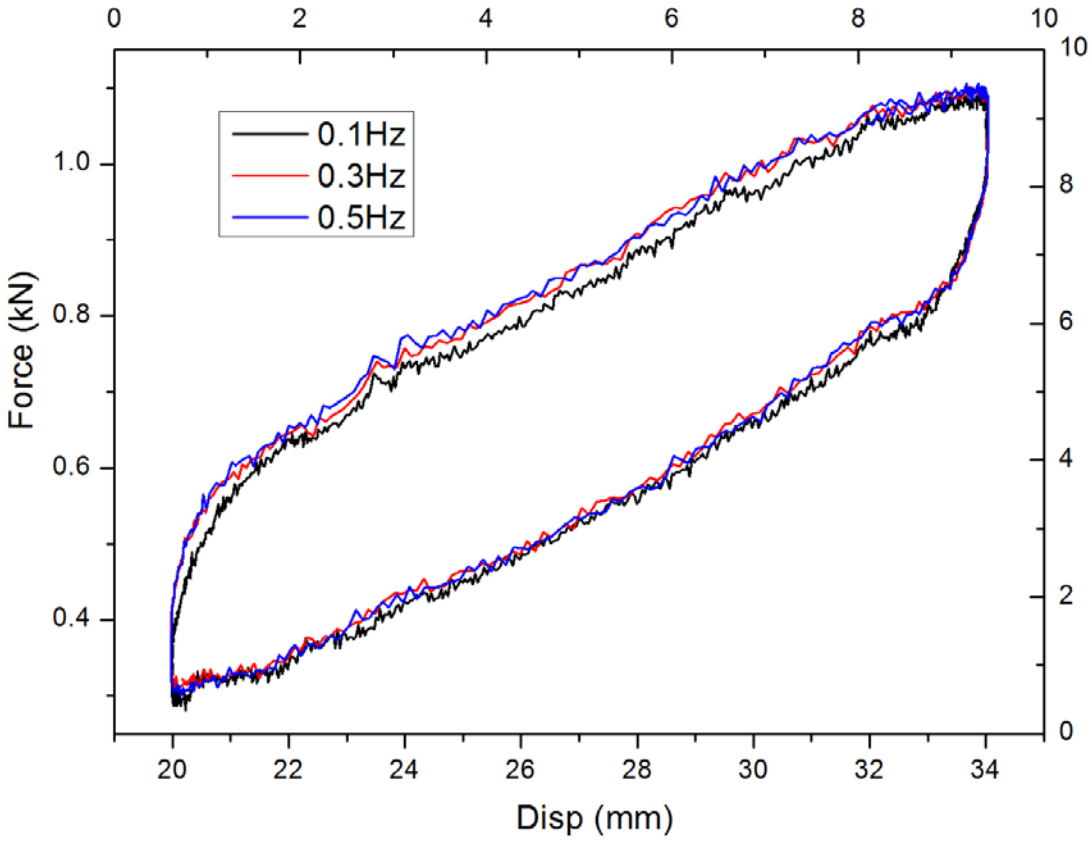

Figure 5.9 Force-displacement loops under different frequencies.

5.5 Modelling and parameter identification

5.5.1 Development of a new 3-DOF model

Based on the motivation to better predict the VSVD suspension response in real-time control, a new 3-DOF dynamic model, which includes two modified Bouc-Wen models and an extra mass block m_k with Newton's second law description was proposed, and it is shown in Figure 5.10. The mathematical description for the model is described as follows:

$$
\begin{aligned}
F &= F_d + k_{s1}(z - z_k) + F_s, \\
\dot{y}_1 &= \frac{1}{c_{01}+c_{11}}[\alpha_1 z_{d1} + k_{01}(z - y_1) + C_{01}\dot{z}], \\
\dot{y}_2 &= \frac{1}{c_{02}+c_{12}}[\alpha_2 z_{d2} + k_{02}(z - y_1) + C_{02}\dot{z}], \\
m_k \cdot \ddot{z_k} &= F_s + k_{s1}(z_k - z) - k_{s2} \cdot z_k,
\end{aligned}
\tag{5.3}
$$

where

$$
\begin{aligned}
F_d &= c_{11}\dot{y}_1 + k_{11}(z - Z_{01}), \\
F_s &= c_{12}\dot{y}_2 + k_{12}(z - z_k - Z_{02}), \\
\dot{z_{d1}} &= -\gamma_1|\dot{z} - \dot{y}_1| \cdot z_{d1}|z_{d1}| - \beta_1 \cdot (\dot{z} - \dot{y}_1){z_{d1}}^2 + A_{d1}(\dot{z} - \dot{y}_1), \\
\dot{z_{d2}} &= -\gamma_2|\dot{z} - \dot{y}_2| \cdot z_{d2}|z_{d2}| - \beta_2 \cdot (\dot{z} - \dot{y}_2){z_{d2}}^2 + A_{d2}(\dot{z} - \dot{y}_2), \\
\alpha_1 &= \alpha_{1a} + \alpha_{1b} \cdot I_1, \\
C_{01} &= C_{01a} + C_{01b} \cdot I_1, \\
C_{11} &= C_{11a} + C_{11b} \cdot I_1, \\
\alpha_2 &= \alpha_{2a} + \alpha_{2b} \cdot I_2, \\
C_{02} &= C_{02a} + C_{02b} \cdot I_2, \\
C_{12} &= C_{12a} + C_{12b} \cdot I_2.
\end{aligned}
$$

F is the force generated by the VSVD suspension; z and z_k are the displacement of the suspension and the mass block, respectively; y_1 and y_2 are internal pseudo-displacement of the two dampers; and I_1 and I_2 are the command voltages sent to the current driver. In this model, the parameters for adjusting the hysteresis are represented by $\gamma, \beta,$ and A; and a is the evolutionary coefficient; c_0 and c_1 are the viscous damping observed at larger and small velocities, respectively; k_0 is the stiffness at large velocities. Furthermore, k_1 is the accumulator stiffness; Z_0 is the initial displacement of spring k_1 associated with the nominal damper force due to the accumulator.

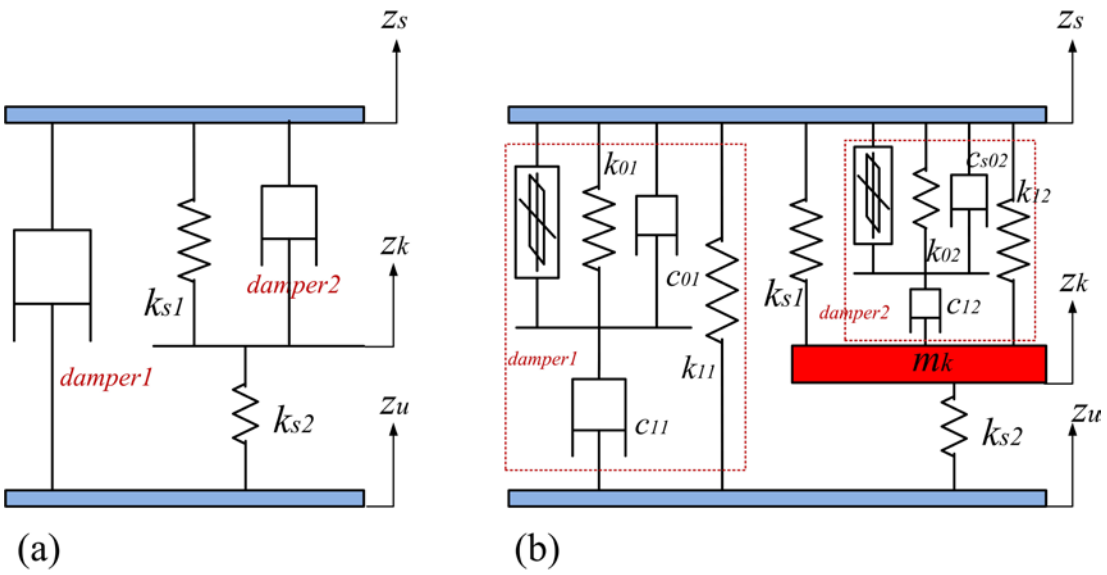

Figure 5.10 Mathematic model for the VSVD suspension: (a) 2-DOF conventional model; (b) 3-DOF double Bouc-Wen model.

5.5.2 Parameter identification

By analysing the experimental data using the GA algorithm whose calculating program is shown in Figure 5.11, parameters were determined to fit the proposed model. The estimated parameters are shown in Table 5.2. Figure 5.12 shows the fitting results for the stiffness variability and the damping variability. It can be seen that the predicted hysteresis loops by the model match well with the experimentally obtained data. This means that the proposed phenomenological model is able to predict the behaviors of the variable stiffness and damping damper in high accuracy.

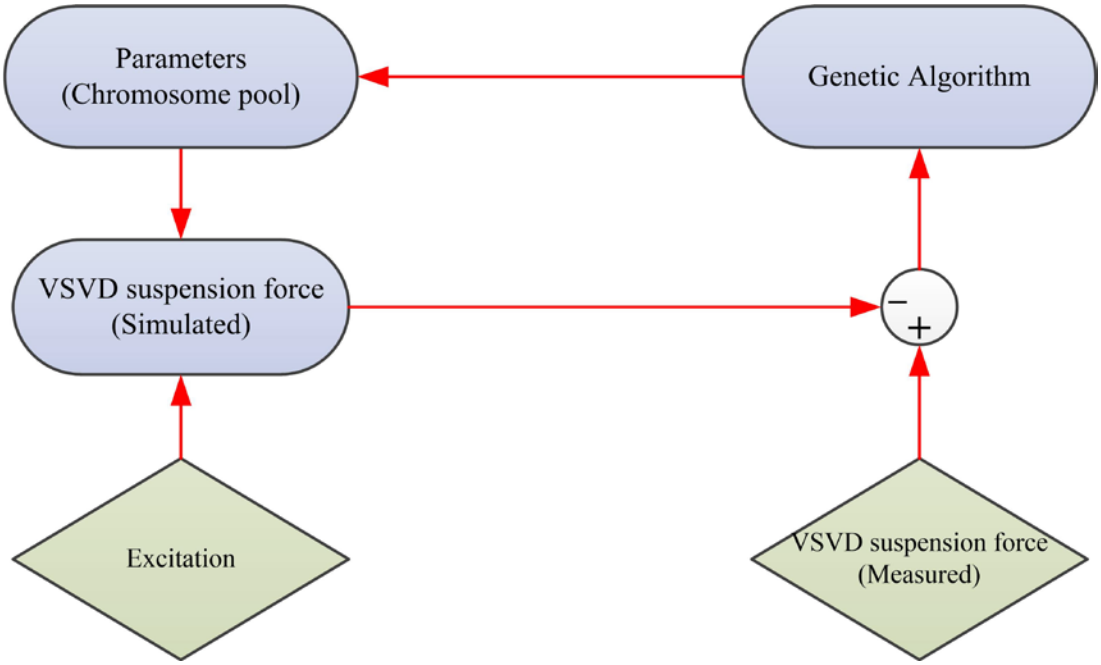

Figure 5.11 Flowchart of parameter identification using GA.

In addition to the graphical evidence of the superiority of the proposed model, a quantitative study was conducted that to analyse the errors between the classic 2-DOF model and the proposed 3-DOF model and the experimental data. For the two models considered here, the error between the predicted force and the measured force was calculated as a function of time E_t, displacement E_z,and velocity $E_{\dot{z}}$ over 5 complete cycles (see [40] for full calculation steps). The resulting normalized errors are given in Table 5.3. It can be seen that the error norms calculated for the proposed model are smaller than that calculated for the norm 2-DOF model considered.

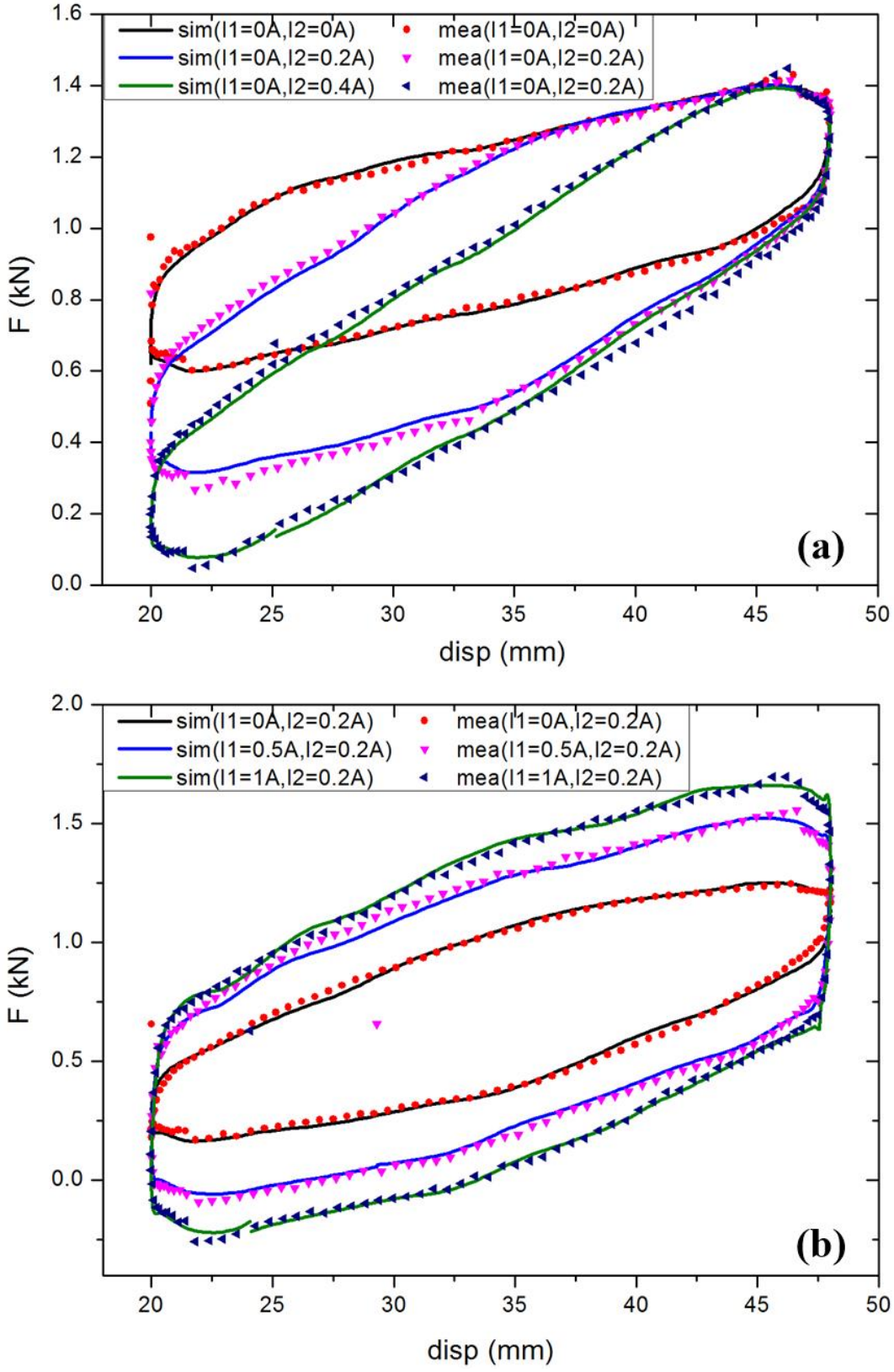

Figure 5.12 Comparison between the simulated response and the measured response: (a) variable stiffness; (b) variable damping.

Table 5.2 Identified values for the parameters

Parameters	Values	Parameters	Values
A_{d1}	106	A_{d2}	168
β_1	207000	β_2	1755259
r_1	295900	r_2	156956
Z_{01}	0.19	Z_{02}	0.28
α_{1a}	8895	α_{1b}	22814
α_{2a}	13044	α_{2b}	46360
C_{01a}	7037	C_{01b}	7534
C_{02a}	16045	C_{02b}	1637
C_{11a}	56485	C_{11b}	102756
C_{12a}	1211	C_{12b}	2513550
k_{01}	73	k_{02}	30232
k_{11}	242	k_{12}	4487
k_{s1}	29976	k_{s2}	38500
m_k	4.8		

Table 5.3 Error norms for VSVD models

Parameters	2-DOF Bingham	3-DOF BoucWen
E_t	0.207	0.0557
E_z	0.0554	0.0125
$E_{\dot{z}}$	0.197	0.0854

5.6 Numerical evaluation of the proposed suspension

In order to verify the effectiveness of the advanced VSVD suspension on vibration control, the quarter of a car mounted with the suspension is evaluated in this section by simulation software. As the developed VSVD suspension presented in the above section has been established with the optimal design base on the quarter-car test rig parameters, the force generated by the suspension is well suited to the existing quarter-car model, which is applied in the simulation conducted in this section. A control system and the quarter-car model including VSVD suspension are presented in Figure 5.13. Simulink® is used to establish the dynamic model of the car. The model established in this study is a 2-DOF quarter car containing a sprung mass, the VSVD suspension, unsprung mass, and the spring k_t representing the stiffness of tyre. A vertical excitation is applied on the spring k_t to represent the road profile. During the simulation process, the real-time state of the quarter-car model are transferred to the damping controller and the stiffness controller to control the damping and stiffness of the advance suspension, respectively.

5.6.1 Simple on-off control strategy for simulation work

The control strategy involved in this study contains two parts. The first is the damping control algorithm. The main purpose of the damping controller is to determine the desired damping. The control strategy adopted in this section is skyhook. Detail of the skyhook control strategy is as follows:

$$I_1 = \begin{cases} 0.8\ \text{A}, & \dot{z}_s(\dot{z}_s - \dot{z}_u) \geq 0, \\ 0\ \text{A}, & \dot{z}_s(\dot{z}_s - \dot{z}_u) < 0. \end{cases} \tag{5.4}$$

The second item is the stiffness controller. The control method is also skyhook control algorithm and the detail is expressed as:

$$I_2 = \begin{cases} 0.4\ \text{A}, & \dot{z}_s(z_s - z_u) \geq 0, \\ 0\ \text{A}, & \dot{z}_s(z_s - z_u) < 0, \end{cases} \tag{5.5}$$

where I_1 and I_2 are the currents controlling damping and stiffness items, respectively, z_s and $\dot{z}_s$ are the displacement and velocity of the sprung mass while z_u and $\dot{z}_u$ are the displacement and velocity of the unsprung mass. The working currents are determined as $I_1 = 0.8$ A and $I_2 = 0.4$ A.

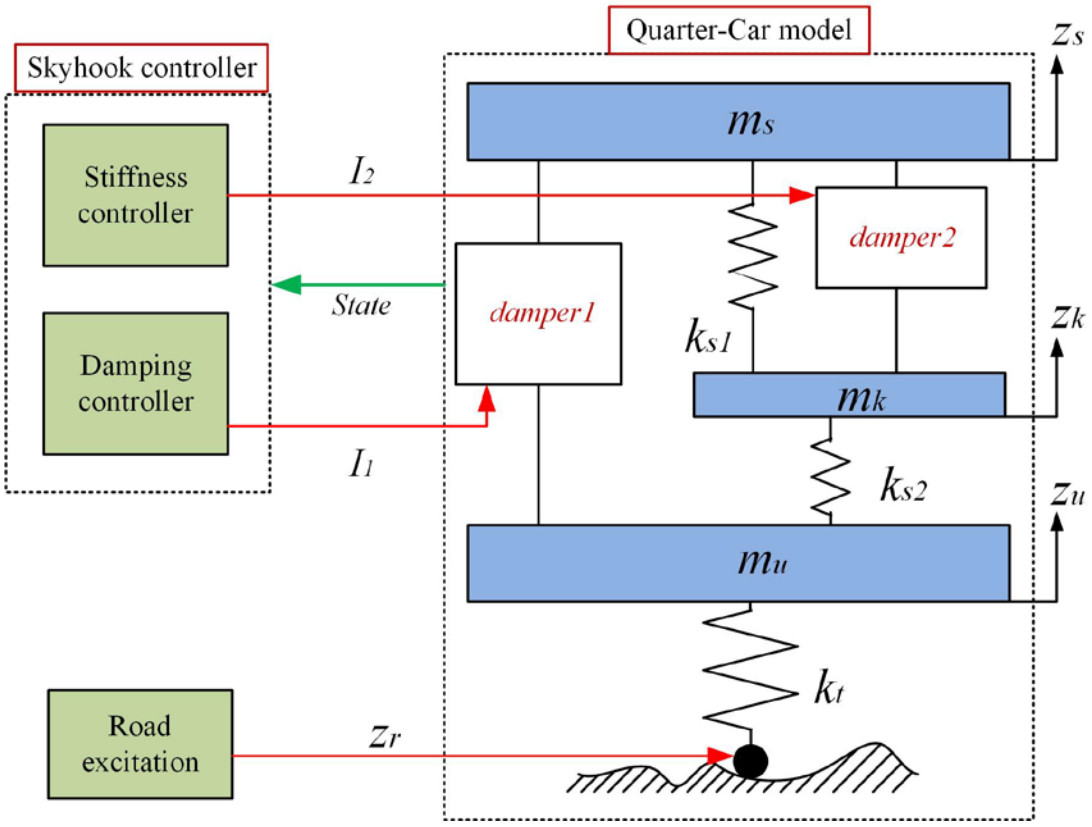

Figure 5.13 Control system of variable stiffness and damping suspension.

5.6.2 Numerical results and discussions

In this section, four different types of suspension were simulated. The four suspensions are passive suspension, damping variable suspension, stiffness variable suspension, and variable stiffness and variable damping suspension. In this simulation, the quarter-

car runs on two types excitation, a bump and random road profile. The simulation results of the SMA of the system in time domain is shown in Figure 5.14 and Figure 5.15. As a comparison, the performances of the quarter-car with other three kind suspensions were also evaluated, and the results are plotted in the two figures.

From these figures, it can be seen that semi-active suspensions perform better on SMA attenuation than the passive suspension. It also can be seen that the system applied with variable stiffness and damping control performs best compared with passive suspension, only variable stiffness one, and only variable damping case.

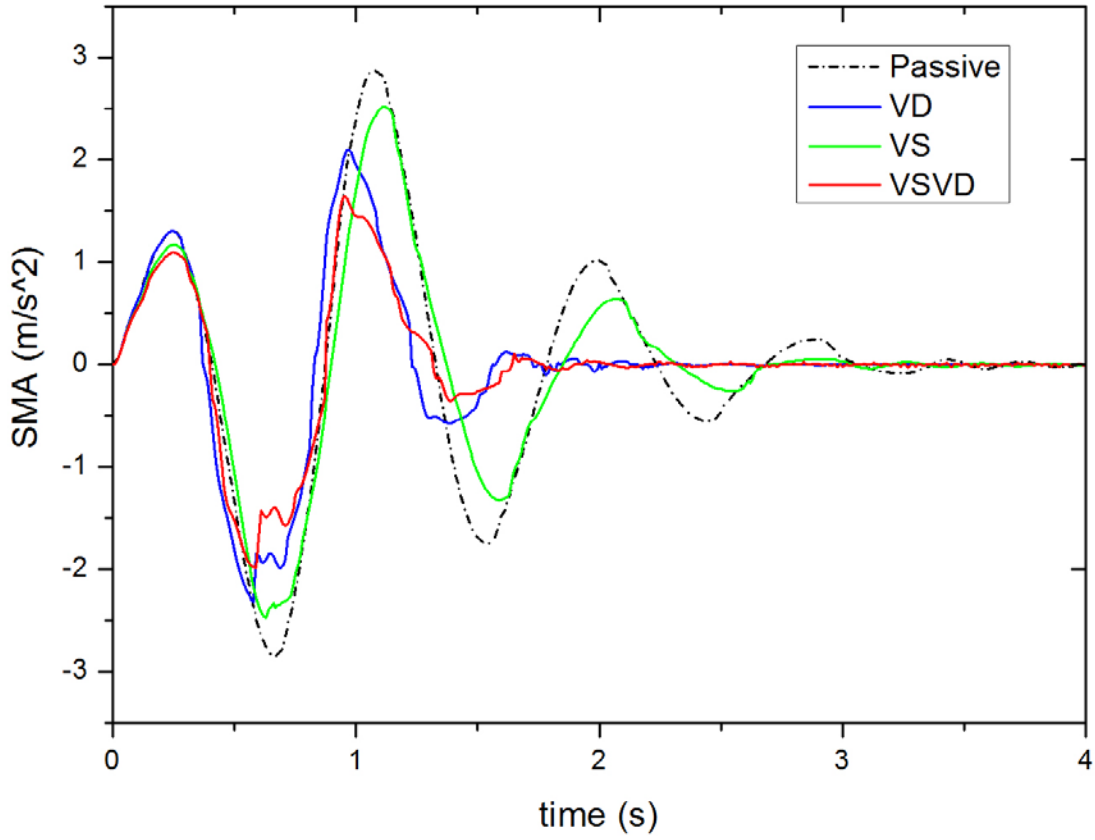

Figure 5.14 Car body response for bump case.

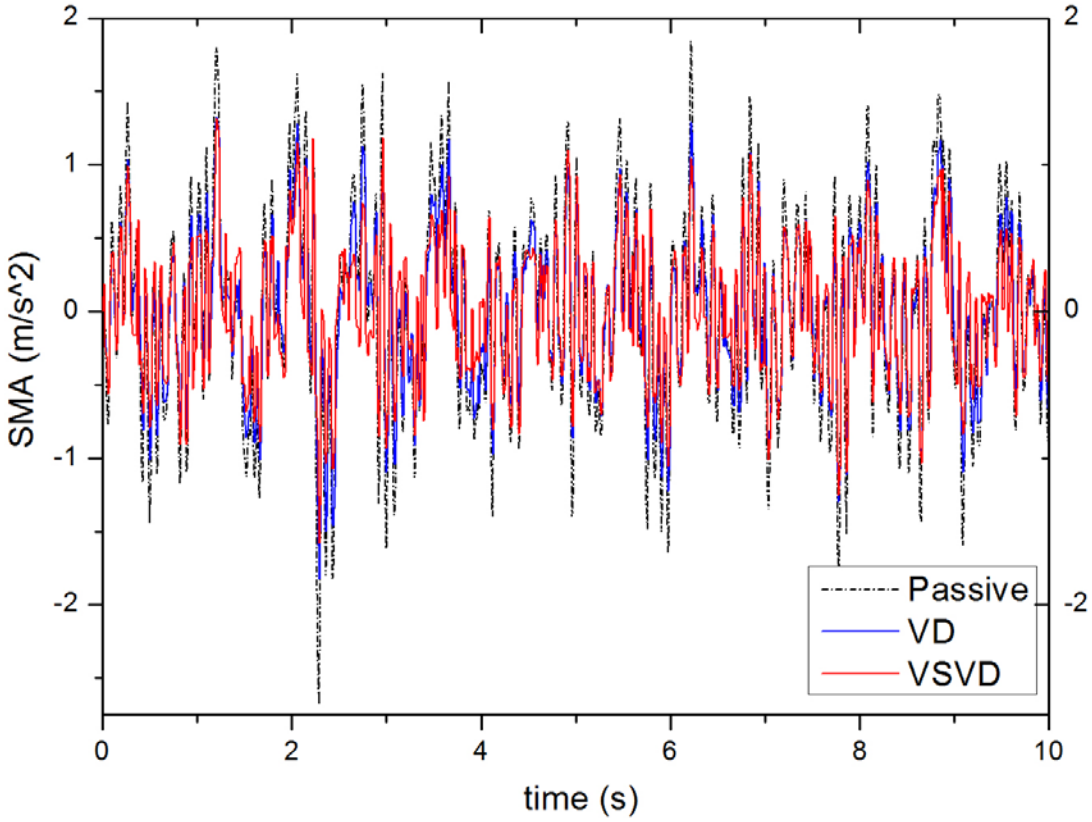

Figure 5.15 Car body response for random road in time domain (only three types are shown for brevity).

Figure 5.16 shows the RMS value of the vertical SMA excited by random road disturbance. Four different suspensions were compared by bar graph. It illustrates that variable damping suspension and variable stiffness suspension decrease the vibration by 23.7% and 7.6%, respectively, relative to the passive case. Furthermore, the variable stiffness and damping suspension can improve the vibration attenuation effectiveness by 30.3%.

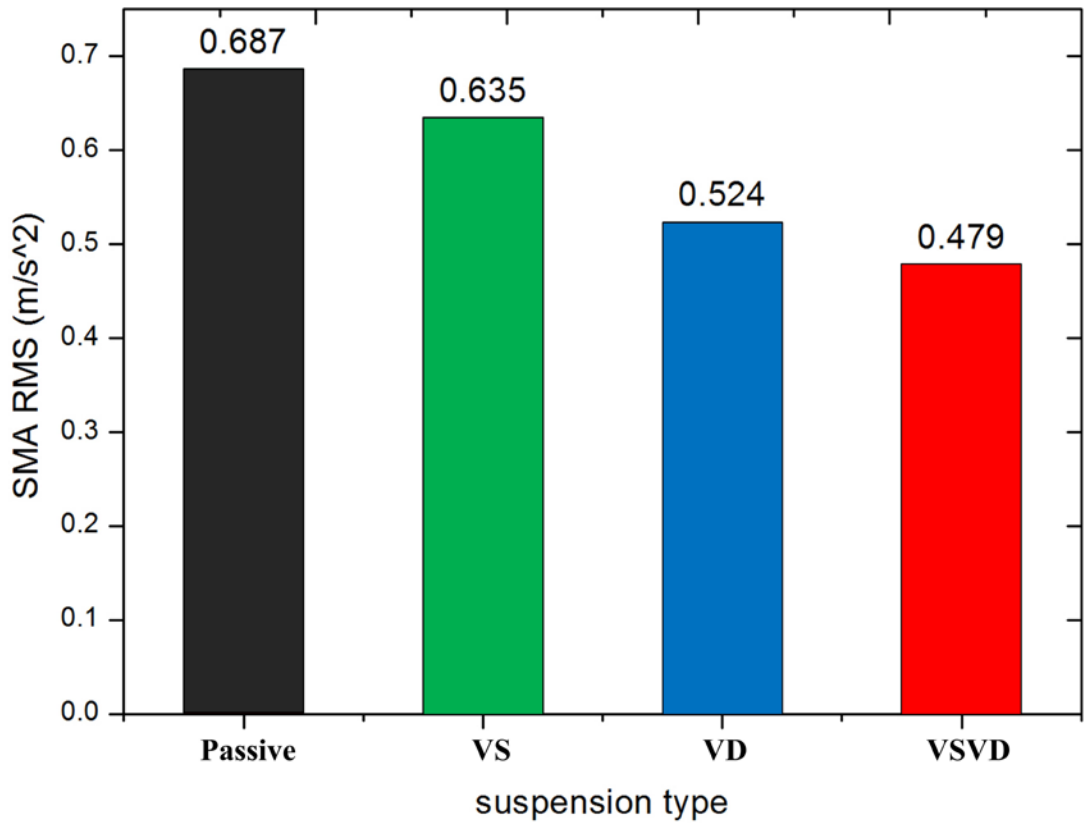

Figure 5.16 Acceleration RMS value of car body.

5.7 Conclusion

An advanced MR suspension with variable stiffness and damping characteristics that can be practically applied to vehicle body was designed, optimized, and tested. The analysis and test results by an INSTRON machine verified that both the stiffness and the damping properties of the damper can be controlled properly. With optimal design for the prototype structure, the stiffness of the suspension can vary from 18.2 kN/m to 38.5 kN/m while the equivalent damping coefficient has the ability to change from 796 $kN/(m/s)$ to 1658 $kN/(m/s)$, which are feasible to a real vehicle suspension for practical application. To describe the dynamic characteristic of the VSVD suspension accurately, a new 3-DOF phenomenological model with double Bouc-Wen model was proposed and compared to the classical models. Then, the effectiveness of

the VSVD suspension which is described by the 3-DOF model was verified by simulation work under bump and random road excitation.

6 A TS FUZZY MODELLING BASED CONTROL STRATEGY FOR VARIABLE STIFFNESS AND VARIABLE DAMPING SUSPENSION

6.1 Introduction

The previous chapter focus on improving the structure of variable stiffness and variable damping (VSVD) suspension and establishing the corresponding phenomenological model. In order to further enhance the vibration reduction performance of the VSVD suspension, a new TS fuzzy modelling based VSVD controller was designed and tested. The controller includes a skyhook damping controller and a stiffness controller which considering road dominant frequency. To estimate the frequency information in real-time, a state observer was designed and integrated in the controller. Considering the nonlinear dynamic characteristics of MR dampers, a TS fuzzy modelling program was applied to the suspension model in the state observer design process. Then, the performance of the VSVD control algorithm was evaluated experimentally on the quarter-car test rig which equipping the VSVD suspension.

6.2 Modelling of a quarter car system with VSVD suspension

For the purpose of developing a real-time controller for the quarter-car installed with the VSVD suspension, a simple and effective model for the suspension itself are necessary. In this section, a modified model derived from the 3-DOF double Bouc-Wen model was proposed to better adapt real-time control for VSVD system. Then the quarter-car system the was modelled by TS fuzzy modelling approach to effectively build the state observer.

6.2.1 Simplified VSVD model for real-time control

The Bouc-Wen model has been widely accepted in describing MR behavior for its mathematical simplicity and accuracy [132]. Thus, the model proposed in this section includes two Bouc-Wen models, which not only has simple and measurable state (the state y in modified Bouc-Wen model is almost unmeasurable), but also the accuracy to describe the hysteretic behavior of an MR structure.

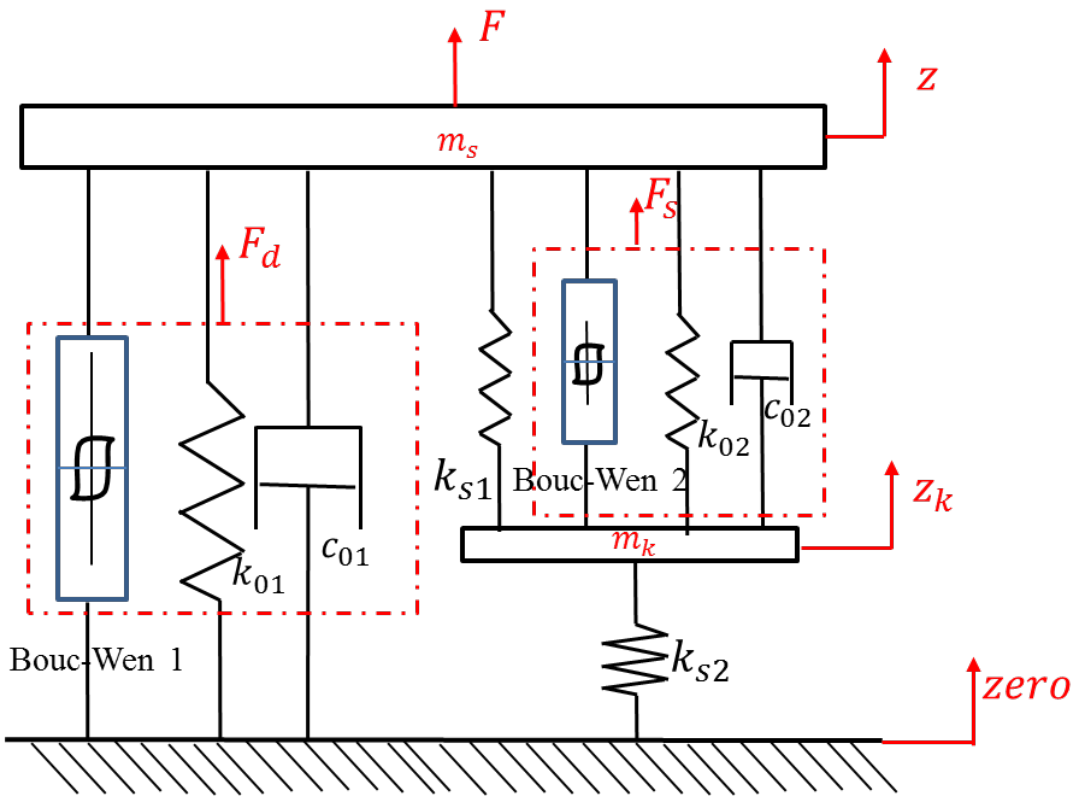

Figure 6.1 Schematic diagram of the proposed phenomenological model for controller design.

Figure 6.1 shows the schematic diagram of the proposed phenomenological model which includes two Bouc-Wen models. The mathematical description for this model is as follows:

$$
\begin{aligned}
F &= F_d + k_{s1}(z - z_k) + F_s, \\
F_d &= \alpha_1 z_{d1} + k_{01} \cdot z + C_{01} \cdot \dot{z}, \\
F_s &= \alpha_2 z_{d2} + k_{02} \cdot (z - z_k) + C_{02} \cdot (\dot{z} - \dot{z_k}), \\
m_k \cdot \ddot{z_k} &= F_s + k_{s1}(z_k - z) - k_{s2} \cdot z_k,
\end{aligned}
\tag{6.1}
$$

where

$$
\begin{aligned}
\dot{z_{d1}} &= -\gamma_1 |\dot{z}| \cdot z_{d1} |z_{d1}| - \beta_1 \cdot \dot{z} {z_{d1}}^2 + A_{d1}(\dot{z}), \\
\dot{z_{d2}} &= -\gamma_2 |\dot{z} - \dot{z_k}| \cdot z_{d2} |z_{d2}| - \beta_2 \cdot (\dot{z} - \dot{z_k}) {z_{d2}}^2 + A_{d2}(\dot{z} - \dot{z_k}), \\
\alpha_1 &= \alpha_{1a} + \alpha_{1b} \cdot I_1, \\
C_{01} &= C_{01a} + C_{01b} \cdot I_1, \\
\alpha_2 &= \alpha_{2a} + \alpha_{2b} \cdot I_2, \\
C_{02} &= C_{02a} + C_{02b} \cdot I_2,
\end{aligned}
$$

and A_{d1}, A_{d2}, β_1, β_2, $\gamma_1$and γ_2 are used to describe the hysteresis behaviour; α_1 and α_2 are the evolutionary coefficient; C_{01} and $C_{02}$are the viscous damping ; k_{01} and k_{02} are the stiffness.

To evaluate the accuracy of the proposed model in describing the suspension performance, numerical simulation was conducted to identify the optimal parameters for the model to fit the measured dynamic characteristic of the VSVD MR suspension. A least-square method in combination with the trust-region-reflective algorithm available in MATLAB was used to determine the parameters in this model. Table 6.1 lists the identified values for these parameters.

Table 6.1 Identified values for the parameters

Parameters	Values	Parameters	Values
A_{d1}	120	A_{d2}	89
β_1	237602	β_2	266259
γ_1	219872	γ_2	1277656
α_{1a}	7211	α_{1b}	23415
α_{2a}	18654	α_{2b}	43876
C_{01a}	15036	C_{01b}	11221
C_{02a}	20657	C_{02b}	1876
k_{01}	347	k_{02}	29032
k_{s1}	29976	k_{s2}	38500

6.2.2 Quarter car model with VSVD suspension

A quarter car model installed with this VSVD MR suspension was built in Simulink. Eq. (6.2) describes the complete system:

$$\begin{aligned} m_s \cdot \ddot{z}_s = &-[(\alpha_{1a} + \alpha_{1b} \cdot I_1) \cdot z_{d1} + k_{01}(z_s - z_u) + \\ &(c_{01a} + c_{01b} \cdot I_1)(\dot{z}_s - \dot{z}_u) + k_{s1}(z_s - z_k) + \\ &(\alpha_{2a} + \alpha_{2b} \cdot I_2) \cdot z_{d2} + k_{02}(z_s - z_k) + \\ &(c_{02a} + c_{02b} \cdot I_2)(\dot{z}_s - \dot{z}_k)], \\ m_u \cdot \ddot{z}_u = &(\alpha_{1a} + \alpha_{1b} \cdot I_1) \cdot z_{d1} + k_{01}(z_s - z_u) + \\ &(c_{01a} + c_{01b} \cdot I_1)(\dot{z}_s - \dot{z}_u) + k_{s2}(z_k - z_u) - k_t(z_u - z_r), \\ m_k \cdot \ddot{z}_k = &\, k_{s1}(z_s - z_k) + (\alpha_{2a} + \alpha_{2b} \cdot I_2) z_{d2} - k_{s2}(z_k - z_u) \\ &+ k_{02}(z_s - z_k) + (c_{02a} + c_{02b} \cdot I_2)(\dot{z}_s - \dot{z}_k), \end{aligned} \tag{6.2}$$

where $m_s$is the sprung mass, $m_u$is the unsprung mass, m_u is the mass of the top cylinder of the suspension, z_s is the displacement of the sprung mass, z_u is the displacement of the unsprung mass, z_k is the displacement of the top damper cylinder. Define the state variables as follows:

$$\begin{aligned} x_1 = \dot{z}_s, \quad x_2 = \dot{z}_u, \quad x_3 = \dot{z}_k, \quad x_3 = \dot{z}_k, \\ x_5 = z_k - z_u, \quad x_6 = z_u - z_r, \quad x_7 = z_{d1}, \quad x_8 = z_{d2}, \end{aligned} \tag{6.3}$$

and the state vector as:

$$x = [x_1 \quad x_2 \quad x_3 \quad x_4 \quad x_5 \quad x_6 \quad x_7 \quad x_8]^T. \tag{6.4}$$

In order to simplify the highly nonlinearity of the proposed model, define $\widetilde{f_1}$, $\widetilde{f_2}$as:

$$\begin{aligned} \widetilde{f_1} &= -\gamma_1|\dot{z}_s - \dot{z}_u| \cdot z_{d1}|z_{d1}| - \beta_1(\dot{z}_s - \dot{z}_u)|z_{d1}|^2, \\ \widetilde{f_2} &= -\gamma_2|\dot{z}_s - \dot{z}_k| \cdot z_{d2}|z_{d2}| - \beta_2(\dot{z}_s - \dot{z}_k)|z_{d2}|^2. \end{aligned} \tag{6.5}$$

Then define:

$$\begin{aligned} f_1 &= \frac{\widetilde{f_1}}{x_7}, \\ f_2 &= \frac{\widetilde{f_2}}{x_8}, \\ f_3 &= \alpha_{1b} \cdot x_7 + c_{01b}(x_1 - x_2), \\ f_4 &= \alpha_{2b} \cdot x_8 + c_{02b}(x_1 - x_3). \end{aligned} \tag{6.6}$$

Then Eq. (6.2) can be written as:

$$
\begin{aligned}
m_s \cdot \dot{x_1} = -[&\alpha_{1a} \cdot x_7 + k_{01} \cdot x_4 + c_{01a} x_1 - c_{01a} x_2 + f_3 I_1 \\
&+ k_{s1} x_4 - k_{s1} x_5 + \alpha_{2a} \cdot x_8 + k_{02} x_4 - k_{02} x_5 \\
&+ c_{02a} \cdot x_1 - c_{02a} \cdot x_3 + f_4 \cdot I_2],
\end{aligned}
$$

$$
\begin{aligned}
m_u \cdot \dot{x_2} = &\alpha_{1a} \cdot x_7 + k_{01} \cdot x_4 + c_{01a} x_1 - c_{01a} x_2 + k_{s2} x_5 \\
&- k_t x_6 + f_3 \cdot I_1,
\end{aligned}
$$

$$
\begin{aligned}
m_k \cdot \dot{x_3} = &k_{s1} x_4 - k_{s1} x_5 + \alpha_{2a} \cdot x_8 + k_{02} x_4 - k_{02} x_5 \\
&+ c_{02a} \cdot x_1 - c_{02a} \cdot x_3 - k_{s2} x_5 + f_4 \cdot I_2,
\end{aligned}
\tag{6.7}
$$

$$
\begin{aligned}
\dot{x_4} &= x_1 - x_2, \\
\dot{x_5} &= x_3 - x_2, \\
\dot{x_6} &= x_2 - \dot{z_r}, \\
\dot{x_7} &= f_1 x_7 + A d_1 (x_1 - x_2), \\
\dot{x_8} &= f_2 x_8 + A d_1 (x_1 - x_3).
\end{aligned}
$$

We can write a state-space for system Eq. (6.4) as:

$$
\dot{x}(t) = Ax + B_1 w + B_2 u, \tag{6.8}
$$

where

$$
A = \begin{bmatrix}
\frac{c_{01a}+c_{02a}}{-m_s} & \frac{-c_{01a}}{-m_s} & \frac{-c_{02a}}{-m_s} & \frac{k_{01}+k_{s1}+k_{02}}{-m_s} & \frac{-k_{s1}-k_{02}}{-m_s} & \frac{0}{m_u} & \frac{\alpha_{1a}}{-m_s} & \frac{\alpha_{2a}}{-m_s} \\
\frac{c_{01a}}{m_u} & \frac{-c_{01a}}{m_u} & \frac{0}{m_u} & \frac{k_{01}}{m_u} & \frac{k_{s2}}{m_u} & \frac{-k_t}{m_u} & \frac{\alpha_{1a}}{m_u} & \frac{0}{m_u} \\
\frac{c_{02a}}{m_k} & \frac{0}{m_k} & \frac{-c_{02a}}{m_k} & \frac{k_{s1}+k_{02}}{m_k} & \frac{-k_{s1}-k_{02}-k_{s2}}{m_k} & \frac{0}{m_k} & \frac{0}{m_k} & \frac{\alpha_{2a}}{-m_k} \\
1 & -1 & 0 & 0 & 0 & 0 & 0 & 0 \\
0 & -1 & 1 & 0 & 0 & 0 & 0 & 0 \\
0 & 1 & 0 & 0 & 0 & 0 & 0 & 0 \\
Ad_1 & -Ad_1 & 0 & 0 & 0 & 0 & f_1 & 0 \\
Ad_1 & 0 & Ad_1 & 0 & 0 & 0 & 0 & f_2
\end{bmatrix},
$$

$$
B_1 = [0 \quad 0 \quad 0 \quad 0 \quad 0 \quad -1 \quad 0 \quad 0]^T,
$$

$$B_2 = \begin{bmatrix} \frac{f_3}{-m_s} & \frac{f_4}{-m_s} \\ \frac{f_3}{m_u} & \frac{0}{m_u} \\ \frac{0}{m_k} & \frac{f_4}{m_k} \\ 0 & 0 \\ 0 & 0 \\ 0 & 0 \\ 0 & 0 \\ 0 & 0 \end{bmatrix},$$

$w = z_r$.

6.2.3 TS fuzzy modelling of quarter-car with VSVD suspension

Considering that the state variables x_1, x_2, x_7, and x_8 are actually limited in practice for a stable system, the nonlinear f_1 ,f_2, f_3, and $f_4$should also be bounded in operation. We represent f_1 ,f_2, f_3, and f_4 using their minimum values and maximum values by following "sector nonlinearity" approach [125]:

$$\begin{aligned} f_1 &= M_1 \cdot f_{1max} + M_2 \cdot f_{1min}, \\ f_2 &= N_1 \cdot f_{2max} + N_2 \cdot f_{2min}, \\ f_3 &= T_1 \cdot f_{3max} + T_2 \cdot f_{3min}, \\ f_4 &= H_1 \cdot f_{4max} + H_2 \cdot f_{4min}, \end{aligned} \tag{6.9}$$

where $f_{(i)max}\ (i = 1,2,3,4)$ represents the maximum values and $f_{(i)min}\ (i = 1,2,3,4)$ is the minimum values of the nonlinear $f_{(i)}\ (i = 1,2,3,4)$. $M_{(i)}$, $N_{(i)}$, $T_{(i)}$, and $H_{(i)}\ (i = 1,2)$ are fuzzy membership functions and satisfy:

$$\begin{aligned} M_1 + M_2 &= 1, \\ N_1 + N_2 &= 1, \\ T_1 + T_2 &= 1, \\ H_1 + H_2 &= 1, \end{aligned} \tag{6.10}$$

and the member functions are defined as:

$$M_1 = \frac{f_1 - f_{1min}}{f_{1max} - f_{1min}}, \quad M_2 = \frac{f_{2max} - f_2}{f_{2max} - f_{2min}},$$
$$N_1 = \frac{f_2 - f_{2min}}{f_{2max} - f_{2min}}, \quad N_2 = \frac{f_{2max} - f_2}{f_{2max} - f_{2min}},$$
$$T_1 = \frac{f_3 - f_{3min}}{f_{3max} - f_{3min}}, \quad T_2 = \frac{f_{3max} - f_3}{f_{3max} - f_{3min}}, \tag{6.11}$$
$$H_1 = \frac{f_4 - f_{4min}}{f_{4max} - f_{4min}}, \quad H_2 = \frac{f_{4max} - f_4}{f_{4max} - f_{4min}}.$$

Then the nonlinear quarter car system can be described by the abovementioned linear subsystems. For each possibility, there is a corresponding state-space equation:

If $f_1 = M_1, f_2 = N_1, f_3 = T_1, f_4 = H_1,$
then $\dot{x} = A_{(1)}\mathrm{x} + B_1 w + B_{2(1)} u.$

If $f_1 = M_1, f_2 = N_1, f_3 = T_1, f_4 = H_2,$
then $\dot{x} = A_{(2)}\mathrm{x} + B_1 w + B_{2(2)} u.$

If $f_1 = M_1, f_2 = N_1, f_3 = T_2, f_4 = H_1,$
then$\dot{x} = A_{(3)}\mathrm{x} + B_1 w + B_{2(3)} u.$

If $f_1 = M_1, f_2 = N_1, f_3 = T_2, f_4 = H_2,$
then$\dot{x} = A_{(4)}\mathrm{x} + B_1 w + B_{2(4)} u.$

If $f_1 = M_1, f_2 = N_2, f_3 = T_1, f_4 = H_1,$
then$\dot{x} = A_{(5)}\mathrm{x} + B_1 w + B_{2(5)} u.$

If $f_1 = M_1, f_2 = N_2, f_3 = T_2, f_4 = H_1,$
then$\dot{x} = A_{(6)}\mathrm{x} + B_1 w + B_{2(6)} u.$

If $f_1 = M_1, f_2 = N_2, f_3 = T_2, f_4 = H_2,$
then$\dot{x} = A_{(7)}\mathrm{x} + B_1 w + B_{2(7)} u.$

If $f_1 = M_2, f_2 = N_1, f_3 = T_1, f_4 = H_1,$
then$\dot{x} = A_{(8)}\mathrm{x} + B_1 w + B_{2(8)} u.$

If $f_1 = M_2, f_2 = N_2, f_3 = T_1, f_4 = H_1,$
then$\dot{x} = A_{(9)}\mathrm{x} + B_1 w + B_{2(9)} u.$

If $f_1 = M_2, f_2 = N_2, f_3 = T_2, f_4 = H_1,$
then$\dot{x} = A_{(10)}\mathrm{x} + B_1 w + B_{2(10)} u.$

If $f_1 = M_2, f_2 = N_2, f_3 = T_2, f_4 = H_2,$

then$\dot{x} = A_{(11)}\mathrm{x} + B_1 w + B_{2(11)} u.$

If $f_1 = M_1, f_2 = N_2, f_3 = T_1, f_4 = H_2,$

then$\dot{x} = A_{(12)}\mathrm{x} + B_1 w + B_{2(12)} u.$

If $f_1 = M_2, f_2 = N_1, f_3 = T_1, f_4 = H_2,$

then$\dot{x} = A_{(13)}\mathrm{x} + B_1 w + B_{2(13)} u.$

If $f_1 = M_2, f_2 = N_1, f_3 = T_2, f_4 = H_1,$

then$\dot{x} = A_{(14)}\mathrm{x} + B_1 w + B_{2(14)} u.$

If $f_1 = M_2, f_2 = N_1, f_3 = T_2, f_4 = H_2,$

then$\dot{x} = A_{(15)}\mathrm{x} + B_1 w + B_{2(15)} u.$

If $f_1 = M_2, f_2 = N_2, f_3 = T_1, f_4 = H_2,$

then$\dot{x} = A_{(16)}\mathrm{x} + B_1 w + B_{2(16)} u,$

where $A_{(i)}$ $(i = 1,2,3, \dots, 16)$. ($i = 1,2,3, \dots, 16$) are obtained by replacing $f_{(i)}$ $(i = 1,2)$ in matrix A of Eq. (6.8) with $f_{(i)max}$ and $f_{(i)min}$, respectively.

Then the TS fuzzy model for the nonlinear quarter car under the bounded state variables is obtained as:

$$\dot{x} = \sum_{i=1}^{16} h_i \left[A_{(i)}\mathrm{x} + B_1 w + B_{2(i)} \dot{u}\right] = A_h \mathrm{x} + B_1 w + B_{2h} \dot{u}, \tag{6.12}$$

where $A_h = \sum_{i=1}^{16} h_i A_{(i)}$, $B_{2h} = \sum_{i=1}^{16} h_i B_{2(i)}$,

$h_1 = M_1 N_1 T_1 H_1, \quad h_2 = M_1 N_1 T_1 H_2,$

$h_3 = M_1 N_1 T_2 H_1, \quad h_4 = M_1 N_1 T_2 H_2,$

$h_5 = M_1 N_2 T_1 H_1, \quad h_6 = M_1 N_2 T_2 H_1,$

$h_7 = M_1 N_2 T_2 H_2, \quad h_8 = M_2 N_1 T_1 H_1,$

$h_9 = M_2 N_2 T_1 H_1, \quad h_{10} = M_2 N_2 T_2 H_1,$

$h_{11} = M_2 N_2 T_2 H_2, \quad h_{12} = M_1 N_2 T_1 H_2,$

$h_{13} = M_2 N_1 T_1 H_2, \quad h_{14} = M_2 N_1 T_2 H_1,$

$h_{15} = M_2 N_1 T_2 H_2, \quad h_{16} = M_2 N_2 T_1 H_2,$

and $h_{(i)}$ $(i = 1,2,3, \ldots, 16)$ satisfy: $\sum_{i=1}^{16} h_i = 1$.

6.3 The VSVD controller design

For the controller design, an observer was designed to estimate the velocity of the pavement input so that the real-time frequency information of road profile can be obtained. Then, a control algorithm for the proposed VSVD suspension system was developed on the basis of the state observer and TS fuzzy modelling method.

As the stiffness and the damping of the suspension are separately adjusted and controlled, two different controllers have to be designed. For the variable damping, we chose the classic skyhook controller which is simple while effective. The description for skyhook controller is:

$$F_{sky} = \begin{cases} C_{max}\dot{z_s}, & \dot{z_s}(\dot{z_s} - \dot{z_u}) \geq 0, \\ C_{min}\dot{z_s}, & \dot{z_s}(\dot{z_s} - \dot{z_u}) < 0\,, \end{cases} \tag{6.13}$$

where C_{max} and C_{min} are the maximum and minimum skyhook gains, which correspond to the command voltages I_{max} and I_{min}, respectively. In this experiment, the specific skyhook force is expressed as the MR damper force with the control output voltage, I_{max}=0.8A and $I_{min} = 0$V.

In terms of the control strategy for the stiffness component, it is to avoid the resonance of the quarter car under a pavement input. As the stiffness is controlled according to the dominant excitation frequency, the real-time frequency information of the pavement input is very important in determining the stiffness. At the same time, ideal switching frequencies, where the high stiffness should be switched to the low stiffness or vice versa, should also be obtained as a reference for the real-time frequency. In addition, the stroke limitation should be taken into consideration to protect the suspension from any collision.

Table 6.2 Correspondence between the switching frequency and the applied current

Damper current I_d (A)	Switching frequency (Hz)
0.0	1.50
0.1	1.49
0.2	1.47
0.3	1.46
0.4	1.45
0.5	1.43
0.6	1.41
0.7	1.40
0.8	1.38

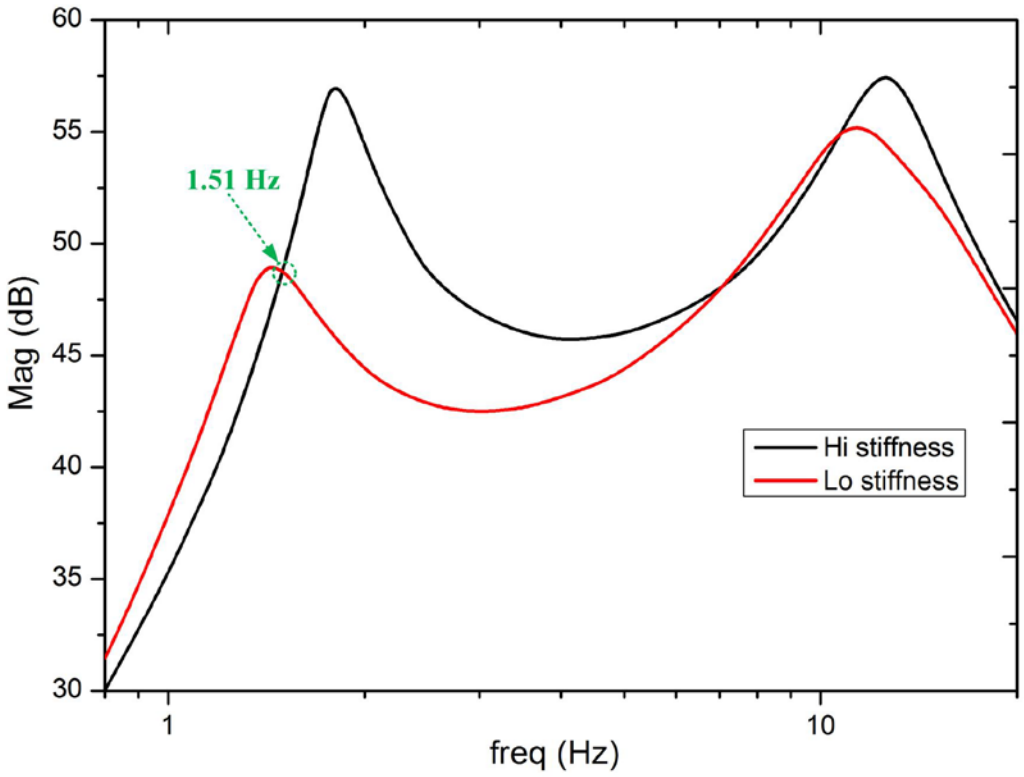

Figure 6.2 Simulation result of the switching frequency.

Determining the switching frequency is to guarantee that an optimal or minimal transmissibility (ratio of the quarter car response to the excitation signal) can be obtained. For example, the simulation result shown in Figure 6.2 in terms of the transmissibility from the excitation z_r to the sprung mass acceleration $\ddot{z}_s$, the switching frequency is 1.51Hz and the desired minimum transmissibility is composed of the black segment which is indicated as high stiffness before the 1.51Hz and the red segment indicated as low stiffness after 1.51Hz. In terms of the simulation results, the switching frequency is also related to the damping force F_d of the VSVD suspension. As the damping force F_d is controlled by current I_d, the switching frequency is a function of I_d. Table 6.2 lists the correspondence between the switching frequency and I_d. It can be calculated that the relationship between the switching frequency and the current is linear, therefore, the switching frequency can be defined as linear function of the applied current:

$$f_c = -0.15I_d + 1.50\,. \tag{6.14}$$

Real time dominant frequency of the pavement input is needed to compare with the above obtained switching frequency. Then the stiffness will be determined according to their relationship. To measure the real time dominant frequency, we have to firstly collect the velocity data ($\dot{z}_r$) of the pavement input. Then the dominant frequency information of the pavement input will be obtained by analyzing the velocity using STFT. As $\dot{z}_r$ is immeasurable in practice, we designed an observer to estimate the information. The design of the observer is based on the TS fuzzy model built in Section 6.2.3. The observer is designed as follow:

Define the measurable suspension deflection as:

$$y = [z_s - z_u], \tag{6.15}$$

and its state-space equation is: $y = C \cdot x$,

then $C = [0\ 0\ 0\ 0\ 1\ 0\ 0\ 0]$.

Then define the proposed observer as:

$$\begin{aligned} \dot{\hat{x}} &= A_h\hat{x} + L_h(y - \hat{y}) + B_{2h} \cdot u, \\ \hat{y} &= C\hat{x}, \end{aligned} \tag{6.16}$$

where $\hat{x}$ is the observer state vector, $\hat{y}$ is the estimated output, L_h is the observer gain matrix to be designed. Considering Eq. (6.8) and Eq. (6.16), the error dynamics model is defined as:

$$\begin{aligned} \dot{e} &= \dot{x} - \dot{\hat{x}} \\ &= A_h x + B_1 w + B_{2h} u - A_h\hat{x} - L_h y + L_h\hat{y} - B_{2h} u \\ &= A_h(x - \hat{x}) - L_h(\mathrm{y} - \hat{y}) + B_1 w \\ &= A_h \cdot e - L_h \cdot \mathrm{C} \cdot \mathrm{e} + B_1 w \\ &= (A_h - L_h \cdot \mathrm{C}) \cdot \mathrm{e} + B_1 w, \end{aligned} \tag{6.17}$$

where $\mathrm{e} = \mathrm{x} - \hat{x}$ is the estimated error.

Suppose that $A_{oh} = (A_h - L_h) \cdot \mathrm{C}$, then

$$\dot{e} = A_{oh} \cdot \mathrm{e} + B_1 w. \tag{6.18}$$

By defining an objective output as:

$$z_0 = e = \mathrm{x} - \hat{x} = E_0 \cdot e, \tag{6.19}$$

where $E_0 = 1$.

Then if there exists a matrix P>0 such that the following LMI is satisfied:

$$\begin{bmatrix} PA_{oh} + A_{oh}^T & PB_1 & E_0^T \\ * & -r_0^2 I & 0 \\ * & * & -I \end{bmatrix} < 0\,. \tag{6.20}$$

Then the system Eq. (6.8) is stable with H_∞ disturbance attenuation $r_0 > 0$. Using the definition $\mathrm{Y} = \mathrm{P}L_h$ and solving the LMI, the observer gain matrix can be obtained

as $L_h = P^{-1}Y$. Then the observer is successfully designed and it can estimate $\dot{z_r}$in real-time control.

Apart from the switching frequency, the determination of the stiffness also depends on stroke limitation. Once the suspension deflection is not less than the stoke limitation, the maximum stiffness will be turned on to avoid any collision. This value guarantees that the deformation of spring slows down before any collision under the maximum stoke limitation. Therefore, the controller to determine the stiffness is:

$$k_s = \begin{cases} k_{max}(I_s = 0.4A)\,, & f_{req} < f_c \; OR \; |z_s - z_u| \geq s_t, \\ k_{min}(I_s = 0\text{A})\,, & \text{Otherwise.} \end{cases} \tag{6.21}$$

where f_c is the switching frequency, f_{req} is the real time dominant frequency of the pavement input signal. Substituting Eq. (6.13) into Eq. (6.21) gives the complete VSVD control algorithm as:

$$\begin{cases} [k_s = k_{max}(I_s = 0.4A)] \; and \; [c_s = c_{sky}], freq < f_c \; OR \; z_s - z_u \geq s_t, \\ [k_s = k_{min}(I_s = 0\text{A})] \; and \; [c_s = c_{sky}], \quad \text{Otherwise.} \end{cases} \tag{6.22}$$

After constructing the controller, the TS fuzzy model is left aside in the experiment and the closed-loop control system is shown in Figure 6.3.

For the convenience of the reader, the signal processing module, the controller, and the quarter-car are represented by blue, green, and orange, respectively. It can be seen that the measurable variables, z_s and $z_s - z_u$, are transmitted to the skyhook variable damping (VD) controller and thus the desired damping can be determined. As for the variable stiffness (VS) controller, it needs three inputs and produces one output. One of the inputs, $\dot{z_r}$, needs to be estimated by the observer designed in the above section as this variable is immeasurable in practice.

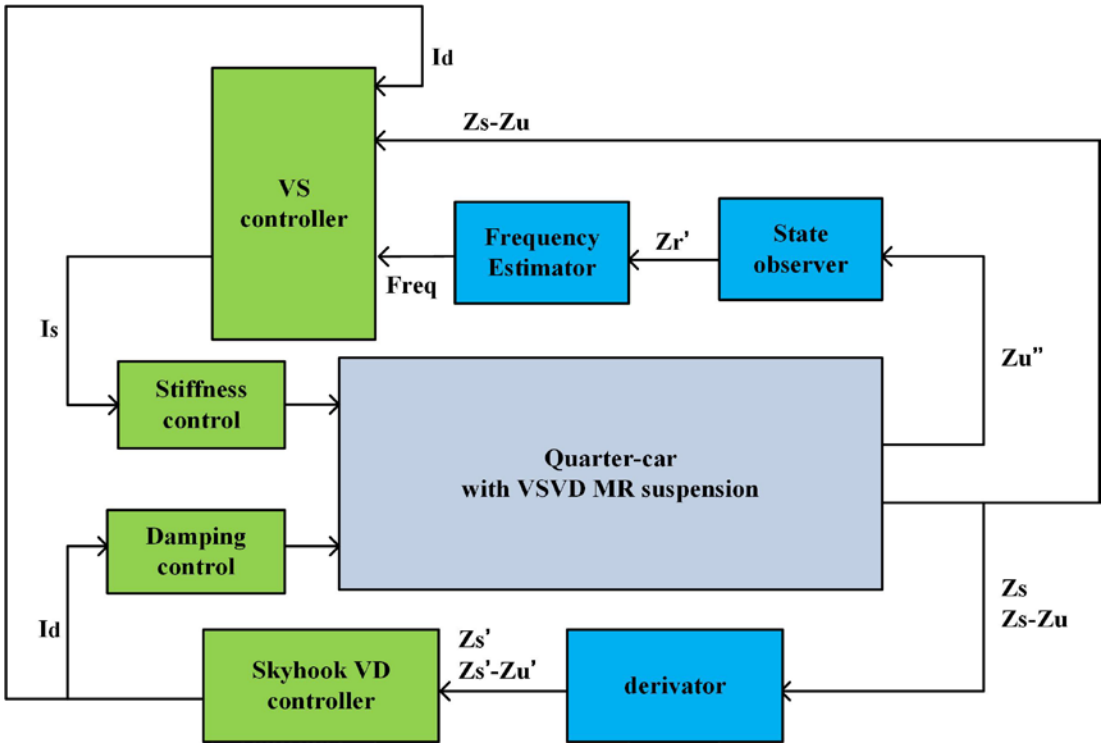

Figure 6.3 The control flow of the VSVD system.

After the estimation of $\dot{z}_r$, a frequency estimator will calculate the real time dominant frequency of the velocity using the Short-time Fourier Transform [133]. I_d provides the information of the switching frequency according to Eq. (6.14) and the deflection $(z_s - z_u)$ will compare with the suspension stoke limitation. Then the VS controller can determine the desired stiffness of the MR suspension.

6.4 Experimental validation of the VSVD controller

In this section, the proposed TS fuzzy controller was applied to control the variable stiffness and damping suspension which is installed on the quarter car test rig. Then, by applying the two kinds of road profiles to the tyre, the responses of the passive suspension, the VD one, the VS one, and the VSVD suspension were evaluated experimentally.

6.4.1 Description of the test rig setup and road excitations

Figure 6.4 shows the experimental set up of the quarter car test rig. The sprung mass m_s is 257.6 Kg and the tyre mass m_u is 33.2 Kg. The tyre is excited by a vertical road profile generated by a hydraulic system manufactured by the CRAM Corporation. The hydraulic actuator is controlled by the real-time control board (Model: myRio-1900, NI Corp.) with a PID controller. Acting as the external disturbance of the system, the imposed road profile displacement is measured by a laser displacement sensor (Model: LB-11, Keyence Corp.) and sent to the PID controller for the close-loop control.

Regarding the quarter-car structure, two displacement input signals, the SD and the sprung mass displacement (SMD), are measured by the two laser sensors (Model: LB-11, Keyence Corp.); and two acceleration input signals, the SMA and the unsprung mass acceleration (UMA), are measured by the two accelerometers (Model: ADXL327, Analog Devices Corp.). In terms of the VSVD MR suspension control, it is a multi-input-multi-output (MIMO) system. The signals, SD and SMD, are the inputs of the VD skyhook controller that SD and the absolute displacement SMD is the inputs of the digital differentiator to generate the velocities for the VD skyhook controller. The signals, UMA, SD, and I_d, are the inputs of the VS controller that UMA is processed by the state observer and the frequency estimator to output the real-time road dominant frequency. By running the VSVD control algorithm based on these inputs, the real-time control board || (Model: myRio-1900, NI Corp.) calculates the command currents, I_d and I_s, and sends them to power amplifiers. After amplifying the power of the signals, the currents considered as the system outputs will be sent to the two MR dampers. Furthermore, SMA and SD are also used as the reference signals to measure the comfort index of the applied suspensions.

Four kinds of excitation profile are applied in the test. In the first stage, to indicate the response of the VSVD controller to various excitation frequencies, a 10 seconds variable frequency sinusoidal excitation is applied, which is shown in Figure 6.5. In the first 5 seconds, the profile is described as 30 mm peak to peak amplitude with 1 Hz frequency, and it changes to 15 mm peak to peak amplitude with 2 Hz frequency in the last 5 seconds.

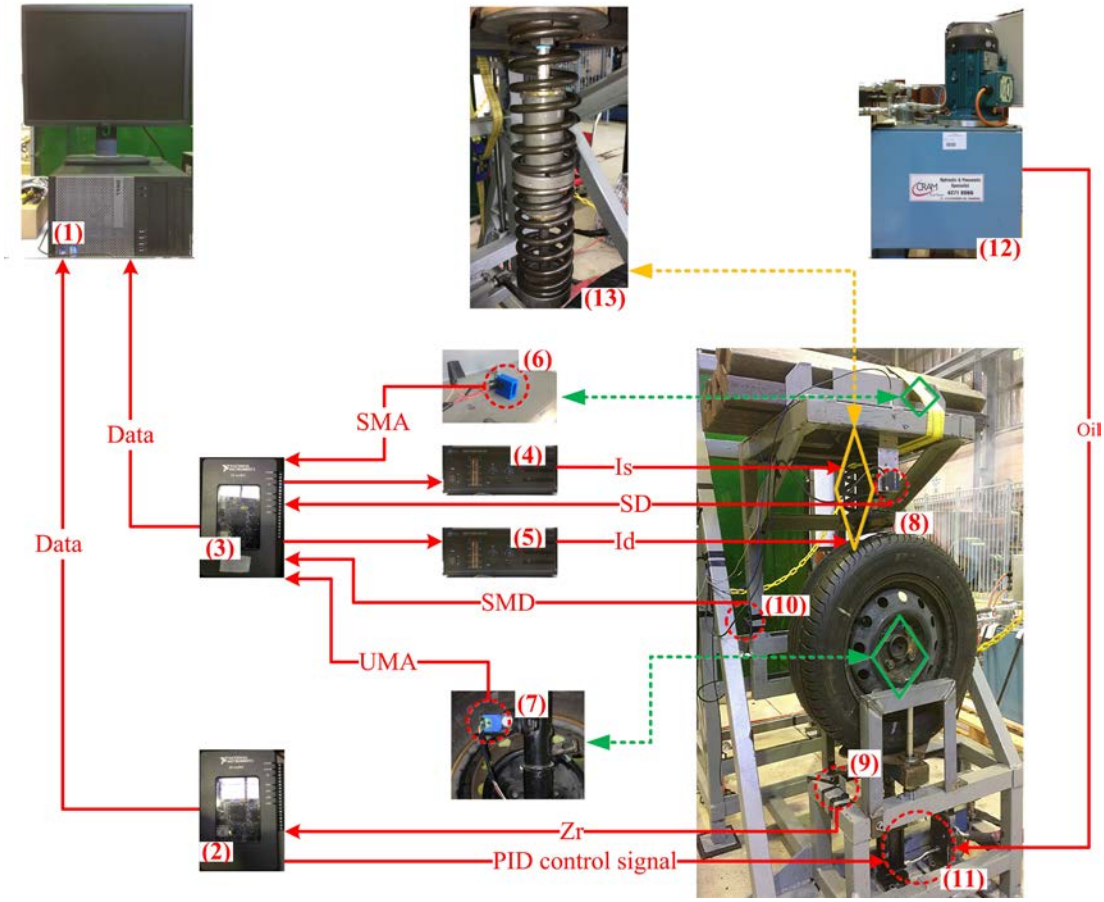

Figure 6.4 The experimental setup (1) computer, (2) NI real-time control board I, (3) NI real-time control board II, (4, 5) power amplifiers, (6,7) accelerometers, (8-10) laser sensors, (11) hydraulic actuator, (12) hydraulic station, and (13) the VSVD suspension.

A random excitation generated by this system is chosen as the second input signal. The displacement of the random road profile is generated according to [116, 123], as shown below:

$$\dot{z}_r(t) + \rho V_0 Z_r(t) = V_0 W_n \,, \tag{6.23}$$

where W_{n} is white noise with the intensity $2\sigma^2\rho V$, ρ is the road roughness parameter, σ^2 is the covariance of road irregularity, and V_0 is the vehicle speed. In the simulation, $\rho = 0.45\mathrm{m}^{-1}$, $\sigma^2 = 300\mathrm{mm}^2$, V_0 is 20m/s.

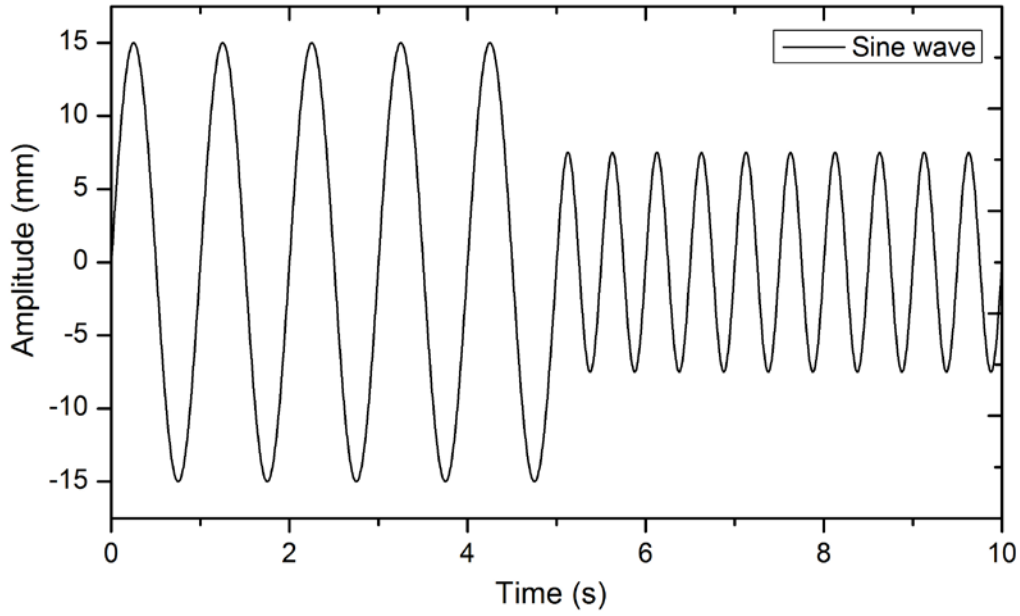

Figure 6.5 Sinusoidal excitation with variable frequency and magnitude.

In this experiment, the variable vehicle speed is also taken into consideration. The vehicle is assumed to travel on an off-road profile with the speed $V_0 = 20\ \mathrm{m/s}$ in the first 15 seconds, and keep $10\ \mathrm{m/s}$ in the last 15 seconds.

To investigate the ability of the controller on preventing end-stop phenomenon, two big bumps are added to the off-road profile as the fourth kind of road excitations. The off-road profile in time domain, the off-road profile with big bumps, and the corresponding vehicle speed are shown in Figures 6.6(a), 6.6(b) and 6.6(c).

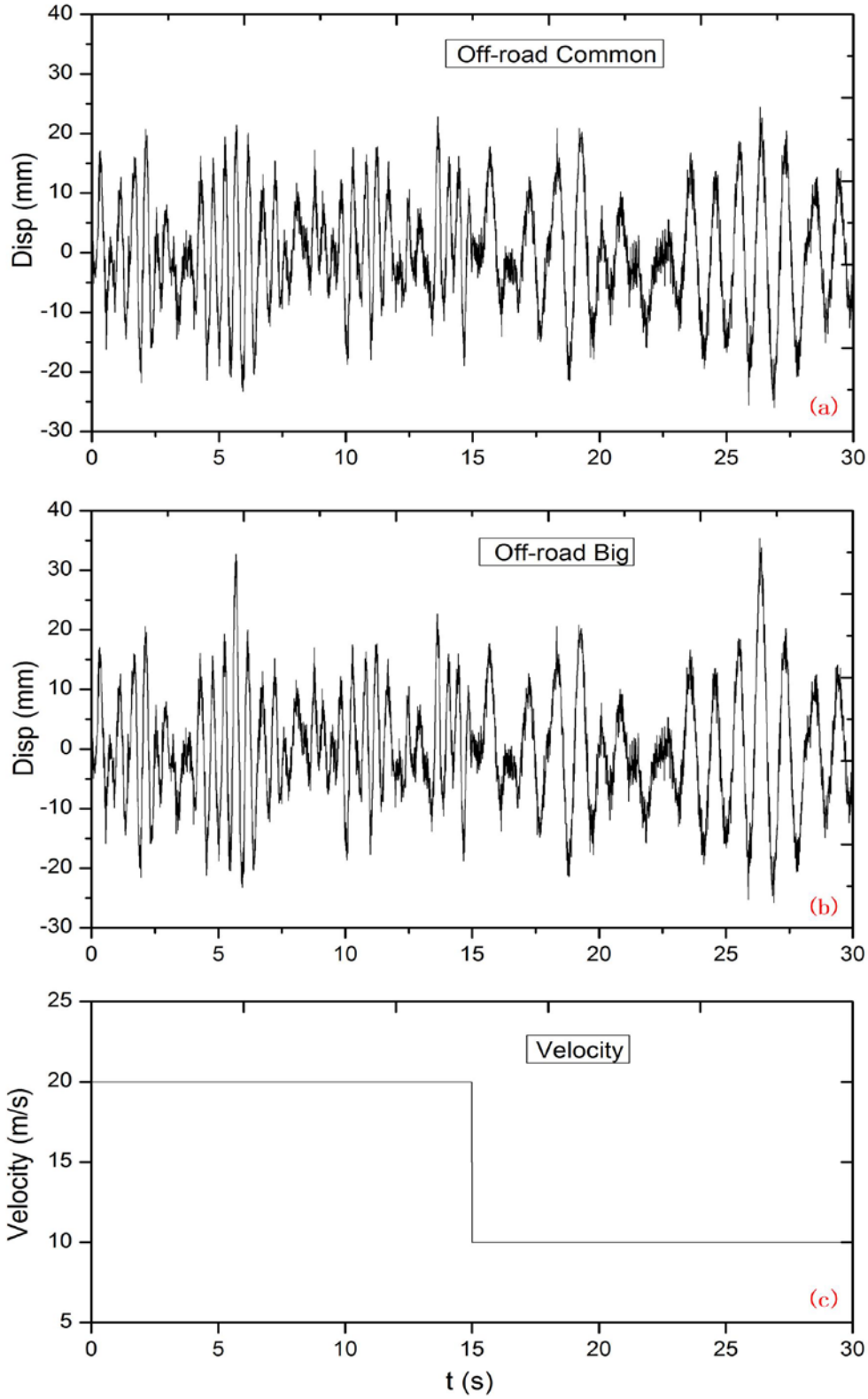

Figure 6.6 Test excitation: (a) normal off-road profile; (b) off-road with big bumps; (c) the vehicle speed of the excitation.

6.4.2 Experimental results

By applying the four kinds of excitation to the quarter-car system, the responses of the passive suspension, variable damping suspension, and the variable stiffness and variable damping suspension were evaluated.

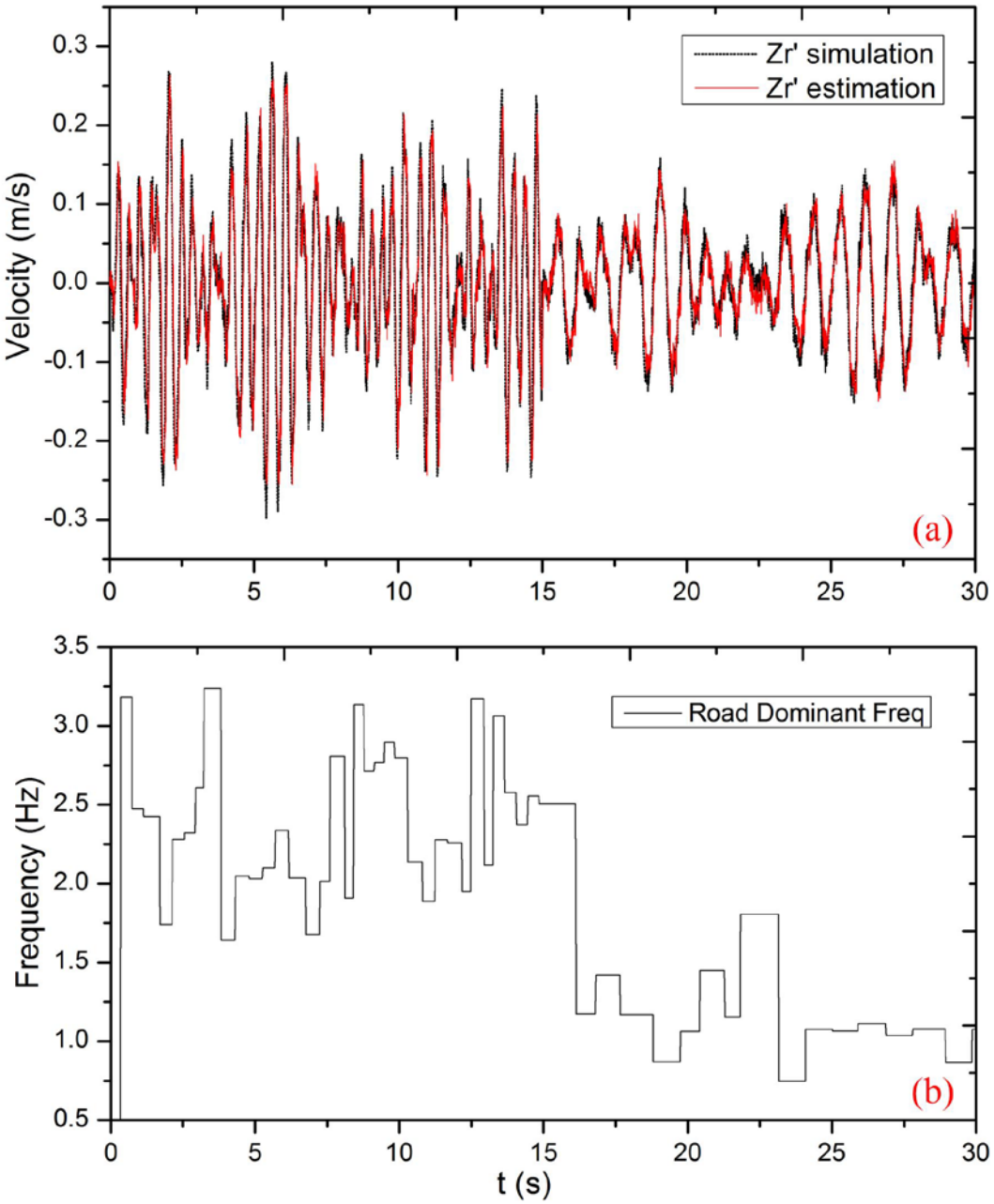

Figure 6.7 The performances of: (a) the state observer; (b) frequency estimator.

Figure 6.7 plots the results of estimated sprung mass velocity and the calculated road profile dominant frequency, respectively. The result indicates that the proposed state observer and frequency estimator can estimate the suspension states in real-time and accurate road profile dominant frequency information for the variable stiffness controller.

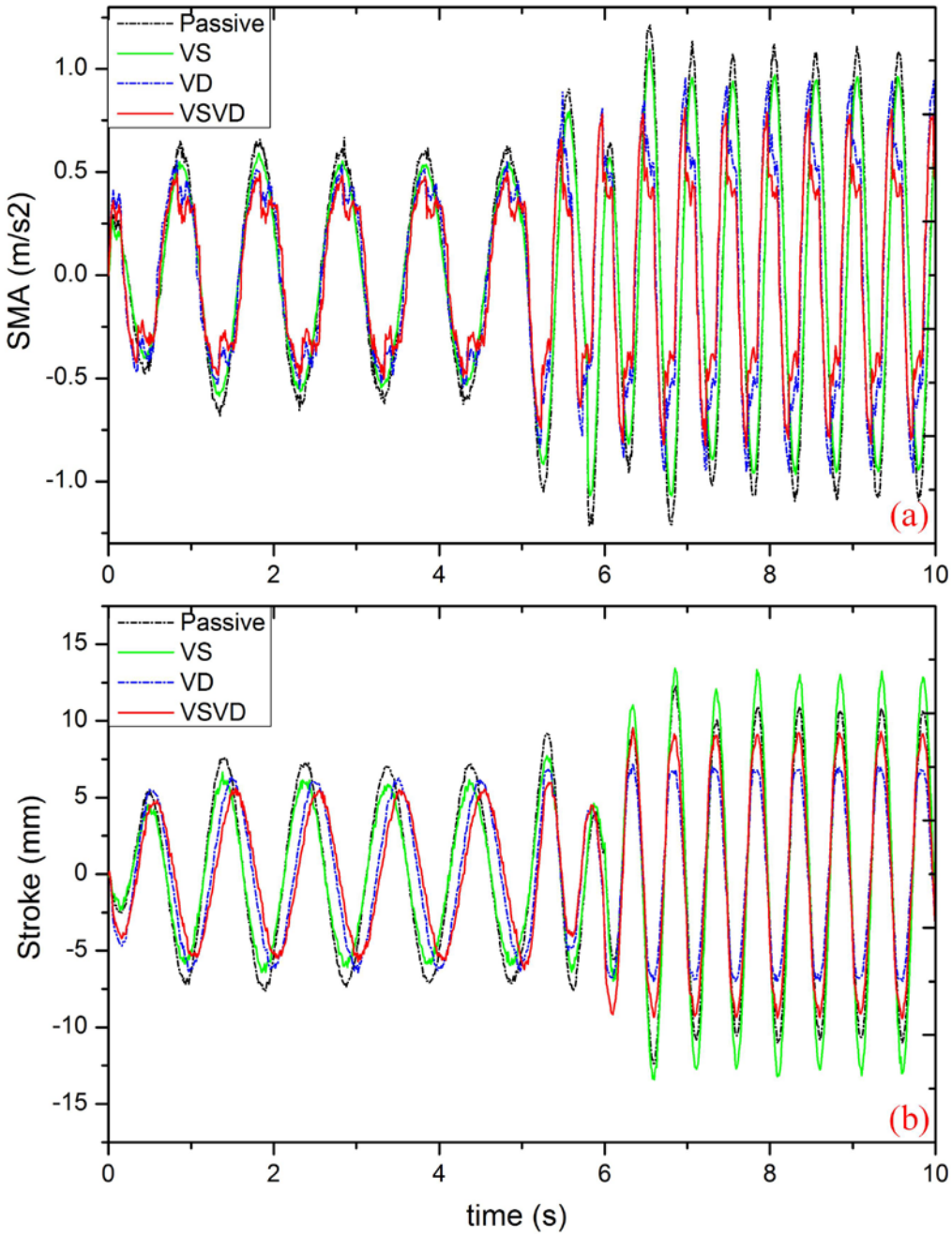

Figure 6.8 The results on the sine wave excitation: (a) sprung mass acceleration response; (b) suspension deflection response.

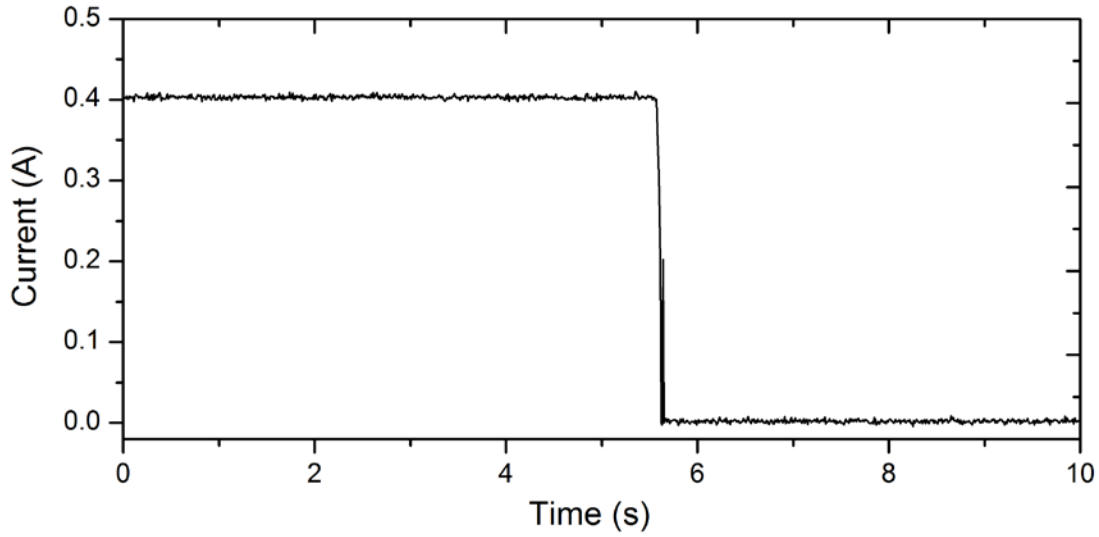

Figure 6.9 The applied current I_s of VS controller for sine wave excitation.

In the first stage of the experiment, sinusoidal excitation was carried out to evaluate the systems. Time histories of the test rig response in terms of the two performance criteria, sprung mass acceleration and suspension deflection, were recorded and plotted in Figure 6.8, respectively. The applied current I_s of VS controller was demonstrated in Figure 6.9. The figure shows that the applied current keeps high (big stiffness) in the low excitation frequency area, and it becomes zero (low stiffness) in the high excitation frequency area.

It can be seen that the vibration of the system, indicated as SMA value, is significantly suppressed under variable stiffens and variable damping control compared to the passive case. The VSVD controller performs best in SMA among these three suspensions, while the VD controller performs better during the last 5 seconds on suspension deflection, which could be attributed to the constantly large stiffness the VD system has. By comparing the four suspensions, it is clear that the lower is the suspension stiffness, the bigger is the suspension deflection. Specifically, the suspension travel of single VS control is worse than the passive case. Nevertheless, it

can be seen from the result of VSVD control that by combining a good damping controller with a low stiffness value, the suspension deflection can still be controlled and smaller than the value of passive suspension.

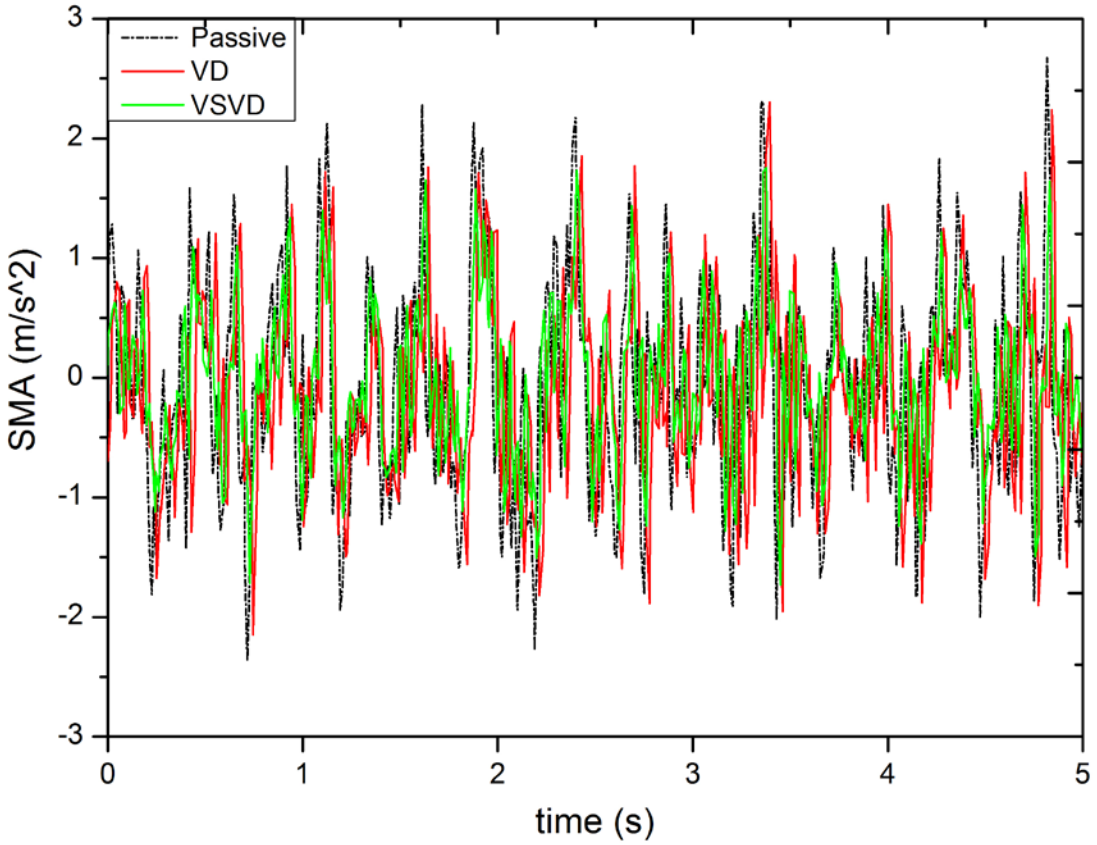

Figure 6.10 SMA under random road excitation in time domain.

Figures 6.10 and 6.11 show the experimental results on the random road profile in time domain and frequency domain, respectively. Three cases were considered: passive case where conventional passive suspension is used; variable damping case where the variable stiffness and damping suspension is used but the stiffness which is fixed by setting the applied current I_s as 0.35A; VSVD case where the variable stiffness and damping suspension is used and both the damping and stiffness can be controlled; the consequence of VS case which is similar with the one in the sinusoidal test is omitted for brevity.

Time history of the quarter car response in terms of the sprung mass acceleration is shown in Figure 6.10. It can be seen that the sprung mass acceleration under the passive case has the biggest peak value during the whole-time history. VSVD case and VD case both perform better than the passive case. However, the sprung mass acceleration under VSVD case is further reduced than that under VD case. This means that the quarter-car system performs best under VSVD case where the damping and the stiffness of the suspension are both controlled in real time. In order to illustrate the experimental results more clearly, the sprung mass acceleration responses under the three cases are compared in Table 6.3 in terms of their RMS values. It is seen that the acceleration RMS under VSVD case has the smallest value. And the reduction percentage compared to the passive case show that VSVD case is more effective on reducing the sprung mass acceleration than the VD case.

Table 6.3 Acceleration RMS value under random road profile

Variable	Passive	VD	VSVD
RMS (m/s^2)	0.967	0.821	0.772
Reduction percentage (%)	N/A	-15.1	-20.2

Figure 6.11 shows the frequency spectrum of the sprung mass acceleration under the random excitation. Close observations reveal that VSVD control case shows the best effectiveness on reducing the vibration power, especially at the frequency (2.1Hz) where the quarter car system suffers the most severe vibration.

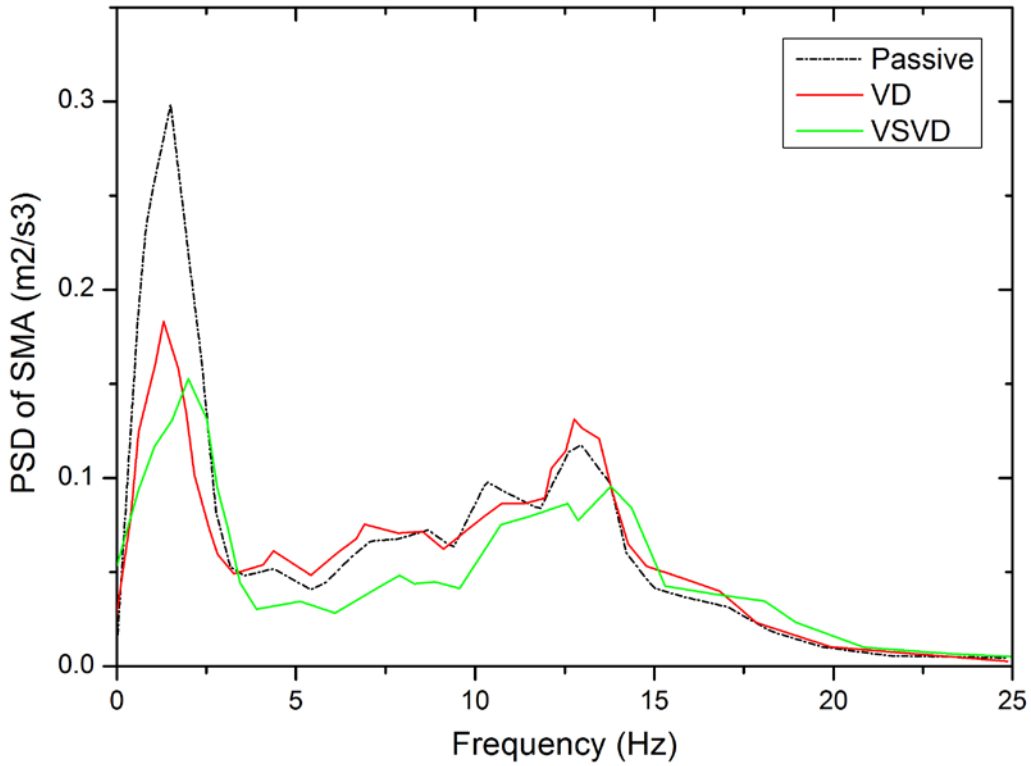

Figure 6.11 Sprung mass acceleration under random excitation in frequency domain.

Time histories of the test rig response to off-road excitation are recorded and plotted in Figure 6.12, where two objectives, the results of sprung mass acceleration and the suspension deflection, are shown in Figures 6.12(a) and 6.12(b), respectively. On the basis of the RMS value decrease made by VD control, the SMA value is further decreased by VSVD controller in the whole-time range. Regarding to SD, the VSVD controller performs better in low vehicle speed range (10 m/s) but has bigger value in high speed range (20 m/s) comparing with the suspension controlled by VD controller.

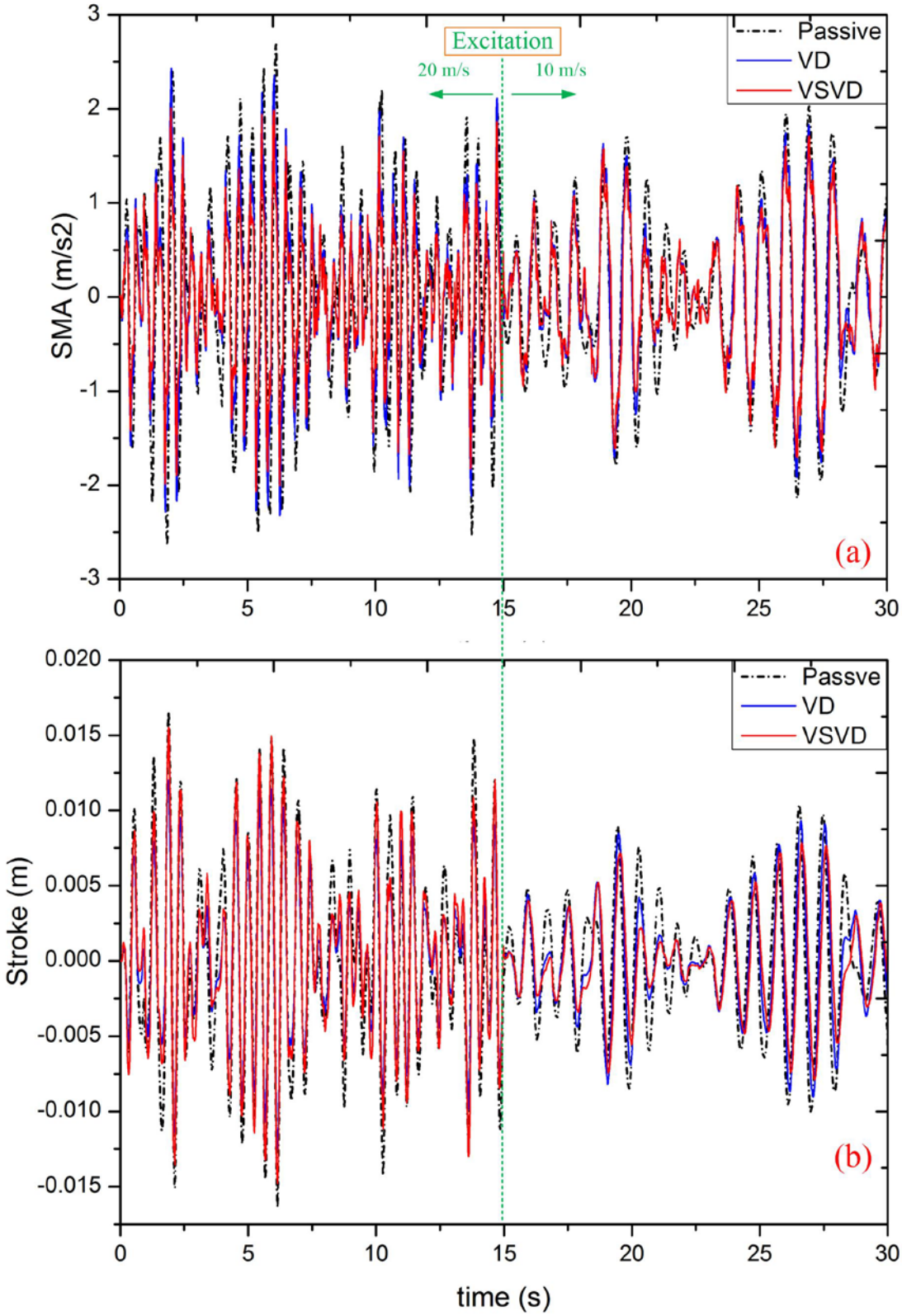

Figure 6.12 SMA and SD under variable speed off-road profile.

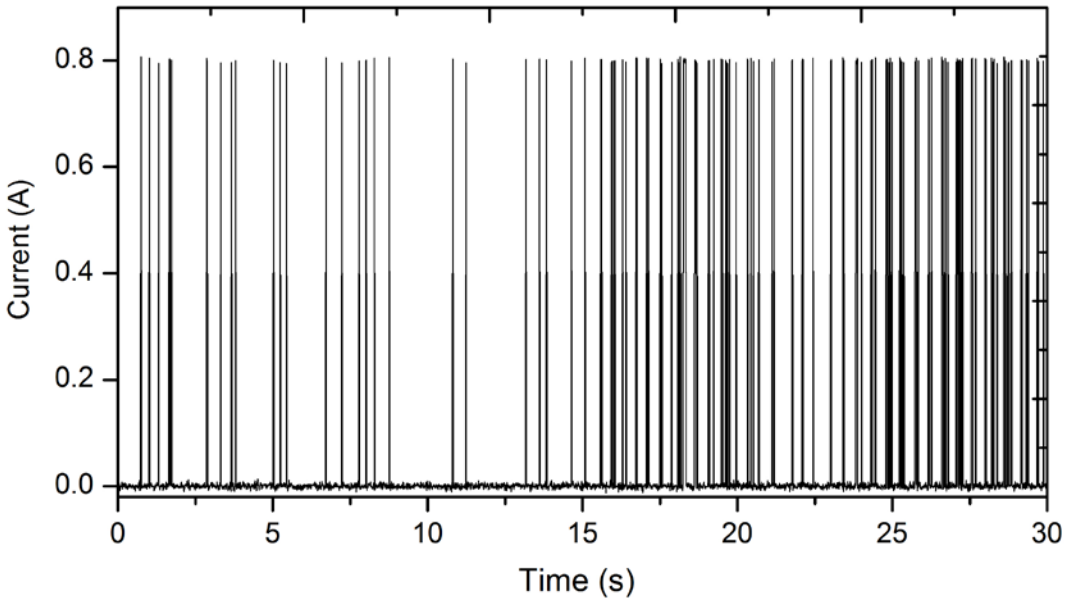

Figure 6.13 The applied current I_d of basic VSVD controller for off-road profile.

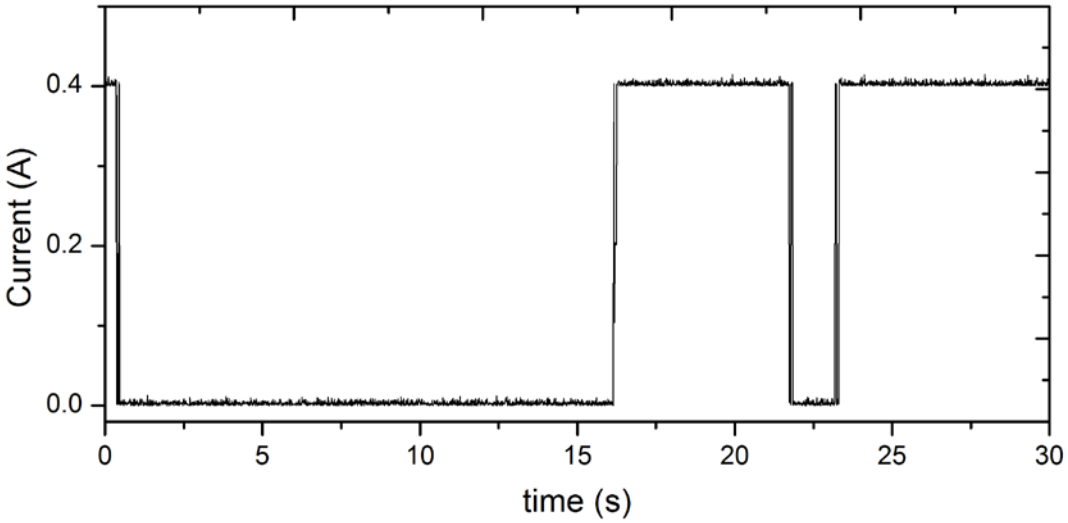

Figure 6.14 The applied current I_s of basic VSVD controller for off-road profile.

The applied currents to control damping and stiffness under off-road profile are shown in Figure 6.13 and Figure 6.14, respectively. Figure 6.14 shows the applied current to control system stiffness under off-road profile. The figure indicates that the applied current keeps zero (low stiffness) while the vehicle speed is relative high which increases the road dominant frequency, and it becomes big (large stiffness) when the vehicle speed decreases to 10 m/s (relative low road dominant frequency).

In order to illustrate the experimental results more clearly, the response of the three suspensions and the improved percentages to the conventional passive one is compared in Table 6.4 in terms of the RMS values. It can be seen that the suspension with VSVD controller has lowest RMS value in SMA but higher RMS value in SD compared with the suspension with VD controller. The distinctive result of VSVD case might be attributed by the small system stiffness controlled by the VSVD controller for the high road dominant frequency situation around 0-15 seconds (high vehicle speed), that the small stiffness reduces the vibration effectively but increases the movement distance of the suspension.

Table 6.4 RMS value of SMA and SD under off-road profile

Variable	Passive	VD	VSVD
SMA RMS (m/s^2)	0.974	0.783	0.732
Reduction (%)	N/A	-19.6	-24.8
SD RMS (m/s^2)	0.00555	0.00398	0.00441
Reduction (%)	N/A	-28.3	-20.6

To investigate the ability of the VSVD controller when dealing with end-stop phenomenon, the off-road profile with big bump excitation was applied to the quarter-car system, and the experimental results are demonstrated in Figure 6.15. Around the 5.5 second that the small stiffness is applying to the quarter-car system, the end-stop appears in the suspension system.

In Figure 6.15(a), the increase of SMA in area A is attributed by the big bump which leads to a sudden rise of the quarter-car system. The area B indicates the end-stop of the VSVD system that the small stiffness of the suspension cannot prevent the sprung mass and unsprung mass from moving closer so that the suspension stroke reaches the

limit and collision happened. The crash causes a huge increase in SMA, which could make the driver and passengers very uncomfortable.

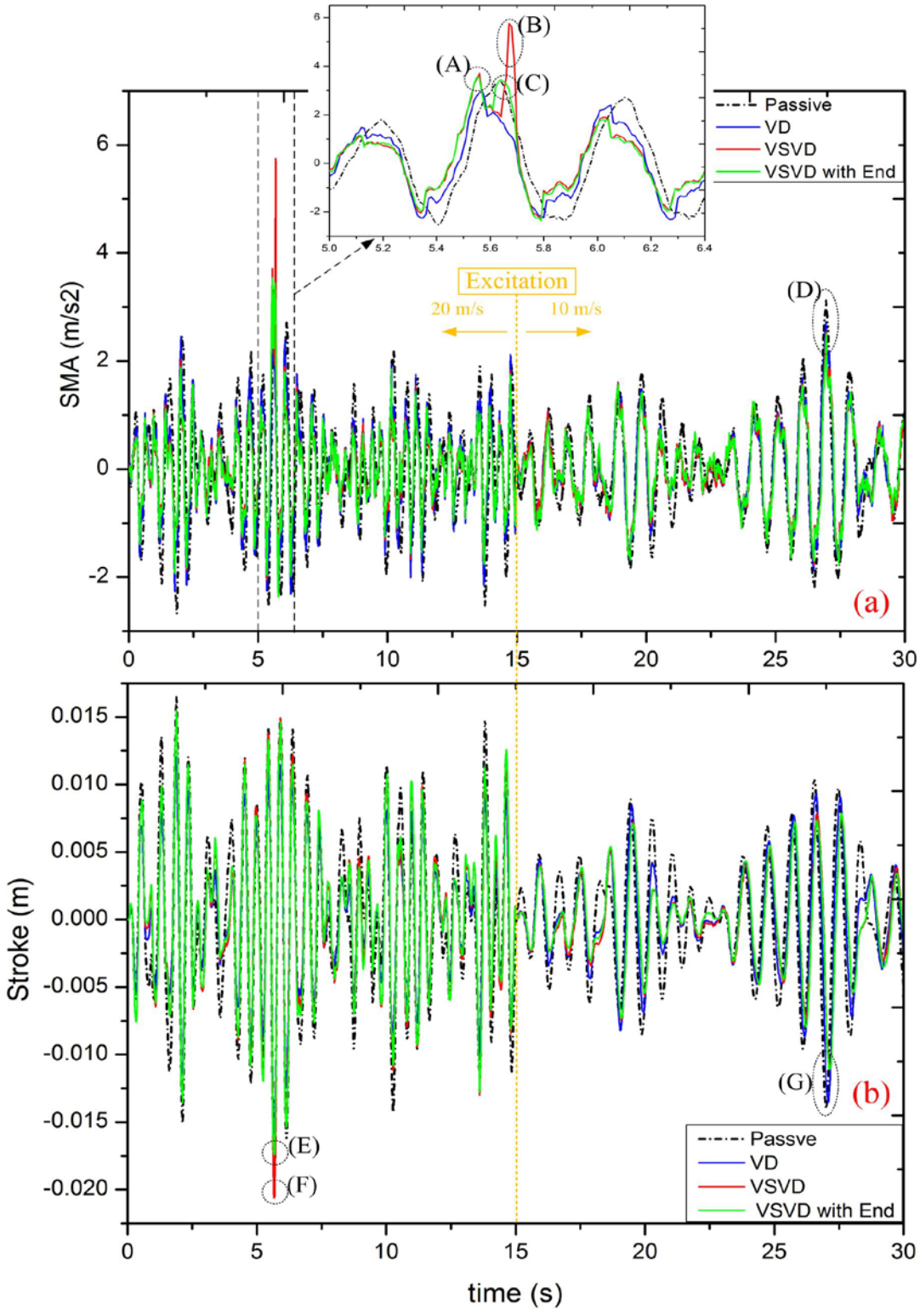

Figure 6.15 SMA and SD under variable speed off-road profile with big bump.

The result of VSVD controller considering end-stop is shown in area C. The big bump is detected and the system stiffness changes to big enough in advance, so that no crash happens in the suspension. The area D indicates the unobvious effect in SMA made by the second bump that the continuous big stiffness of the system prevents the collision. The results of the suspension deflection are shown in Figure 6.15(b). It can be seen that the basic VSVD controller meets the stroke limit which is shown in area F and the VSVD controller considering end-stop does not reach the limit shown in area E. Area G illustrates the continuous big stiffness of the suspension systems avoid end-stop.

When the quarter-car test rig meets a big bump that causes a rapid compression of the VSVD suspension, an end-stop crash would happen between the top cover and the cylinder 2 of the suspension. The area where the end-stop happened on the suspension system is shown in Figure 6.16.

Figure 6.16 The location of the suspension where the end-stop happened.

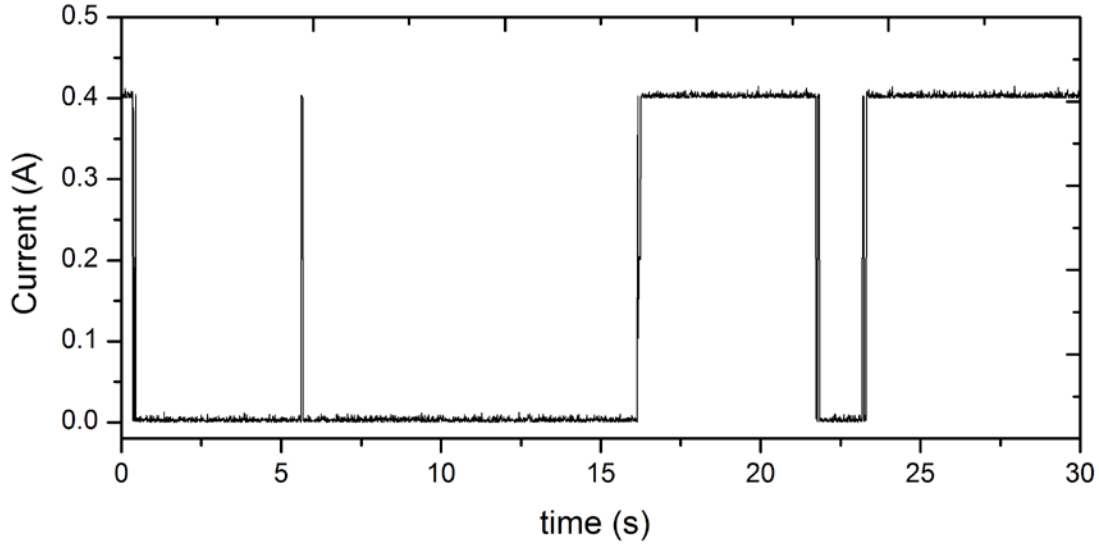

Figure 6.17 The applied current I_s of VSVD controller considering end-stop for off-road with big bumps excitation.

The applied current to control stiffness for end-stop case is shown in Figure 6.17. it is noticed that a high current is generated around the 5.5 second to increase the suspension stiffness.

6.5 Conclusion

A control algorithm on the basis of TS fuzzy modelling, STFT, skyhook and a state observer was built to control the advanced MR suspension and a quarter car test rig was used to evaluate the performance of the VSVD suspension on vibration control. Experimental tests were conducted under four excitations, which includes sine wave, random road, off-road, and off-road with big bump. Comparing with the conventional passive suspension, the SMA reduction (20.2%) of VSVD control is much more effective than the one of the VD control (15.1%). Moreover, the experiment result of off-road case illustrates that the reduction on the RMS SMA of VSVD suspension achieves 24.8% while no end-stop happened. Therefore, it is worthwhile to mention

that the VSVD controller can increase riding comfort of a vehicle effectively, especially under off-road or outfield working condition.

7 CONCULSIONS AND FUTURE WORK

In order to satisfy human's increasing demand on the performance of vehicle, the development direction of automobile industry has developed into a new stage which includes multiple disciplines and technologies. In view of the wide range of applications of MR technology in the automobile industry, this thesis presented the development of MR control for vehicle suspension and the corresponding design of MR devices to improve the vibration control performance. The major findings from this study are summarised in the following section.

7.1 Summary of the main findings

7.1.1 Theoretical analysis of vehicle suspension and MR damper design

MacPherson nonlinear suspension model and linear quarter-car model were established and compared. Experiment result shows quarter-car model can exactly describe the suspension's dynamic characteristics with fewer model parameters than MacPherson model. In order to improve the vibration control performance, an optimization program which based on the existing test rig characteristic was done for MR damper and controller design. During the design program, stiffness and damping are normally most fundamental elements needed for proper performance. Different stiffness values correspond to the different resonance frequency of a vibration system and increase damping, which then reduces the transmittable resonance. Thus, suspension equivalent damping and stiffness were carefully analysed and optimized. In the program, a multi-objective method was used to deal with the driver's demand of a vehicle suspension under different driving status. Based on the optimization results, An MR damper for a quarter-car suspension was designed, fabricated. It was

also tested comparing with a LORD MR damper. The test results show the OMRD performs better than the LORD damper on the existing quarter-car test rig.

7.1.2 A TS fuzzy control for the vehicle suspension with MR damper

A state observer-based TS fuzzy controller was designed and investigated on the quarter-car test-rig. To build the controller, a TS fuzzy modelling approach for the quarter-car semi-active suspension was proposed. Considering practical application, a state observer was established to estimate the suspension state in real-time. The measured result shows that the observer can estimate the state of the quarter-car system accurately and the time delay of the estimated result is less than 30 ms. Experimental results under different road excitations were measured. The results show that by using the proposed state observer-based TS fuzzy controller, the reductions on the three objectives, the PTP values of SMA, SD, and TD, are about 28%, 23%, and 14% compared to the ones of passive system, respectively. It verifies that the state observer-based TS fuzzy controller outperforms the other control algorithms.

7.1.3 A new full-size VSVD vehicle suspension based on MR dampers

A full-size variable stiffness and damping vehicle suspension was designed, prototyped, tested, and analysed, and the results verify that the stiffness and damping value of the suspension can be controlled and its range is suitable for a real car; indeed with optimal design for the prototype structure, the stiffness of the suspension can vary from 18.2 $\mathrm{kN/m}$ to 38.5 $\mathrm{kN/m}$ while the equivalent damping coefficient has the ability to change from 796 $\mathrm{kN/(m/s)}$ to 1658 $\mathrm{kN/(m/s)}$, and therefore this development makes the suspension feasible for vehicle in practical application. In order to describe the dynamic characteristic of the VSVD suspension accurately, a new 3-DOF phenomenological model with double Bouc-Wen model was established. Then,

the effectiveness the VSVD suspension which is described by the 3-DOF model was verified by the simulation work under bump and random road excitation. The results illustrate that the proposed model can accurately predict the dynamic performance of the variable stiffness and damping MR suspension in real-time control.

7.1.4 A TS fuzzy modelling based controller for VSVD suspension

A control algorithm on the basis of TS fuzzy modelling, short time Fourier transform, skyhook and a state observer was built to control the advanced MR variable stiffness and damping suspension and a quarter car test rig was used to evaluate the performance of the VSVD damper on vibration control. Experimental tests were conducted under four excitations, which includes sine wave, random road, off-road, and off-road with big bump. The results illustrate the suspension controlled by the variable stiffness and damping controller highly improves the comfort and robustness of the vehicle system, with respect to different road input conditions. Specifically, the SMA RMS value of the variable stiffness and damping suspension performs further approximate 25% reduction when comparing to the passive suspension system. Meanwhile, the VSVD control algorithm also prevented end-stop from happening in the test excited by off-road profile. Clearly, reaching the end-stop causes a dramatic deterioration of the comfort performance and a damage of vehicle components to decrease device lifetime. It is successfully verified that the ability of this new controller which can enhance the performance of variable stiffness and damping suspension in terms of improving ride comfort effectively.

7.2 Recommendations for future work

The major effort of this thesis is on developing MR structure and control algorithm for improving the performance of vehicle suspension. It is desirable and valuable to make further effort on the follow three aspects.

7.2.1 Design of interval type-2 TS fuzzy controller for MR damper

The TS fuzzy modelling approach can handle nonlinearities in modelling physical structure by approximating nonlinear terms to any specified accuracy with a family of type-1 fuzzy sets and rules. The type-1 fuzzy model can capture nonlinearities effectively. However, it is worth noticing that there exist not only nonlinearities but also parameter uncertainties when building the model. Since the uncertain parameter exists in the plant, the membership functions would be still uncertain. Based on interval type-2 fuzzy set theory, the parameter uncertainties could be handled with the lower and upper membership functions. How to connect interval type-2 fuzzy method into an TS fuzzy modelling based controller for MR damper should be considered in future studies.

7.2.2 Further improvement of VSVD control in real-time

Due to the typical low pass filtering characteristic of vehicle suspension, the high frequency information of frequency domain response is relatively low utilized for real-time control. The existing VSVD algorithm just estimate the frequency information of road profile in real-time. Based on this process, further frequency domain analysis and frequency information decomposition with weighting should be done to improve the effectiveness of the VSVD control algorithm.

Furthermore, the effectiveness of the observer integrated in control strategies has been demonstrated in this thesis. Considering that the state of vehicle suspension is not only

structural nonlinear but also partly immeasurable, further study on nonlinear state observer is highly recommended. In addition, the time delay issue attributed by observer may also decrease the performance of the controlled system in real-time test. Therefore, how to effectively integrate a state observer and control algorithm should be a topic of interest. Furthermore, based on the road testing methods in the references [72, 134, 135], the developed VSVD suspension system can be installed on a real car to do field test on proving ground to evaluate its control effectiveness and system reliability in future research. In outdoor situation, mud is easy to adhere to the chassis while a vehicle is running. If the surface of laser sensor is covered by mud, the device attached to the suspension may fail to work. Therefore, in a field test, the laser sensor which is used to measure the suspension deflection might be replaced by a magneto-strictive displacement transducer to enhance the stability of the control system. Furthermore, In the future research, we might consider to build a more practical state observer to estimate more state information of VSVD system, such as the displacement between sprung mass and unsprung mass, and the vertical velocity of sprung mass. By doing so, less sensors, especially leaser sensor, might be used in real field test to ensure the stability of the system.

REFERENCES

[1] C. Long, D. H. Shi, R. C. Wang, and H. W. Zhou, "Semi-active control of energy-regenerative suspension based on hybrid control strategy," *Transactions of Beijing Institute of Technology,* 2016.

[2] K. D. Rao and S. Kumar, "Modeling and simulation of quarter car semi active suspension system using LQR controller." *Proceedings of the 3rd International Conference on Frontiers of Intelligent Computing: Theory and Applications (FICTA) 2014*, Springer, Cham, 2015.

[3] H. Du, W. Li, and N. Zhang, "Semi–active control of an integrated full–car suspension with seat suspension and driver body model using ER dampers," *International Journal of Vehicle Design,* vol. 63, pp. 159-184, 2013.

[4] J. S. Esmaeili, A. Akbari, and H. R. Karimi, "Load-dependent LPV/H2 output-feedback control of semi-active suspension systems equipped with MR damper," *International Journal of Vehicle Design,* vol. 68, p. 119, 2015.

[5] H. Du, W. Li, and N. Zhang, "Semi-active variable stiffness vibration control of vehicle seat suspension using an MR elastomer isolator," *Smart Materials & Structures,* vol. 20, p. 105003, 2011.

[6] J. Gu, H. Wang, C. Wang, M. Pang, and X. Jin, "The parameter optimization and performance analysis of the suspension system in the cab of a heavy truck," *International Conference on Computer and Computing Technologies in Agriculture*, Springer, Berlin, Heidelberg, 2013.

[7] G. Z. Yao, F. F. Yap, and G. Chen, "MR damper and semi-active control of vehicle suspension system," *Smart Materials Bulletin,* vol. 2002, p. 13, 2002.

[8] J. N. Yang and A. K. Agrawal, "Semi-active hybrid control systems for nonlinear buildings against near-field earthquakes," *Engineering Structures,* vol. 24, pp. 271-280, 2002.

[9] X. Z. Zhang, X. Y. Wang, W. H. Li, and K. Kostidis, "Variable stiffness and damping MR isolator," *Journal of Physics: Conference Series*, 2009, p. 012088.

[10] C. Greinerpetter, A. Suryadi Tan, and T. Sattel, "A semi-active magnetorheological fluid mechanism with variable stiffness and damping," *Smart Materials & Structures*, vol. 23, 2014.

[11] S. Sun, H. Deng, H. Du, W. Li, J. Yang, G. Liu, *et al.*, "A compact variable stiffness and damping shock absorber for vehicle suspension." *IEEE/ASME Transactions on Mechatronics*, 20(5), 2621-2629, 2015.

[12] L. M. Jugulkar, S. Singh, and S. M. Sawant, "Analysis of suspension with variable stiffness and variable damping force for automotive applications," *Advances in Mechanical Engineering*, vol. 8, 2016.

[13] X. Dong, W. Liu, X. Wang, J. Yu, and P. Chen, "Research on variable stiffness and damping magnetorheological actuator for robot joint," *International Conference on Intelligent Robotics and Applications*, Springer, Cham, 2017.

[14] I. Maciejewski and T. Krzyżyński, "Control design of semi-active seat suspension systems," *Journal of Theoretical and Applied Mechanics*, vol. 49, pp. 1151-1168, 2011.

[15] W. S. Aboud, S. M. Haris, and Y. Yaacob, "Advances in the control of mechatronic suspension systems," *Journal of Zhejiang University SCIENCE C*, vol. 15, pp. 848-860, 2014.

[16] L. Zuo and P.-S. Zhang, "Energy harvesting, ride comfort, and road handling of regenerative vehicle suspensions," *Journal of Vibration and Acoustics*, vol. 135, p. 011002, 2013.

[17] P. W. Nugroho, W. Li, H. Du, G. Alici, and J. Yang, "An adaptive neuro fuzzy hybrid control strategy for a semiactive suspension with magneto rheological damper," *Advances in Mechanical Engineering*, vol. 6, p. 487312, 2014.

[18] K. Yi and B. Song, "A new adaptive sky-hook control of vehicle semi-active suspensions," *Proceedings of the Institution of Mechanical Engineers, part D: Journal of automobile engineering*, vol. 213, pp. 293-303, 1999.

[19] C. Poussot-Vassal, C. Spelta, O. Sename, S. M. Savaresi, and L. Dugard, "Survey and performance evaluation on some automotive semi-active suspension control methods: A comparative study on a single-corner model," *Annual Reviews in Control*, vol. 36, pp. 148-160, 2012.

[20] M. Crosby and D. C. Karnopp, "The active damper—a new concept for shock and vibration control," *Shock and Vibration Bulletin*, vol. 43, pp. 119-133, 1973.

[21] H. E. Tseng and D. Hrovat, "State of the art survey: active and semi-active suspension control," *Vehicle System Dynamics*, vol. 53, pp. 1034-1062, 2015.

[22] W. S. Aboud, S. M. Haris, and Y. Yaacob, "Advances in the control of mechatronic suspension systems," *Journal of Zhejiang Universityence C,* vol. 15, pp. 848-860, 2014.

[23] E. Guglielmino, T. Sireteanu, C. W. Stammers, G. Ghita, and M. Giuclea, *Semi-active suspension control: improved vehicle ride and road friendliness*. Springer Science & Business Media, 2008.

[24] O. Altet, X. Moreau, M. Moze, P. Lanusse, and A. Oustaloup, "Principles and synthesis of hydractive CRONE suspension," *Nonlinear Dynamics,* vol. 38, pp. 435-459, 2004.

[25] R. Gehm, "Delphi improves cadillac's ride," *Automotive Engineering International,* vol. 109, pp. 32-33, 2001.

[26] R. N. Jazar, "Quarter Car Model," *Vehicle Dynamics,* ed: Springer, 2014, pp. 985-1026.

[27] J. K. Ok, D. W. Park, W. S. Yoo, and J. H. Sohn, "Development of a new bushing model for vehicle suspension module design," *Transactions of the Korean Society of Automotive Engineers,* vol. 14, 143-150, 2006.

[28] A. Giua, C. Seatzu, and G. Usai, "A mixed suspension system for a half-car vehicle model," *Dynamics & Control,* vol. 10, pp. 375-397, 2000.

[29] K. S. Hong, D. S. Jeon, W. S. Yoo, H. Sunwoo, S. Y. Shin, and C. M. Kim, "A New Model and an Optimal Pole-Placement Control of the Macpherson Suspension System," *Sae Technical Papers,* 1999.

[30] J. Hurel, A. Mandow, and A. Garcia-Cerezo, "Nonlinear two-dimensional modeling of a McPherson suspension for kinematics and dynamics simulation," *IEEE International Workshop on Advanced Motion Control*, 2012, pp. 1-6.

[31] J. Hurel, A. Mandow, and A. Garcíacerezo, "Kinematic and dynamic analysis of the McPherson suspension with a planar quarter-car model," *Vehicle System Dynamics,* vol. 51, pp. 1422-1437, 2013.

[32] K. S. Hong, D. S. Jeon, W. S. Yoo, H. Sunwoo, S. Y. Shin, C. M. Kim, *et al.*, "A new model and an optimal pole-placement control of the Macpherson suspension system," *SAE Technical Paper,* 0148-7191, 1999.

[33] A. I. I. Mahir, S. P. Deng, and Y. M. Qi, "Gantry robot dynamic analysis based on Lagrange's motion equation," *Key Engineering Materials,* vol. 693, pp. 1741-1746, 2016.

[34] M. Ahmadian and C. A. Pare, "A quarter-car experimental analysis of alternative semiactive control methods," *Journal of Intelligent Material Systems and Structures,* vol. 11, pp. 604-612, 2000.

[35] S. Türkay and H. Akçay, "A study of random vibration characteristics of the quarter-car model," *Journal of Sound & Vibration,* vol. 282, pp. 111-124, 2005.

[36] N. Wereley, A. Chaudhuri, J.-H. Yoo, S. John, S. Kotha, A. Suggs, *et al.*, "Bidisperse magnetorheological fluids using Fe particles at nanometer and micron scale," *Journal of Intelligent Material Systems and Structures,* vol. 17, pp. 393-401, 2006.

[37] B. J. Park, K. H. Song, and H. J. Choi, "Magnetic carbonyl iron nanoparticle based magnetorheological suspension and its characteristics," *Materials Letters,* vol. 63, pp. 1350-1352, 2009.

[38] R. Stanway, J. Sproston, and N. Stevens, "Non-linear modelling of an electro-rheological vibration damper," *Journal of Electrostatics,* vol. 20, pp. 167-184, 1987.

[39] I. H. Shames, *Elastic and inelastic stress analysis*. CRC Press, 1997.

[40] B. Spencer, S. Dyke, M. Sain, and J. Carlson, "Phenomenological model for magnetorheological dampers," *Journal of Engineering Mechanics,* vol. 123, pp. 230-238, 1997.

[41] Y. K. Wen, "Method for random vibration of hysteretic systems," *Journal of the engineering mechanics division,* vol. 102, pp. 249-263, 1976.

[42] M. Ismail, F. Ikhouane, and J. Rodellar, "The hysteresis Bouc-Wen model, a survey," *Archives of Computational Methods in Engineering,* vol. 16, pp. 161-188, 2009.

[43] R. Alkhatib, G. Nakhaie Jazar, and M. Golnaraghi, "Optimal design of passive linear suspension using genetic algorithm," *Journal of Sound and Vibration,* vol. 275, pp. 665-691, 2004.

[44] R. Prabakar, C. Sujatha, and S. Narayanan, "Response of a quarter car model with optimal magnetorheological damper parameters," *Journal of Sound and Vibration,* vol. 332, pp. 2191-2206, 2013.

[45] R. S. Prabakar, C. Sujatha, and S. Narayanan, "Response of a half-car model with optimal magnetorheological damper parameters," *Journal of Vibration and Control,* p. 1077546314532300, 2014.

[46] C. C. Smith, D. Y. McGehee, and A. J. Healey, "The prediction of passenger riding comfort from acceleration data," *Journal of Dynamic Systems, Measurement, and Control,* vol. 100, pp. 34-41, 1978.

[47] J. Hedrick, R. Ravera, and J. Anderes, "The effect of elevated guideway construction tolerances on vehicle ride quality," *Journal of Dynamic Systems, Measurement, and Control,* vol. 97, pp. 408-416, 1975.

[48] L. Hoberock, "A survey of longitudinal acceleration comfort studies in ground transportation vehicles," *Journal of Dynamic Systems, Measurement, and Control,* vol. 99, pp. 76-84, 1977.

[49] J. J. Fearnsides, J. Hendrick, and H. Firouztash, "Specification of ride quality criteria for transportation systems: the state of the art and a new approach," *High Speed Ground Transportation Journal,* vol. 8, 1974.

[50] ISO, *Mechanical Vibration and Shock: Evaluation of Human Exposure to Whole-body Vibration. Part 1, General Requirements: International Standard ISO 2631-1: 1997 (E)*: ISO, 1997.

[51] A. Kuznetsov, M. Mammadov, I. Sultan, and E. Hajilarov, "Optimization of improved suspension system with inerter device of the quarter-car model in vibration analysis," *Archive of Applied Mechanics,* vol. 81, pp. 1427-1437, 2011.

[52] G. Verros, S. Natsiavas, and C. Papadimitriou, "Design optimization of quarter-car models with passive and semi-active suspensions under random road excitation," *Journal of Vibration and Control,* vol. 11, pp. 581-606, 2005.

[53] D. Hrovat, "Survey of advanced suspension developments and related optimal control applications," *Automatica,* vol. 33, pp. 1781-1817, 1997.

[54] G. Georgiou, G. Verros, and S. Natsiavas, "Multi-objective optimization of quarter-car models with a passive or semi-active suspension system," *Vehicle System Dynamics,* vol. 45, pp. 77-92, 2007.

[55] D. Simon and M. Ahmadian, "Vehicle evaluation of the performance of magneto rheological dampers for heavy truck suspensions," *Transactions-*

American Society of Mechanical Engineers Journal of Vibration and Acoustics, vol. 123, pp. 365-375, 2001.

[56] Y. Shen, M. Golnaraghi, and G. Heppler, "Semi-active vibration control schemes for suspension systems using magnetorheological dampers," *Journal of Vibration and Control*, vol. 12, pp. 3-24, 2006.

[57] C. Park and D. Jeon, "Semiactive vibration control of a smart seat with an MR fluid damper considering its time delay," *Journal of intelligent material systems and structures*, vol. 13, pp. 521-524, 2002.

[58] D. Karnopp, M. J. Crosby, and R. Harwood, "Vibration control using semi-active force generators," *Journal of Manufacturing Science and Engineering*, vol. 96, pp. 619-626, 1974.

[59] S. Guo, S. Li, and S. Yang, "Semi-active vehicle suspension systems with magnetorheological dampers," *Vehicular Electronics and Safety, 2006. ICVES 2006. IEEE International Conference on*, 2006, pp. 403-406.

[60] S. Abramov, S. Mannan, and O. Durieux, "Semi-active suspension system simulation using Simulink," *International Journal of Engineering Systems Modelling and Simulation*, vol. 1, pp. 101-114, 2009.

[61] P. W. Nugroho, W. Li, H. Du, G. Alici, and J. Yang, "An adaptive neuro fuzzy hybrid control strategy for a semiactive suspension with magneto rheological damper," *Advances in Mechanical Engineering*, vol. 2014, 2014.

[62] M. Valášek, M. Novak, Z. Šika, and O. Vaculin, "Extended ground-hook-new concept of semi-active control of truck's suspension," *Vehicle System Dynamics*, vol. 27, pp. 289-303, 1997.

[63] V. Sankaranarayanan, M. Emekli, B. Gilvenc, L. Guvenc, E. Ozturk, Ş. Ersolmaz, *et al.*, "Semiactive suspension control of a light commercial vehicle," *Mechatronics, IEEE/ASME Transactions on*, vol. 13, pp. 598-604, 2008.

[64] P. J. Gawthrop, S. A. Neild, and D. J. Wagg, "Semi-active damping using a hybrid control approach," *Journal of Intelligent Material Systems and Structures*, p. 1045389X12436734, 2012.

[65] G. Yao, F. Yap, G. Chen, W. Li and S. Yeo, "MR damper and its application for semi-active control of vehicle suspension system," *Mechatronics*, vol. 12, pp. 963-973, 2002.

[66] H. Du, J. Lam, and N. Zhang, "Modelling of a magneto-rheological damper by evolving radial basis function networks," *Engineering Applications of Artificial Intelligence,* vol. 19, pp. 869-881, 2006.

[67] L. M. Jansen, "Semiactive control strategies for MR dampers-comparative study," *Journal of Engineering Mechanics,* vol. 126, pp. 795-803, 2000.

[68] A. Shojaei, H. Metered, S. Shojaei, and S. O. Oyadiji, "Theoretical and experimental investigation of magneto-rheological damper based semi-active suspension systems," *International Journal of Vehicle Structures & Systems,* vol. 5, p. 109, 2013.

[69] A. M. Tusset, M. Rafikov, and J. M. Balthazar, "An intelligent controller design for magnetorheological damper based on a quarter–car model," *Journal of Vibration and Control,* 2009.

[70] M. N. Khajavi and V. Abdollahi, "Comparison between optimized passive vehicle suspension system and semi active fuzzy logic controlled suspension system regarding ride and handling," *Proceedings of world academy of science, engineering and technology*, 2007, pp. 57-61.

[71] X. P. Do, K. Shah, and S. B. Choi, "Damping force tracking control of MR damper system using a new direct adaptive fuzzy controller," *Shock and Vibration,* 2015.

[72] M. Yu, C. Liao, W. Chen, and S. Huang, "Study on MR semi-active suspension system and its road testing," *Journal of Intelligent Material Systems and Structures*, vol. 17, pp. 801-806, 2006.

[73] M. M. Rashid, N. A. Rahim, M. A. Hussain, and M. Rahman, "Analysis and experimental study of magnetorheological-based damper for semiactive suspension system using fuzzy hybrids," *Industry Applications, IEEE Transactions on,* vol. 47, pp. 1051-1059, 2011.

[74] M. Biglarbegian, W. Melek, and F. Golnaraghi, "A novel neuro-fuzzy controller to enhance the performance of vehicle semi-active suspension systems," *Vehicle System Dynamics,* vol. 46, pp. 691-711, 2008.

[75] L. A. Zadeh, B. Yuan, and G. J. Klir, "Fuzzy sets, fuzzy logic, and fuzzy systems: selected papers by Lotfi A. Zadeh," *Archive for Mathematical Logic,* vol. 32, pp. 1-32, 1996.

[76] T. Takagi and M. Sugeno, "Fuzzy identification of systems and its applications to modeling and control," *IEEE transactions on systems, man, and cybernetics*, vol.1, 116-132, 1985.

[77] L. Félix-Herrán, D. Mehdi, R. Soto, J. de J Rodríguez-Ortiz, and R. Ramírez-Mendoza, "Control of a semi-active suspension with a magnetorheological damper modeled via Takagi-Sugeno," *Control & Automation (MED), 2010 18th Mediterranean Conference on*, 2010, pp. 1265-1270.

[78] H. Du and N. Zhang, "Model-based fuzzy control for buildings installed with magneto-rheological dampers," *Journal of Intelligent Material Systems and Structures*, 2009.

[79] H. Zhang, J. Yang, and C.Y. Su, "TS fuzzy-model-based robust H-inf design for networked control systems with uncertainties," *IEEE Transactions on Industrial Informatics*, 3(4), 289-301, 2007.

[80] L. Félix-Herrán, D. Mehdi, J. Rodríguez-Ortiz, R. Ramírez-Mendoza, and R. Soto, "Takagi-Sugeno fuzzy model of a one-half semiactive vehicle suspension: lateral approach," *Mathematical Problems in Engineering*, vol. 2015, 2015.

[81] N. N. Karnik, J. M. Mendel, and Q. Liang, "Type-2 fuzzy logic systems," *IEEE Transactions on Fuzzy Systems*, vol. 7, pp. 643-658, 1999.

[82] M. M. Zirkohi and T. C. Lin, "Interval type-2 fuzzy-neural network indirect adaptive sliding mode control for an active suspension system," *Nonlinear Dynamics*, vol. 79, pp. 513-526, 2015.

[83] S. D. Nguyen, D. Jung, and S. B. Choi, "A robust vibration control of a magnetorheological damper based railway suspension using a novel adaptive type 2 fuzzy sliding mode controller," *Shock and Vibration*, vol. 2017, 2017.

[84] A. Sakalli, T. Kumbasar, E. Yesil, and H. Hagras, "Analysis of the performances of type-1, self-tuning type-1 and interval type-2 fuzzy PID controllers on the Magnetic Levitation system," *Fuzzy Systems (FUZZ-IEEE), 2014 IEEE International Conference on*, 2014, pp. 1859-1866.

[85] C. Lauwerys, J. Swevers, and P. Sas, "Robust linear control of an active suspension on a quarter car test-rig," *Control Engineering Practice*, vol. 13, pp. 577-586, 2005.

[86] P. Brezas, M. C. Smith, and W. Hoult, "A clipped-optimal control algorithm for semi-active vehicle suspensions: Theory and experimental evaluation," *Automatica,* vol. 53, pp. 188-194, 2015.

[87] J. L. Yao, W. K. Shi, J. Q. Zheng, and H. P. Zhou, "Development of a sliding mode controller for semi-active vehicle suspensions," *Journal of Vibration and Control,* vol. 19, pp. 1152-1160, 2013.

[88] J. Fei and M. Xin, "Robust adaptive sliding mode controller for semi-active vehicle suspension system," *International Journal of Innovative Computing, Information and Control,* vol. 8, pp. 691-700, 2012.

[89] H. Zhang, E. Wang, N. Zhang, F. Min, R. Subash, and C. Su, "Semi-active sliding mode control of vehicle suspension with magneto-rheological damper," *Chinese Journal of Mechanical Engineering,* vol. 28, pp. 63-75, 2015.

[90] M. C. Chen, W. Y. Wang, S. F. Su, and Y. H. Chien, "Robust TS fuzzy-neural control of uncertain active suspension systems," *International Journal of Fuzzy Systems,* vol. 12, pp. 321-329, 2010.

[91] H. Li, J. Yu, C. Hilton, and H. Liu, "Adaptive sliding-mode control for nonlinear active suspension vehicle systems using T-S fuzzy approach," *Industrial Electronics, IEEE Transactions on,* vol. 60, pp. 3328-3338, 2013.

[92] D. K. Shin and S. B. Choi, "Design of a new adaptive fuzzy controller and its application to vibration control of a vehicle seat installed with an MR damper," *Smart Materials and Structures,* vol. 24, p. 085012, 2015.

[93] D. Hernandez-Alcantara, J. C. Tudon-Martinez, L. Amezquita-Brooks, C. Vivas-Lopez, and R. Morales-Menendez, "State observers for semi-active suspensions: Experimental results," *Control Applications (CCA), 2014 IEEE Conference on*, 2014, pp. 53-58.

[94] L. Xiaodong and Z. Qingling, "New approaches to H∞ controller designs based on fuzzy observers for TS fuzzy systems via LMI," *Automatica,* vol. 39, pp. 1571-1582, 2003.

[95] H. Ren, Y. Zhao, S. Chen, and G. Liu, "State observer based adaptive sliding mode control for semi-active suspension systems," *Journal of Vibroengineering,* vol. 17, 2015.

[96] Y. Liu, H. Matsuhisa, and H. Utsuno, "Semi-active vibration isolation system with variable stiffness and damping control," *Journal of Sound and Vibration,* vol. 313, pp. 16-28, 2008.

[97] G. Y. Pan and F. Q. Fan, "Research on semi-active suspension system with variable stiffness and damping," *Applied Mechanics and Materials*, 2012, pp. 584-589.

[98] S. C. Liu, "Resonance suppression through variable stiffness and damping mechanisms," *Proceedings of SPIE - The International Society for Optical Engineering,* vol. 3671, 1999.

[99] K. K. Walsh, K. D. Grupenhof, K. L. Little, A. Martin, and C. A. M. Jr, "Development and testing of a newly proposed continuously variable stiffness/damping device for vibration control," *Proceedings of SPIE - The International Society for Optical Engineering,* vol. 8345, p. 69, 2012.

[100] G. J. Liao, X. L. Gong, S. H. Xuan, C. J. Kang, and L. H. Zong, "Development of a real-time tunable stiffness and damping vibration isolator based on magnetorheological elastomer," *Journal of Intelligent Material Systems & Structures*, vol. 23, pp. 25-33, 2012.

[101] X. Zhang, X. Wang, W. Li, and K. Kostidis, "Variable stiffness and damping MR isolator," *Journal of Physics: Conference Series*, 2009, p. 012088.

[102] W. H. Li, X. Y. Wang, X. Z. Zhang, and Y. Zhou, "Development and analysis of a variable stiffness damper using an MR bladder," *Smart Materials & Structures*, vol. 18, p. 074007, 2009.

[103] S. Sun, H. Deng, and W. Li, "A variable stiffness and damping suspension system for trains," *SPIE Smart Structures and Materials+ Nondestructive Evaluation and Health Monitoring*, 2014, pp. 90570P-90570P-12.

[104] X. Zhu, X. Jing, and L. Cheng, "A magnetorheological fluid embedded pneumatic vibration isolator allowing independently adjustable stiffness and damping," *Smart Materials & Structures,* vol. 20, pp. 85025-85042(18), 2011.

[105] P. Raja, X. Wang, and F. Gordaninejad, "A high-force controllable MR fluid damper-liquid spring suspension system," *Smart Materials & Structures,* vol. 23, p. 015021, 2014.

[106] C. Greinerpetter, A. S. Tan, and T. Sattel, "A semi-active magnetorheological fluid mechanism with variable stiffness and damping," *Smart Materials & Structures*, vol. 23, 2014.

[107] Y. Liu, H. Matsuhisa, H. Utsuno, and J. G. Park, "Vibration isolation by a variable stiffness and damping system," *Jsme International Journal*, vol. 48, pp. 16–28, 2005.

[108] S. Sun, J. Yang, W. Li, H. Deng, H. Du, and G. Alici, "Development of a novel variable stiffness and damping magnetorheological fluid damper," *Smart Materials & Structures*, vol. 24, 2015.

[109] Z. Xing, M. Yu, S. Sun, J. Fu, and W. Li, "A hybrid magnetorheological elastomer-fluid (MRE-F) isolation mount: development and experimental validation," *Smart Materials and Structures*, vol. 25, p. 015026, 2015.

[110] Y. Xu, M. Ahmadian, and R. Sun, "Improving vehicle lateral stability based on variable stiffness and damping suspension system via MR damper," *IEEE Transactions on Vehicular Technology*, 63.3, pp. 1071-1078, 2014.

[111] Y. Xu and M. Ahmadian, "Improving the capacity of tire normal force via variable stiffness and damping suspension system," *Journal of Terramechanics*, vol. 50, pp. 121-132, 2013.

[112] O. M. Anubi and C. D. Crane III, "A new active variable stiffness suspension system using a nonlinear energy sink-based controller," *Vehicle System Dynamics*, vol. 51, pp. 1588-1602, 2013.

[113] O. M. Anubi and C. Crane, "A new semiactive variable stiffness suspension system using combined skyhook and nonlinear energy sink-based controllers," *Control Systems Technology, IEEE Transactions on*, vol. 23, pp. 937-947, 2015.

[114] Y. Liu, J. Hozumi, and M. Tabata, "Ride comfort and wheel load fluctuation compatible control using variable stiffness and damping," *Proceedings of the FISITA 2012 World Automotive Congress*, 2013, pp. 355-365.

[115] C. Spelta, F. Previdi, S. M. Savaresi, P. Bolzern, M. Cutini, C. Bisaglia, *et al.*, "Performance analysis of semi-active suspensions with control of variable damping and stiffness," *Vehicle System Dynamics*, vol. 49, pp. 237-256, 2011.

[116] S. B. Choi and W. K. Kim, "Vibration control of a semi-active suspension featuring electrorheological fluid dampers," *Journal of Sound and Vibration,* vol. 234, pp. 537-546, 2000.

[117] M. Shinozuka and G. Deodatis, "Simulation of stochastic processes by spectral representation," *Applied Mechanics Reviews,* vol. 44, pp. 191-204, 1991.

[118] Y. H. Liu, F. Li, and Y. H. Huang, "Numerical simulation methods of railway track irregularities," *Journal of Traffic and Transportation Engineering,* vol. 6, pp. 29-33, 2006.

[119] L. D. Lutes, *Stochastic analysis of structural and mechanical vibrations*. Prentice Hall, 1997.

[120] D. Karnopp, "How significant are transfer function relations and invariant points for a quarter car suspension model?," *Vehicle system dynamics,* vol. 47, pp. 457-464, 2009.

[121] Ö. Gündoğdu, "Optimal seat and suspension design for a quarter car with driver model using genetic algorithms," *International Journal of Industrial Ergonomics,* vol. 37, pp. 327-332, 2007.

[122] Z. Michalewicz, *Genetic algorithms+data structures=evolution programs*. Springer Science & Business Media, 1996.

[123] H. Du, J. Lam, K. Cheung, W. Li, and N. Zhang, "Direct voltage control of magnetorheological damper for vehicle suspensions," *Smart Materials and Structures,* vol. 22, p. 105016, 2013.

[124] X. Tang, W. Li, and H. Du, "Speed dependent optimisation for variable stiffness vehicle suspension," *11th World Congr. Struct. Multidiscip. Optim.*, Sydney, 2015.

[125] K. Tanaka and H. O. Wang, *Fuzzy control systems design and analysis: a linear matrix inequality approach*. John Wiley & Sons, 2004.

[126] F. Zhang, *The Schur complement and its applications*. Springer Science & Business Media, 2006.

[127] S. M. Savaresi and C. Spelta, "A single-sensor control strategy for semi-active suspensions," *Control Systems Technology, IEEE Transactions on,* vol. 17, pp. 143-152, 2009.

[128] S. Sulaiman, P. M. Samin, H. Jamaluddin, R. A. Rahman, and M. S. Burhaumudin, "Groundhook control of semi-active suspension for heavy

vehicle," *International Journal of Research in Engineering and Technology (IJRET)*, vol. 1, pp. 146-152, 2012.

[129] F. Tyan, Y. F. Hong, S. H. Tu, and W. S. Jeng, "Generation of random road profiles," *Journal of Advanced Engineering*, vol. 4, pp. 1373-1378, 2009.

[130] H. Ren, S. Chen, Y. Zhao, G. Liu, and L. Yang, "State observer-based sliding mode control for semi-active hydro-pneumatic suspension," *Vehicle System Dynamics*, pp. 1-23, 2015.

[131] W. Li, G. Yao, G. Chen, S. Yeo, and F. Yap, "Testing and steady state modeling of a linear MR damper under sinusoidal loading," *Smart Materials and Structures*, vol. 9, p. 95, 2000.

[132] D. Wang and W. Liao, "Magnetorheological fluid dampers: a review of parametric modelling," *Smart Materials and Structures*, vol. 20, p. 023001, 2011.

[133] S. Sun, H. Deng, J. Yang, W. Li, H. Du, G. Alici, *et al.*, "An adaptive tuned vibration absorber based on multilayered MR elastomers," *Smart Materials & Structures*, vol. 24, 2015.

[134] S. Choi, H. Lee, and E. Chang, "Field test results of a semi-active ER suspension system associated with skyhook controller," *Mechatronics*, vol. 11, pp. 345-353, 2001.

[135] S. B. Choi, Y. M. Han, H. J. Song, J. W. Sohn, and H. J. Choi, "Field test on vibration control of vehicle suspension system featuring ER shock absorbers," *Journal of Intelligent Material Systems and Structures*, vol. 18, pp. 1169-1174, 2007.

LIST OF PUBLICATIONS

Refereed Journal Paper

- X. Tang, H. Du, S. Sun, D. Ning, Z. Xing, and W. Li, “Takagi–Sugeno fuzzy control for semi-active vehicle suspension with a magnetorheological damper and experimental validation,” IEEE/ASME Transactions on Mechatronics, vol. 22, pp. 291-300, 2017.

- S. Sun, X. Tang, J. Yang, D. Ning, H. Du, S. Zhang, and W. Li, “Advanced variable stiffness and damping magnetorheological fluid damper towards next generation vehicle suspension systems,” IEEE Transactions on Industrial Informatics, 2017. (submitted).

Conference Paper

- X. Tang, W. Li, and H. Du, “Speed dependent optimisation for variable stiffness vehicle suspension,” in WCSMO-11, Sydney, Australia, 2015.

- X. Tang, S. Sun, H. Du, and W. Li, “Variable stiffness and damping control with MR suspension for vehicle system,” in ICAVP-2017, Hangzhou, China, 2017.

- S. Sun, X. Tang, W. Li, and H. Du, "Advanced vehicle suspension with variable stiffness and damping MR damper," in IEEE International Conference on Mechatronics, 2017, pp. 444-448.

APPENDIX A: MACPHERSON SUSPENSION MODELLING PROCESS

Lagrange motion equation is normally expressed as follows:

$$\frac{d}{dt}\left(\frac{\partial T}{\partial \dot{q}_j}\right) - \frac{\partial T}{\partial q_j} + \frac{\partial U}{\partial q_j} = Q_j, \quad j = 1,2,\dots N, \tag{A.1}$$

where T is the system dynamics that is also the function of $\dot{q}_j$, U is system potential energy that is also the function of q_j; Q_j is the non-dominant generalized forces including damping force. As for viscous damping, Q_j can be expressed as follows:

$$Q_j = -\frac{\partial D}{\partial \dot{q}_j}. \tag{A.2}$$

(A.2) is called Rayleigh's dissipation function. To define A, B, C as (x_A, y_A), (x_B, y_B), (x_C, y_C), respectively, and the angle between the connecting lead of traveller's and below transverse arm's junction points, and X axis is α; during the motion, the displacement of sprung mass is z_s, and the anti-clock angle of lower controlling swing arm is θ; in addition, the sprung mass only move in vertical direction; then A, B, and C can be expressed as follows:

$$\begin{aligned} x_A &= 0, \\ y_A &= z_s, \end{aligned} \tag{A.3}$$

$$\begin{aligned} x_B &= l_{OB}[\cos(\theta + \theta_0) - \cos(\theta_0)], \\ y_B &= z_s + l_{OB}[\sin(\theta + \theta_0) - \sin(\theta_0)], \end{aligned} \tag{A.4}$$

$$\begin{aligned} x_C &= l_{OC}[\cos(\theta + \theta_0) - \cos(\theta_0)], \\ y_C &= z_s + l_{OC}[\sin(\theta + \theta_0) - \sin(\theta_0)]. \end{aligned} \tag{A.5}$$

By defining $\beta = \alpha + \theta_0$, the equation of triangle OAB can be described as

$$l_{AB} = \sqrt{(l_{OA}^2 + l_{OB}^2 - 2l_{OA}l_{OB}\cos\beta)}, \tag{A.6}$$

$$l'_{AB} = \sqrt{[l_{OA}^2 + l_{OB}^2 - 2l_{OA}l_{OB}\cos(\beta - \theta)]}, \tag{A.7}$$

where l_{AB} is the original distance, and l_{AB} is the distance between A and B during the suspension system's movement. Then the distance variation of AB is $\Delta l_{AB} = l_{AB} - l'_{AB}$. The derivative of Δl_{AB} is

$$\Delta \dot{l}_{AB} = \dot{l}_{AB} - \dot{l}'_{AB} = {\mathrm{a}\sin(\beta-\theta)\,\dot{\theta}}\Big/{2\sqrt{\mathrm{a}-2b\cos(\beta-\theta)}}, \tag{A.8}$$

where $\mathrm{a} = (l_{OA}^2 + l_{OB}^2)$, $\mathrm{b} = (l_{OA}^2 + l_{OB}^2)$.

As for simplified MacPherson suspension model, the system dynamic energy T, the potential energy U and the dissipation function D could be separately expressed as:

$$\mathrm{T} = \tfrac{1}{2} m_s \dot{z}_s^2 + \tfrac{1}{2} m_u \left(\dot{z}_{ux}^2 + \dot{z}_{uy}^2\right), \tag{A.9}$$

$$\mathrm{U} = \tfrac{1}{2} k_s (\Delta l_{AB})^2 + \tfrac{1}{2} k_t (z_u - z_r)^2, \tag{A.10}$$

$$\mathrm{D} = \tfrac{1}{2} c_s \Delta \dot{l}_{AB}^2. \tag{A.11}$$

Substituting (A.1)-(A.8) into (A.9)-(A.11) gives

$$\mathrm{T} = \tfrac{1}{2}(m_s + m_u)\dot{z}_s^2 + \tfrac{1}{2} m_u l_{OC}^2 \dot{\theta}^2 + m_u l_{OC} \cos(\theta + \theta_0)\,\dot{\theta}\dot{z}_s, \tag{A.12}$$

$$\begin{aligned} U = {} & \tfrac{1}{2} k_s \{2\mathrm{a} - \mathrm{b}[\cos\beta + \cos(\beta-\theta)]\} \\ & - k_s \sqrt{\{\mathrm{a}^2 - \mathrm{ab}[\cos\beta + \cos(\beta-\theta)] + b^2 \cos\beta\cos(\beta-\theta)\}} \\ & + \tfrac{1}{2} k_t \{z_s + l_{OC}[\sin(\theta+\theta_0) - \sin(\theta_0)] - z_r\}^2, \end{aligned} \tag{A.13}$$

$$\mathrm{D} = {c_s b^2 \sin^2(\beta-\theta)\,\dot{\theta}^2}\Big/{8[\mathrm{a} - \mathrm{b}\cos(\beta-\theta)]}. \tag{A.14}$$

Based on generalized coordinate $g_1 = z_s$ and $g_2 = \theta$, the simplified MacPherson suspension model's dynamic equation can be represented as:

$$\begin{aligned} & (m_s + m_u)\ddot{z}_s^2 + m_u l_{OC}\left[\cos(\theta+\theta_0)\,\ddot{\theta} - \sin(\theta+\theta_0)\,\dot{\theta}^2\right] \\ & \quad + k_t\{z_s + l_{OC}[\sin(\theta+\theta_0) - \sin(-\theta_0) - z_r]\} = 0, \end{aligned} \tag{A.15}$$

$$
\begin{aligned}
&k_t l_{OC}\cos(\theta+\theta_0)\{z_s + l_{OC}[\sin(\theta+\theta_0)-\sin(-\theta_0)-z_r]\}\\
&\quad -\tfrac{1}{2}k_s\sin(\beta-\theta)\left[b+\frac{d}{\sqrt{c-d\cos(\beta-\theta)}}\right]\\
&\quad +m_u l_{OC}^2\ddot{\theta}+m_u l_{OC}\cos(\theta-\theta_0)\,\ddot{z}_s = -c_s l_{OB}\Delta\dot{l}_{AB},
\end{aligned}
\tag{A.16}
$$

where $c = ab\cos(\alpha+\theta_0)$, $d = ab - b^2\cos(\alpha+\theta_0)$. Note that (A.16) is applied in the following approximate relationship during deduction:

$$
Q_j = -\frac{\partial D}{\partial\dot{\theta}} = -c_s\Delta\dot{l}\frac{\partial\Delta\dot{l}}{\partial\dot{\theta}} \approx -c_s l_{OB}\Delta\dot{l}_{AB}. \tag{A.17}
$$

There is coupling between the acceleration, $\ddot{z}_s$ of spring mass equation (A.15) and (A.16), and the acceleration $\ddot{\theta}$, of the below transverse arm. Defining the state variables and the state vector as $X=[x_1 \quad x_2 \quad x_3 \quad x_4]^T=[z_s \quad \dot{z}_s \quad \theta \quad \dot{\theta}]^T$, the MacPherson suspension system can be written as

$$
\begin{aligned}
\dot{x}_1 &= x_2,\\
\dot{x}_2 &= {}^{1}\!/_{[m_s l_{OC}+m_u l_{OC}\sin^2(x_3-\theta_0)]}\,(m_u l_{OC}^2\sin(x_3-\theta_0)\,x_4^2\\
&\quad -\tfrac{1}{2}k_s\sin(\beta-\theta_0)\cos(x_3-\theta_0)\left[b+{}^{d}\!/_{\sqrt{c-d\cos(\beta-x_3)}}\right]\\
&\quad -k_t l_{OC}\sin^2(x_3-\theta_0)\{x_1+l_{OC}[\sin(x_3-\theta_0)-\sin(-\theta_0)]-z_r\}\\
&\quad +c_s l_{OB}\Delta\dot{l}_{AB}\cos(x_3-\theta_0)),\\
\dot{x}_3 &= x_4,\\
\dot{x}_4 &= -{}^{1}\!/_{[m_s m_u l_{OC}^2+m_u^2 l_{OC}^2\sin^2(x_3-\theta_0)]}\,((m_s+m_u)c_s l_{OB}\Delta\dot{l}_{AB}\\
&\quad +m_s k_t l_{OC}\cos(x_3-\theta_0)\{\sin(x_3-\theta_0)-\sin(-\theta_0)-z_r\}\\
&\quad -\tfrac{1}{2}(m_s+m_u)k_s\sin(\beta-\theta_0)\left[b+{}^{d}\!/_{\sqrt{c-d\cos(\beta-x_3)}}\right]\\
&\quad +m_u^2 l_{OC}^2\sin^2(x_3-\theta_0)\cos(x_3-\theta_0)\,x_4^2).
\end{aligned}
\tag{A.18}
$$

APPENDIX B: LINEAR QUARTER-CAR MODELLING PROCESS

The linear quarter-car dynamic equations:

$$\begin{aligned} &m_s\ddot{z}_s + c_s(\dot{z}_s - \dot{z}_u) + k_s(z_s - z_u) = 0, \\ &m_u\ddot{z}_u + k_t(z_u - z_r) - c_s(\dot{z}_s - \dot{z}_u) - k_s(z_s - z_u) = 0. \end{aligned} \tag{B.1}$$

By defining state variables as:

$$\mathrm{x} = [x_1 \quad x_2 \quad x_3 \quad x_4]^T = [\dot{z}_s \quad \dot{z}_u \quad z_s - z_u \quad z_u - z_r]^T. \tag{B.2}$$

Replacing (B.2) into (B.1) gives the dynamic description with state variables as following:

$$\begin{aligned} &m_s\dot{x}_1 + c_s(\dot{x}_1 - \dot{x}_2) + k_s x_3 = 0, \\ &m_u\dot{x}_2 + k_t x_4 - c_s(x_1 - x_2) - k_s x_3 = 0. \end{aligned} \tag{B.3}$$

Re-arrangement of (3.3) gives

$$\begin{aligned} \dot{x}_1 &= -[k_s x_3 + c_s(x_1 - x_2)]/m_s, \\ \dot{x}_2 &= [k_s x_3 - k_t x_4 + c_s(x_1 - x_2)]/m_u, \\ \dot{x}_3 &= \dot{z}_s - \dot{z}_u = x_1 - x_2, \\ \dot{x}_4 &= \dot{z}_u - \dot{z}_r = x_2 - \dot{z}_r. \end{aligned} \tag{B.4}$$

Then, the state-space equation of the quarter-car system can be represented as

$$\dot{x} = Ax + Bw, \tag{B.5}$$

where $w = \dot{z}_r$ is the disturbance matrix,

$$\mathrm{A} = \begin{bmatrix} -\frac{c_s}{m_s} & \frac{c_s}{m_s} & -\frac{k_s}{m_s} & 0 \\ \frac{c_s}{m_u} & \frac{c_s}{m_u} & \frac{k_s}{m_u} & -\frac{k_t}{m_u} \\ 1 & -1 & 0 & 0 \\ 0 & 1 & 0 & 0 \end{bmatrix},$$

$$\mathrm{B} = [0 \quad 0 \quad 0 \quad -1]^T.$$